Ensemble Flood Forecasting using High-Resolution Ensemble Numerical Weather Prediction with Radar Based Prediction Considering Rainfall Forecast Uncertainty

YU Wansik

2014

Ensemble Flood Forecasting using High-Resolution Ensemble Numerical Weather Prediction with Radar Based Prediction Considering Rainfall Forecast Uncertainty

by

YU Wansik

A Dissertation

Submitted in partial fulfillment of the requirement

for the Degree of Doctor of Philosophy

Department of Civil and Earth Resources Engineering

Kyoto University, Japan

2014

Abstract

Many flood forecasting systems rely on rainfall inputs, which come from observation networks (e.g., radar and rain gauges). However, for medium-term forecasts (~ 1 day ahead), numerical weather prediction (NWP) models must be used to produce the advanced flood forecasting with extended lead time. Recent advances in rainfall forecast from NWP models have created opportunities to incorporate forecast outputs directly into flood forecast systems in order to obtain an extended lead time. And flood forecast systems are increasingly moving toward using ensemble outputs of the NWP model, rather than single deterministic forecasts, to take account of uncertainties and to allow for skillful predictions.

Recent research, however, has found that direct application of ensemble outputs from a numerical weather prediction (NWP) model into the flood forecasting area can result in considerable problems regarding variability and uncertainty, which are propagated into hydrological domains. First, the spatial scale of the hydrological model will not match the scale of the meteorological model, which is not at a high enough resolution yet. Second, the ensemble flood forecasting may need to have some kind of correction applied for the under-representation of uncertainty. Therefore, in order to use ensemble forecast outputs of the NWP model for flood forecasting effectively, it is important to establish some kind of methodologies to apply for ensemble flood forecasts.

Given the current issues with ensemble flood forecasting, this study is attempting to deal with high-resolution ensemble information mainly from numerical weather prediction (NWP) and partly from radar-based prediction for the application of flood forecasting with a distributed hydrologic model and to discusses how uncertainty of ensembles is represented in flood forecasting. And several methods are proposed to

improve the accuracy of the flood forecasting considering rainfall forecast uncertainty. Main focuses and findings of this thesis are listed below.

Chapter 2 describes the design of the meteorological experiment for ensemble forecasting, target event and area, and a hydrologic model for the flood forecasting.

Chapter 3 investigates the applicability of ensemble forecasts of a numerical weather prediction (NWP) model for flood forecasting area based on the basic data of Chapter 2. Ensemble outputs with 30 hr forecast time and 2 km horizontal resolution, which is the state-of-the-art technique for operational applications in hydrological fields, are verified temporally and spatially whether they can produce suitable rainfall predictions or not during the Typhoon Talas event. Then, flood forecasting driven by ensemble outputs is carried out over Futatusno (356.1 km^2) and Nanairo (182.1 km^2) dam catchments of Shingu river basin (2,360km^2), located on the Kii Peninsula of the Kinki area, Japan. Through the case study, it shows that ensemble forecast increases forecast accuracy and allows for skillful predictions, but the uncertainty of ensemble NWP rainfall is also significant at longer lead times. Therefore, it is important to establish methodologies to improve the accuracy of the ensemble flood forecasting.

Chapter 4 presents the uncertainty propagation of rainfall forecast into hydrological response with catchment scale through distributed rainfall-runoff modeling based on the forecasted results of Chapter 3. The research questions that this chapter addresses are: How does rainfall forecast error translate to the flood forecast error, and how does flood forecast propagate as a function of catchment scale dependency. It is assumed that contributions to the uncertainty of predicted discharge come from the uncertainty of rainfall forecast, which is the difference between predicted and observed rainfall, so pay no attention to hydrological model uncertainties, which are classified into model parameter and structure errors. Chapter

4 shows that smaller catchments demonstrate a larger uncertainty in the flood forecasting.

Chapter 5 proposes pre-processing methodologies based on appropriate members and a transposition scheme of ensemble forecast outputs from a numerical weather prediction (NWP) model. First, the selection of appropriate members is investigated by comparison of spatial distributions between observed radar rainfall and forecasted ensemble rainfall. And selected ensemble information is applied to the next forecast period to assess the accuracy improvement of flood forecasting. Second, as an approach for the accuracy improvement of the flood forecasting, transposition method, which is a spatial shift of ensemble rainfall distributions considering the correction of misplaced predicted rainfall distributions, is introduced. Finally, the above two methods are integrated in order to use advantages of characteristics of each method at the same time and apply to the next forecast period to confirm the accuracy improvement of the flood forecast skill. Through Chapter 5, the transposition method could enhance the mean and best value of the accuracy on flood forecasting.

Chapter 6 enhances the transposition method proposed in Chapter 5 and suggests real-time updating of flood forecasting using newly proposed transposition scheme considering orographic rainfall for the QPF location correction and the accuracy improvement. In the first step of the proposed method, ensemble forecast rainfalls from a numerical weather prediction (NWP) model are separated into orographic and non-orographic rainfall fields using atmospheric variables (e.g., air temperature, horizontal wind, and relative humidity) and the extraction of topography effect. Then, the non-orographic rainfall fields are examined by the transposition scheme to produce additional ensemble information. And new ensemble NWP rainfall fields are calculated by recombining the transposition results of non-orographic rain fields with separated orographic rainfall fields for a generation of place-corrected ensemble

information. Then, the additional ensemble information is applied to the hydrologic model for post-flood forecasting with 6-hr intervals, which shows the accuracy improvement of flood forecasting with the proposed updating method.

Chapter 7 proposes hybrid system blending of ensemble information from radar-based forecast and numerical weather prediction (NWP) to improve the accuracy of rainfall and flood forecasting. First, an improved radar image extrapolation method, which is comprised of the orographic rainfall identification and the error ensemble scheme, is introduced. Then, ensemble NWP outputs are updated based on 1) mean bias of the error fields considering error structure and 2) transposition scheme considering the orographic rainfall introduced in Chapter 6. Finally, the improved radar-based prediction and two updated NWP rainfall considering 1) bias correction and 2) QPF location correction are blended dynamically with changing weight functions, which are computed from the expected skill of each radar prediction and updated NWP rainfall. The blending result based on bias correction shows sufficient reproducibility in peak discharge value compared with the result based on QPF location correction in updated flood forecasting, whereas the blending based on transposition scheme could reduce the width of the ensemble spread, which is expressed as the uncertainty in the flood forecasting.

In conclusion, major findings that were mainly addressed in this study are: For extreme events, although the ensemble forecasts based on NWP model can generally catch the rainfall pattern, the uncertainties of rainfall in the flood forecasting area were significant, and for this reason, new methodologies (i.e., QPF location correction by transposition scheme, bias correction by error-field scheme, and hybrid blending scheme) using ensemble information from NWP model and radar-based prediction were proposed and could provide a clear indication of the accuracy improvement of flood forecasting.

Acknowledgements

Working as a Ph.D. student in Kyoto University was a magnificent as well as challenging experience to me. In all these years, many people were instrumental directly or indirectly in shaping up my academic career. It was hardly possible for me to thrive in my doctoral course without the precious support of these personalities. Here is a small tribute to all those people.

First of all, I wish to thank my supervisor Prof. Eiichi NAKAKITA for introducing me to the world of hydrometeorology research. It was due to his valuable guidance, cheerful enthusiasm and ever-friendly nature that I was able to complete my research work. I am grateful to Associate Prof. Yoshinobu KIDO for his valuable comment and support to guide my research. Without their assistance and persistent help in Japan, my research work with Kyoto University would not have been possible.

And this dissertation has been more improved by the committee members. I would like to thank my committee members, Prof. Eiichi NAKAKITA, Associate Prof. Sunmin KIM and Prof. Tetsuya SUMI. Their valuable comments and help made it possible to achieve my research career.

I also would like to express my special gratitude towards Associate Prof. Sunmin KIM and Dr. Kosei YAMAGUCHI for helping me out in all aspects and for providing technical support during my work. Then I would like to thank my laboratory members (Mr Yoshiya TOUGE, Mr. Aritoshi MASUDA, Mr. Yuki KITAGAWA, Mr. Kohei FURUTA, Ms. Haruka KUSANO, Mr. Go SATO, MR. Kazuya TAKAMI, Ms. Akiko KANDA and Mr. Hiroto SATO) and Ms. Mayumi TSUJI for helping me kindly in laboratory life.

I am very obliged to Prof. Kwansue JUNG as a supervisor in Chungnam National University, Korea for his valuable guidance and encouragement during an undergraduate and master course student. Then I express thanks to my seniors in Chungnam National University, Korea: Prof. Giha LEE, Prof. Changlae JANG, Dr. Jeongyup KIM, Dr. Yongjun CHOI, Jungsu BOK, Daejin JUNG, Dr. Yeonsu KIM and Dr. Seungsoo LEE.

Finally, I wish to thank my family for their constant support and encouragement in all my professional endeavors. Although I could not express my gratitude for all of the people who helped me a lot, I am sure that their support and encouragement lead me to finalize this thesis.

In addition, this study was partly supported by the sub-project of the field 3 on Next Generation Supercomputer Project, 'Prediction of heavy rainfalls by a cloud-resolving NWP system', and was based on data from J-POWER CO. Ltd. I am grateful for their support. I could finish this course work from the financial support of Japanese Government (Monbukagakusho: MEXT) Scholarship and from HSE program and GCOE program in Kyoto University.

Wansik YU

Contents

List of Figures

List of Tables

Chapter 1

Introduction

1.1 Background

Flood forecasting is an important mechanism to reduce the damaging effects of flood events and to acquire sufficient time for early flood warnings (Demeritt et al., 2007). The identification of the need for flood forecasting and warning systems is witness to the reality of the limitations of structural flood protection systems. Due to the existence of residents in flood-prone areas and the need to meet expectations of community safety and protection of assets, an adequate flood forecasting and warning service is a growing necessity in many countries (WMO, 2011). The primary goal, in most cases, of flood forecasting and warning services is to provide reliable and timely information to civil protection services as well as to the general public. This should be accomplished with enough lead time to allow people to take measures to protect themselves from flooding or take other appropriate actions.

Numerical Weather Prediction (NWP) models take advantage of present weather conditions as input to atmospheric models to predict the advance of weather systems for medium-term forecasts (~ 1 day ahead). Recent advances in NWP models have created opportunities to improve streamflow forecasts. The accuracy of weather forecasts has steadily improved over the years, but it has been challenging to integrate quantitative precipitation forecasts (QPF) into flood forecast systems (Cloke and Pappenberger, 2009; Cuo et al., 2011).

Using the outputs from a number of forecasts or realizations, the relative frequency of events from the ensemble numerical weather prediction can be used

directly to estimate the probability of a given weather or flood event. Ensemble forecasting is a form of Monte Carlo analysis: multiple numerical predictions are conducted using slightly different initial conditions that are all plausible given the past and current set of observations or measurements. Ensemble or probabilistic forecasts are more widely applied to NWP models, with the probabilistic outcome of a number of NWP runs being used to provide the "most likely" scenario for input into a hydrological model of so-called ensemble prediction systems (EPSs).

Several different hydrologic and flood forecasting projects now use EPS operationally or semi-operationally, and many centers may be considering the adoption of such an approach. In 1999, the European Flood Forecasting System (EFFS, 1999 ~ 2003) project was the first European research project based on EPS and addressed early flood warning (De Roo et al., 2003; Kwadijk, 2003; Bartholmes and Todini, 2005). In the light of the EFFS, a European commission created the European Flood Alert System (EFAS). In 2004, the Hydrological Ensemble Prediction Experiment (HEPEX) guided an international initiative to develop cooperative research between the meteorological and hydrological communities (Schaake et al., 2006, 2007; Thielen et al., 2008). Since then, EPS-based research has become a dominant feature of hydrological research and applications on all time scales (Mesoscale Alpine Programme Demonstration of Probabilistic Hydrological and Atmospheric Simulation of Flood Events (MAP D-PHASE) (Zappa et al., 2008), Prevention, Information and Early Warning (PREVIEW) (Bogner and Kalas, 2008), and other research projects on ensemble forecasts: Roulin et al., 2007; Bartholmes et al., 2009; Hopson and Webster, 2008; Olsson and Lindstrom, 2008).

The findings from EPS projects and case studies (hindcasts) evaluating ensemble flood forecasting clearly showed great potential for using EPS to increase flood early warning time, but equally emphasized the need for further research on the interpretation of ensemble outputs, sufficient events for statistical analysis, especially

pre/post-processing (i.e., some kind of correction) of the raw ensemble outputs. Given the current issue and problem with EPSs with NWP models, proper pre-processing and corrections that deal with under-dispersivity (i.e., not enough spread, and thus under-representation) or bias (difference between predictions and observations) should be considered carefully in order to use EPSs effectively in flood forecasting systems on a small catchment scale. There are several ways to deal with NWP model biases in flood forecasting. One is to shift (or transpose) the spatial rainfall distribution that is derived from the ensemble forecasts of the NWP model to consider a QPF location correction. This approach accounts for biases with misplacement of spatial rain distributions, but it is possible to be vulnerable when ensemble forecasts themselves are uncorrected compared to true rainfall distributions. Another approach is to correct biases from previously predicted and observed rainfall and is generally preferred for flood forecasting, but bias correction methods have not been examined well in previous studies. Hamm and Elmore (2004) mentioned that NWP model ensembles perform poorly without bias correction, but a simple bias correction added to each ensemble member appears to significantly enhance the ensemble's utility. Therefore, some kind of method of dealing with QPF location and bias correction for improved accuracy in rainfall and flood forecasting is the main subject to be discussed in this study.

1.2 Research Aims and Objectives

This study attempts to deal with ensemble forecast outputs of NWP model for flood forecasting applications with a distributed hydrologic model. Several methods are introduced herein to improve the accuracy of flood forecasting considering QPF location correction, bias correction of ensemble NWP outputs, hybrid blending of updated NWP rainfall with radar-based prediction by consideration of orographic rainfall identification, the error-field scheme, and the transposition scheme. The

primary objectives of this thesis are as follows:

1) To examine the applicability of ensemble rainfall outputs of probabilistic weather prediction into flood forecasting, considering prediction uncertainty.

2) To understand and assess the prediction uncertainty propagation from ensemble NWP rainfall outputs into a hydrological response with a catchment scale.

3) To explore improvements in accuracy of flood forecasting by determining appropriate ensemble members of NWP rainfall predictions and transposition of NWP rainfall fields for the QPF location correction of misplaced spatial positions.

4) To suggest a post-processed ensemble forecasting method for real-time updating and accuracy improvement of flood forecasts based on the QPF location correction from the enhancement of a transposition scheme that considers the separation of orographic and non-orographic rainfall.

5) To blend the advantages of NWP ensemble information and radar-based prediction for accuracy improvement of rainfall and flood forecasting in viewpoint of the hybrid forecast.

1.3 Outline of Thesis

This thesis consists of eight chapters, and the analysis from chapter 3 to chapter 7 is based on the ensemble NWP rainfall data and distributed hydrologic model presented in chapter 2. Figure 1.1 shows the roadmap of this thesis. The rectangles represent the title and objective of each chapter and the arrow represents the

relationship between the chapters.

Chapter 2 describes the design of meteorological experiment for ensemble prediction, target event and area, and the applied rainfall-runoff model used in this thesis for flood forecasting.

Chapter 3 investigates the applicability of using ensemble forecasts from a numerical weather prediction (NWP) model for flood forecasting area based on the basic data of Chapter 2, and reviews the reasons why NWP model ensembles are so attractive for flood forecasting area than deterministic model runs. Ensemble outputs with 30 hr forecast time and 2 km horizontal resolution, which is the state-of-the-art technique for operational applications in hydrological fields, are verified temporally and spatially as to whether they can produce suitable rainfall predictions or not during the Typhoon Talas event. Then flood forecasting driven by ensemble outputs is carried out for the Futatusno (356.1 km^2) and Nanairo (182.1 km^2) dam catchments of the Shingu river basin (2,360km^2), located in the Kii Peninsula of the Kinki region in Japan.

Chapter 4 presents the propagation of NWP rainfall uncertainty as a hydrological response with spatial scale through distributed rainfall-runoff modeling based on the forecasted results of Chapter 3. Chapter 3 assumed that contributions to discharge uncertainty come from rainfall forecast uncertainty, which is the difference between predicted and observed rainfall; therefore, this chapter pays no attention to hydrological model uncertainties, which are classified into model parameter errors and model structure errors. For the assessment of uncertainty variability and propagation, error indexes (e.g., coefficient of variation, bias, RMSE) are estimated depending on the catchment scale.

Chapter 5 proposes pre-processing methodologies based on appropriate members and a transposition scheme of ensemble forecast outputs from the numerical weather prediction (NWP) model. First, the selection of appropriate members is investigated by comparing the spatial distributions between observed radar rainfall and forecasted ensemble rainfall, and selected ensemble information is applied into the next forecast period to assess the accuracy improvement of flood forecasting. Second, as an approach for improving accuracy in flood forecasting, the transposition method, which is a spatial shift in ensemble rainfall distributions that considers the correction of misplaced predicted rainfall distributions, is introduced. Finally, the above two methods are integrated in order to use advantages of the characteristics of each method at the same time and apply them to the next forecast period to confirm the accuracy improvement in flood forecasting skill.

Chapter 6 enhances the transposition method proposed in Chapter 5 and suggests real-time updating of flood forecasting using a newly proposed transposition scheme that considers the orographic rainfall for the QPF location correction and the previously realized improvements in accuracy. In the first step of the proposed method, ensemble forecast rainfalls from a numerical weather prediction (NWP) model are separated into orographic and non-orographic rainfall fields using atmospheric variables (e.g., air temperature, horizontal wind, and relative humidity) and the extraction of the topography effect. Then the non-orographic rainfall fields are examined with the transposition scheme to produce additional ensemble information and new ensemble NWP rainfall fields are calculated by recombining the transposition results of non-orographic rain fields with the separate orographic rainfall fields to generate place-corrected ensemble information. Then, the additional ensemble information is applied into a hydrologic model for post-flood forecasting with a 6-hour interval.

Chapter 7 proposes a hybrid system that blends ensemble information from radar-based forecasting and numerical weather prediction (NWP) to improve the accuracy of rainfall and flood forecasting. First, an improved radar image extrapolation method, which is comprised of the orographic rainfall identification and the error ensemble scheme, is introduced. Then ensemble NWP outputs are updated based on: 1) mean bias of error fields that consider error structure and 2) transposition scheme that considers orographic rainfall introduced in Chapter 6. Finally, the improved radar-based prediction and two updated NWP rainfall models that consider 1) bias correction and 2) QPF location correction are blended dynamically with changing weight functions, which are computed from the expected skill of each radar prediction and updated NWP rainfall. The proposed method is verified temporally and spatially through target events and is applied to hybrid flood forecasting for updates with a 1-hour interval.

Finally, Chapter 8 summarizes this thesis with concluding remarks containing the research contributions, limitations and further works relevant to this study.

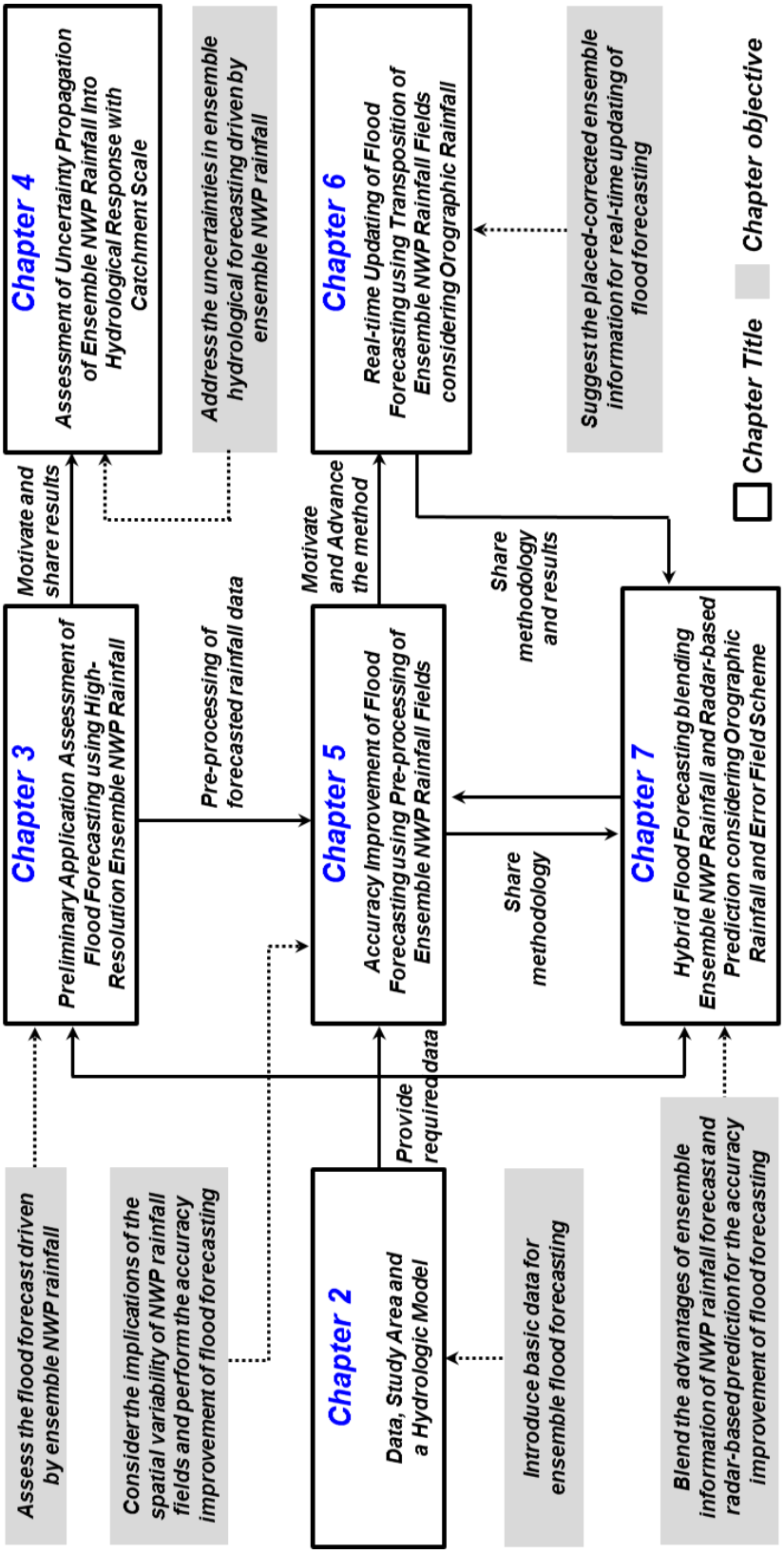

Figure 1.1 Roadmap of this thesis.

Chapter 2

Data, Study Area and a Hydrologic Model

2.1 Design of Meteorological Experiment

In early September 2011 heavy rainfalls happened over Japan due to the season's 12th typhoon, Talas, which caused large flooding and enormous landslide disasters over Japan's Kinki region. It also caused unprecedented human damage, resulting in 78 dead and 16 missing. Talas moved very slowly and had a huge gale diameter throughout its life. The total amount of precipitation from Talas in the Kii Peninsula was estimated to be over 2,000 mm.

In Japan, an operational one-week ensemble prediction model from JMA was developed to provide probabilistic information of 51 ensemble members with a horizontal resolution of 60 km, and it used to be applied for hydrological applications (e.g., prior and optimized release discharge for dam operation; Matsubara et al., 2013). However, operational short-term (1–2 day) ensemble prediction with much finer resolution has not yet been developed. For that reason, studies on ensemble forecast systems that are composed of 11 members (1 unperturbed and 10 perturbed member) with a horizontal resolution of 10 km and 2 km, the latter nested inside the former with a 6-hour lag, have been conducted by the Meteorological Research Institute (MRI) of JMA for the 2011 Typhoon Talas event.

Both 10 km and 2 km resolution systems used the JMA Non-hydrostatic Model (NHM) as the forecast model (Saito et al., 2006; Saito, 2012). Whereas the 10 km resolution forecast adopted the cloud microphysical process and Kain-Fritsch convective scheme, the 2 km resolution forecast did not use a convective scheme

because of its cloud resolving resolutions. The domain of the two ensemble systems with 10 km and 2 km horizontal resolution are illustrated in Figure 2.1.

The coarse resolution system of 10 km had a domain of 361×289 grid points with 50 vertical levels and forecasted up to 36 hours in advance. For initial and lateral boundary conditions, 10 km used the analysis from the JMA non-hydrostatic 4DVAR (JNoVA) data assimilation system (Honda and Sawada, 2008) and the forecasts of JMA's high-resolution (TL959L60) global spectral model (GSM). The control run (cntl) is the forecast with a non-perturbed analysis, and the 10 perturbed forecasts were generated from JMA's 1-week global EPS (WEP) for the initial and boundary perturbations. The fine-resolution 2 km system was conducted from the downscale forecast of 10 km resolution systems. This system had a domain of 350×350 grid points with 60 vertical levels and forecasted up to 30 hours in advance. The initial and boundary conditions for each member at 2 km were interpolated from the forecasts on the corresponding member at 10 km resolution with a 6-hour lag. 10 km started running at 21 JST every day, and 2 km began 6 hours later. Figure 2.2 shows a schematic of forecast runs with 10 km and 2 km resolution.

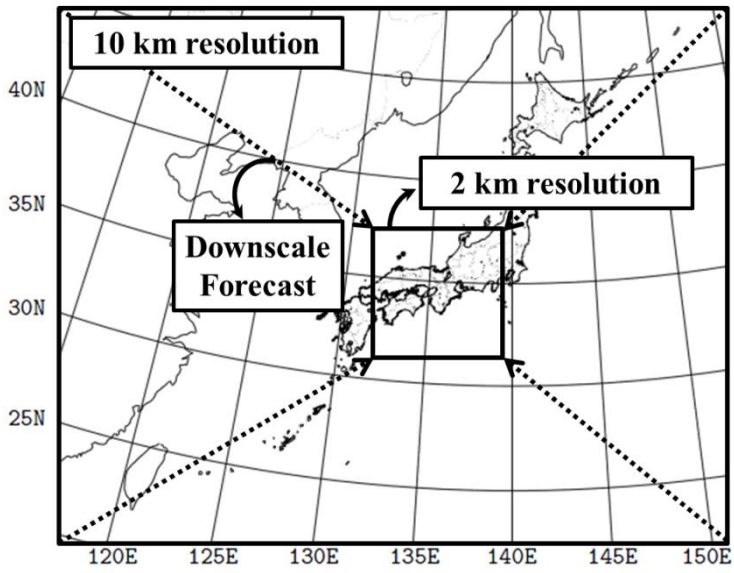

Figure 2.1 Forecast domains of 10 km and 2 km horizontal resolution.

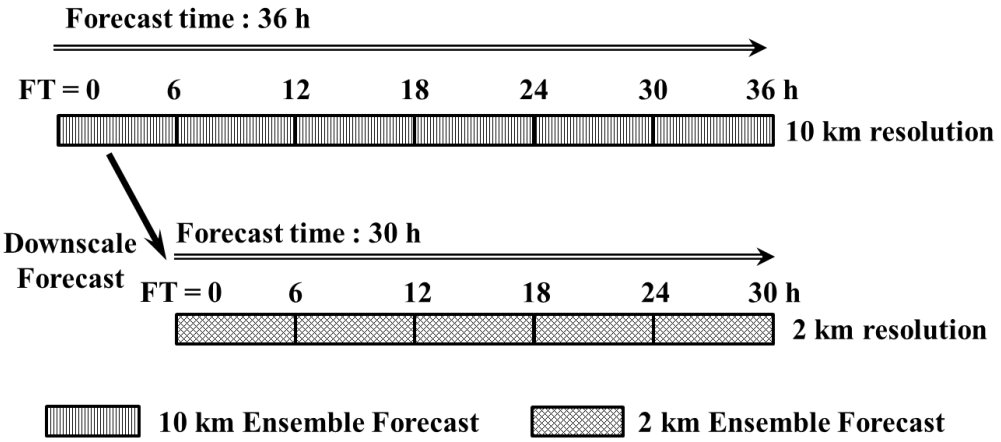

Figure 2.2 Schematic of forecast runs with 10 km and 2 km horizontal resolution

As the first look into the performances of two forecast systems, Figure 2.3 shows the accumulated rainfall by the Ministry of Land, Infrastructure, Transport and Tourism (MLIT)'s C-band composite radar data and its corresponding forecasts by control runs of 10 km and 2 km in the 0- to 30-hour forecasts at 2 km, which were correspondent to 6- to 36-hour forecasts at 10 km. These figures suggest that both control forecasts at 10 km and 2 km predicted well the precipitation amount and spatial location, and the 2 km forecast provided a more detailed distribution of the accumulated rainfall.

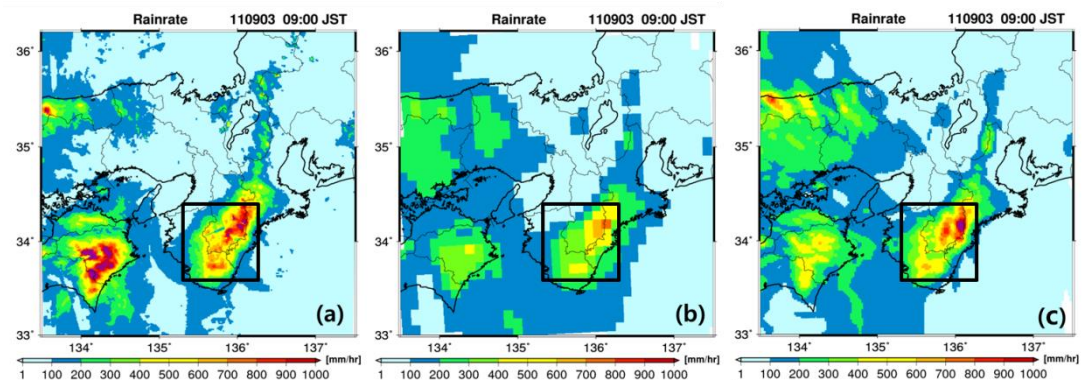

Figure 2.3 (a) Accumulated rainfall by MLIT radar and corresponding control run forecasts at (b) 10 km and (c) 2 km resolution in a 30-hours period (2011/09/02 03:00 ~ 09/03 09:00, 30 hours) over Japan's Kinki region. The rectangle inside the domain denotes the verification area.

Spatial verifications of 10 km and 2 km forecasts are conducted using frequency bias in verification area of Figure 2.3(a). Verifications were carried out with 30 hours forecast time in the 2 km run (2011/09/02 03:00–09/03 09:00), and the average bias values are shown in the plot. The verification rainfall thresholds were considered from light (0.1 mm/h) to intense (30 mm/h). It should be kept in mind that, while high thresholds restrict rain events to heavy rain, low thresholds not only represent light rain but also consider all rains from light to heavy. Figure 2.4 points out that 10 km control forecasts obviously under-predict intense rain events with high thresholds over 10 mm/h, whereas 2 km forecasts predict them well in overall thresholds. It means that a 2 km forecast is better, compared to a 10 km forecast, for predicting heavy rains such as typhoon events. Therefore, in this chapter, we introduced the results of ensemble prediction with a 2 km horizontal resolution due to the viewpoints of high resolution and better predictability of weather phenomena. Figure 2.5 shows the ensemble NWP rainfall forecast at 2 km horizontal resolution during Typhoon Talas (2011/09/02/15:00 JST).

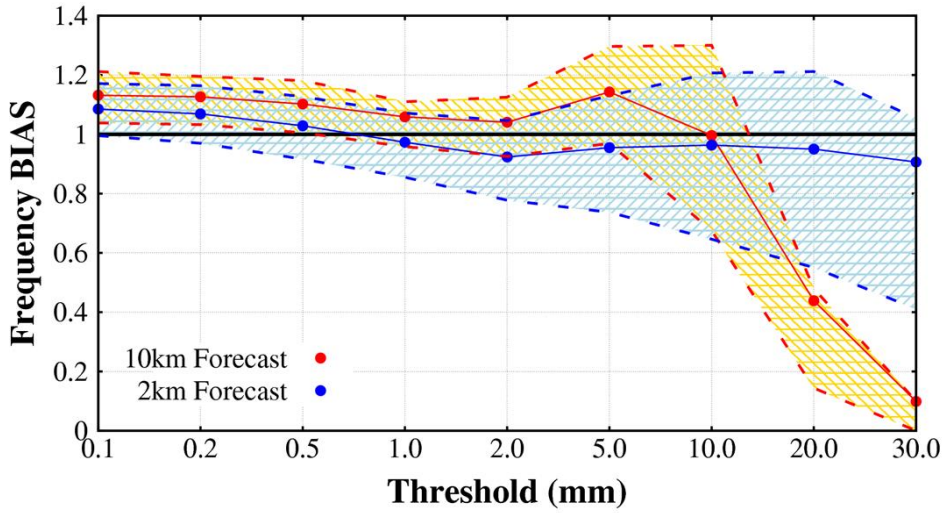

Figure 2.4 Frequency bias from 10 km and 2 km control run forecasts in verification area. The shaded areas are distributions between 25% and 75 % quartile intervals.

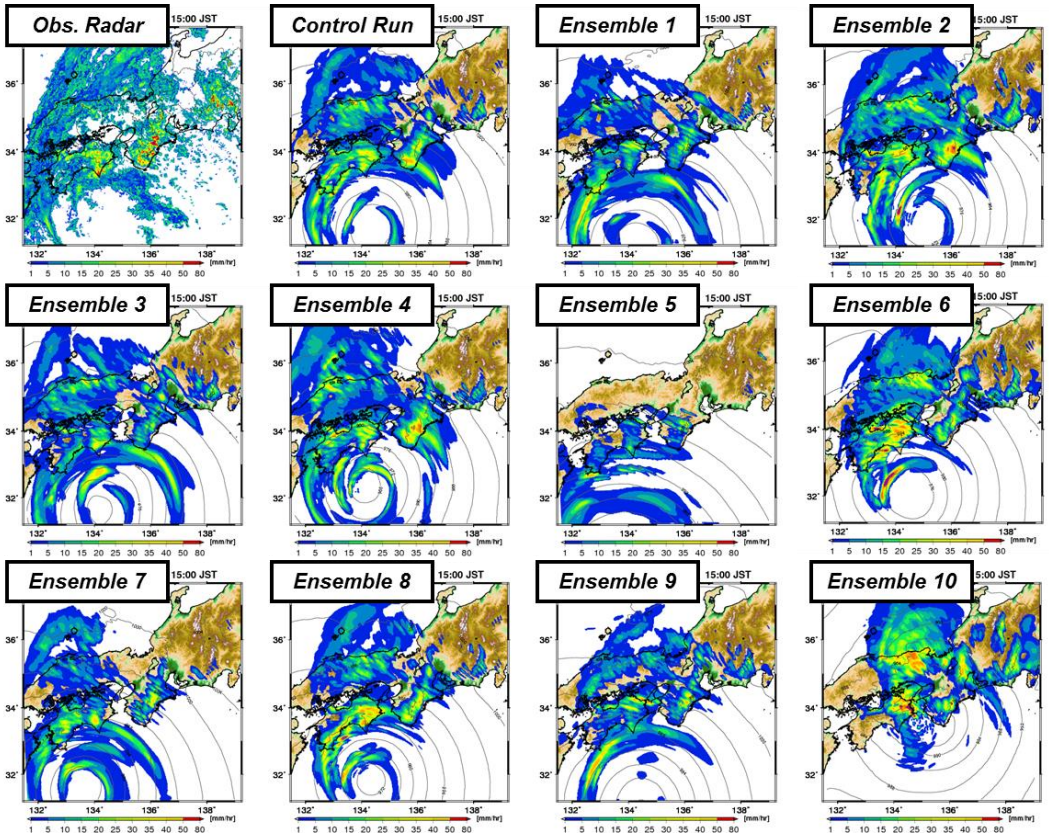

Figure 2.5 Ensemble NWP rainfall forecast at 2km horizontal resolution (2011/09/02/15:00 JST)

2.2 Target Area

The Shingu river basin was selected as the target area to assess the flood forecast applicability using the ensemble NWP rainfall as illustrated in Figure 2.6. The Shingu river Basin is located in the Kii Peninsula of the Kinki area, Japan and covers an area of 2,360 km^2. The average elevation of the study site is 644.6 m, and the slope is steep; this basin is a mountainous area. Figure 2.6(b) shows the drainage network, which consists of channel and hillslope components of the Shingu river basin. The five dams, Futatsuno, Kazeya, Komori, Nanairo, and Ikehara are located upstream. Of the five dam catchments, we focused on two sub-catchments, which are

Futatsuno (356.1 km^2) and Nanairo (182.1 km^2) dam catchments (Nos. 1 and 4 of Figure 2.6(a)). Two additional dams, Kazeya and Ikehara (Nos. 2 and 5 of Figure 2.6(a)), are located upstream of the Futatsuno and Nanairo catchments, respectively. Here, the observed outflows from the Kazeya and Ikehara dam were directly utilized as the upper boundary conditions for the subject dam basins to focus on only the Futatsuno and the Nanairo catchments.

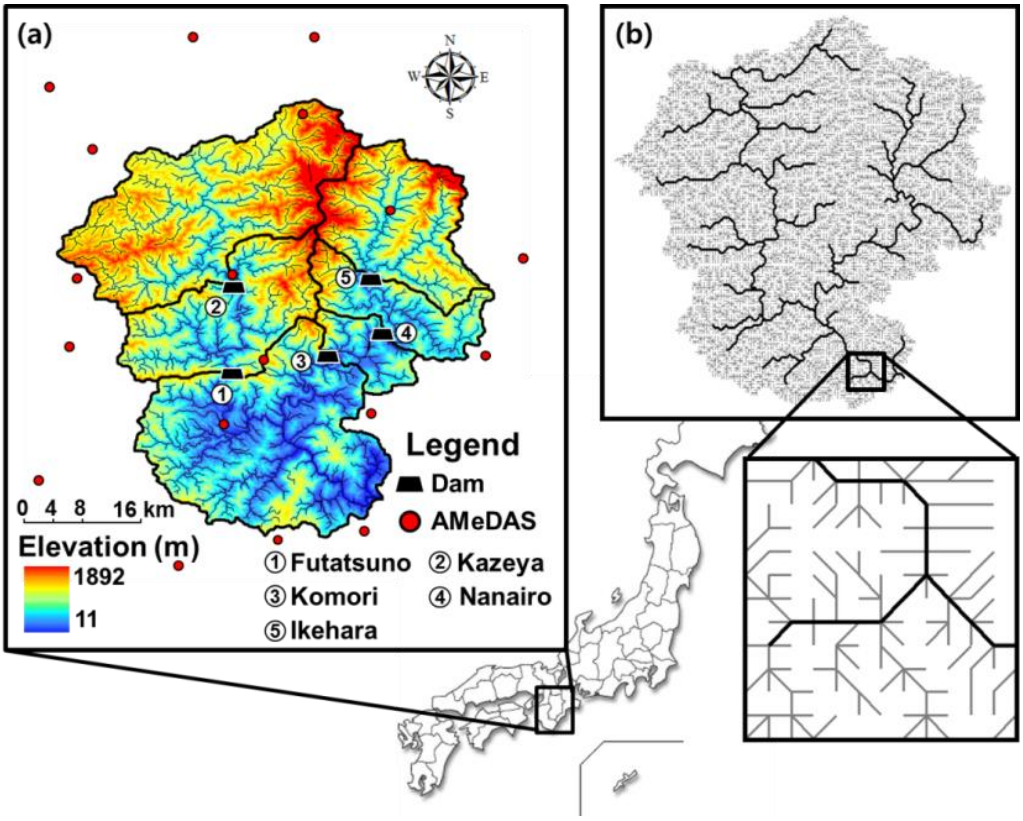

Figure 2.6 (a) Shingu river basin (b) drainage network represented by sets of channel (black line) and slope (gray line) elements.

2.3 Distributed hydrologic model: KWMSS

We used a spatially-distributed hydrologic model, based on one-dimensional kinematic wave method for subsurface and surface flow (hereafter, KWMSS) with a conceptual stage-discharge relationship, which was introduced by Takasao and Shiiba (1988) and enhanced by Tachikawa et al. (2004). This model is based on "Object-oriented Hydrological Modelling System (OHyMoS)". In this model, the rainfall–runoff modeling system accepts spatially variable information in terms of topographic and meteorological data. The drainage network is represented by sets of hillslope and channel elements from digital elevation model (DEM). The drainage network was represented by a 250 m × 250 m spatial resolution of DEM. Figure 2.7 is a conceptualization of spatial flow movement and flow process in hillslope elements of KWMSS. The rainfall over all hillslope elements flows one-dimensionally into the river nodes and then routes to the catchment outlet. The rainfall-runoff transformation conducted by KWMSS is based on the assumption that each hillslope element is covered with a permeable soil layer, as shown in Figure 2.7. This soil layer consists of a capillary layer and a non-capillary layer. In these conceptual soil layers, slow and quick flow are simulated as unsaturated Darcy flow and saturated Darcy flow, respectively, and overland flow occurs if water depth, h [m] exceeds soil water capacity.

$$q = \begin{cases} v_c d_c (h/d_c)^{\beta}, & 0 \le h \le d_c \\ v_c d_c + v_a (h - d_c), & d_c \le h \le d_s \\ v_c d_c + v_a (h - d_c) + \alpha (h - d_s)^m, & d_s \le h \end{cases} \tag{2.1}$$

$$\frac{\partial h}{\partial t} + \frac{\partial q}{\partial x} = r(x,t) \tag{2.2}$$

where $v_c=k_c i$ [m/s], $v_a=k_a i$ [m/s], $k_c=k_a/\beta$ [m/s], $\alpha=i^{1/2}/n$ [$m^{1/3}s^{-1}$], m = 5/3, i is the slope gradient, k_c [m/s] is the hydraulic conductivity of the capillary soil layer, k_a [m/s] is the hydraulic conductivity of the non-capillary soil layer, n [$m^{-1/3}s$] is the roughness coefficient, d_s [m] is the water depth corresponding to the water content, and d_c [m] is the water depth corresponding to maximum water content in the capillary pore. The flow rate of each hillslope element q [m^2/s] is calculated by equation (2.1), and combined with the continuity equation for channel routing by equation (2.2). The KWMSS does not consider vertical flow due to infiltration, but represents lagged subsurface flow with calibrated hydraulic conductivities and soil layer thicknesses (Tachikawa et al., 2004).

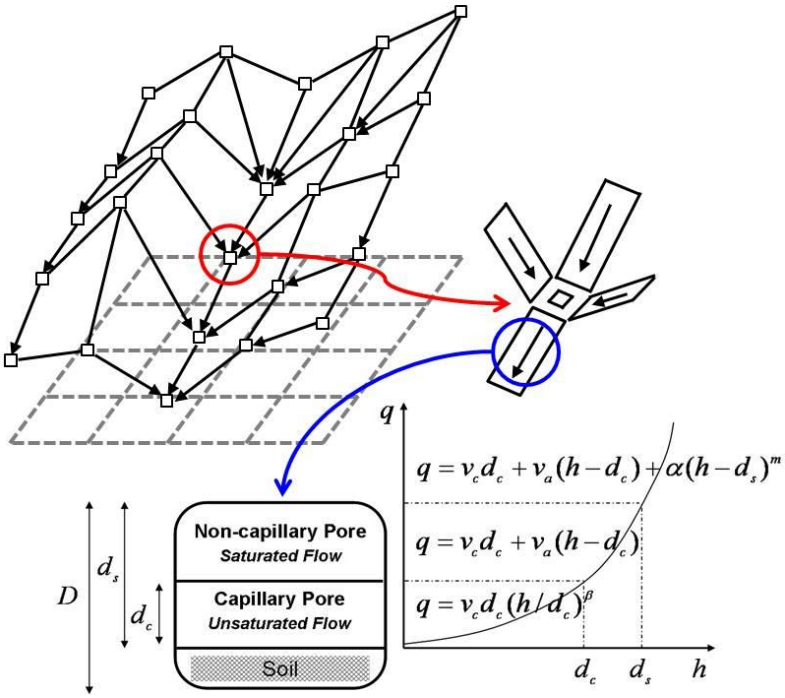

Figure 2.7 Conceptualization of spatial flow movement and flow process in hillslope elements; the arrows indicate element models for calculating hydrological variables, such as water flux.

2.4 Verification Data

The ensemble NWP rainfall forecast in this study is verified spatially against the Ministry of Land, Infrastructure, Transport and Tourism (MLIT) C-band composite radar data (radius of quantitative observation range: 120km, 1km mesh and 5 min resolution). MLIT C-band radar provides wide observation range and is installed to cover the entire nation, and is useful for large river flood-management tool in observing the seasonal rain front or typhoons.

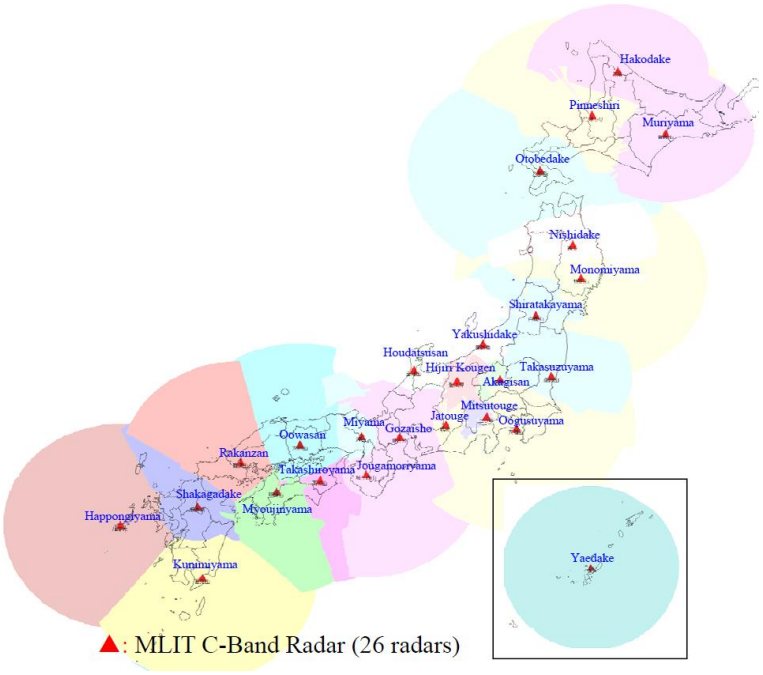

Figure 2.8 Conventional MLIT C-band Radar observation network in Japan

AMeDAS (Automated Meteorological Data Acquisition System) is a high-resolution surface observation network developed by the Japan Meteorological Agency (JMA) used for gathering regional weather data and verifying forecast performance. The system began operating on November 1, 1974, and currently comprises 1,300 stations throughout Japan (of which over 1,100 are unmanned), with an average separation of 17 km. In this study, for temporal verification of QPF with

ensemble NWP rainfall, the areal rainfall intensity of the AMeDAS is used. For comparison, the observed rainfall of AMeDAS over Kinki region (18 stations, 10 min step) is interpolated using the thiessen polygon spatial distribution method.

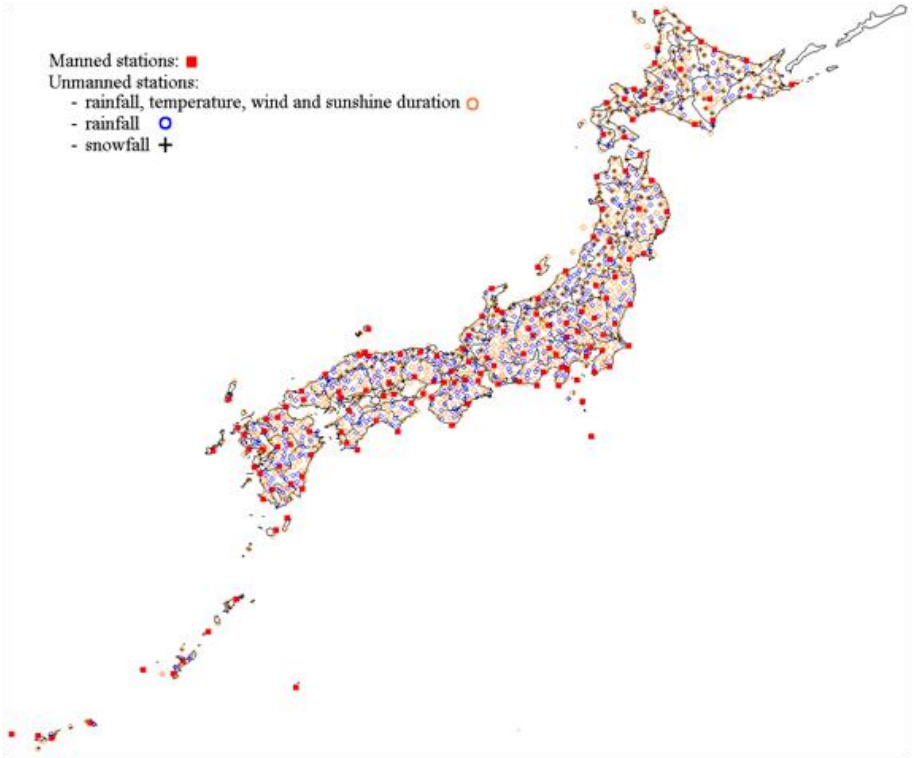

Figure 2.9 Observational sites of AMeDAS
(http://www.jma.go.jp/jma/en/Activities/observations.html)

Chapter 3

Preliminary Application Assessment of Flood Forecasting using High-Resolution Ensemble Numerical Weather Prediction Rainfall

Abstract *This chapter investigates the applicability of ensemble forecasts of numerical weather prediction (NWP) model for flood forecasting area based on the basic data of Chapter 2 and reviews the reasons why ensembles of NWP model are so attractive than deterministic model run. Ensemble outputs with 30hr forecast time and 2 km horizontal resolution are verified temporally and spatially whether they can produce suitable rainfall predictions or not during the Typhoon Talas event. Then flood forecasting driven by ensemble outputs is carried out over the Futatsuno (356.1 km^2) and Nanairo (182.1 km^2) dam catchments of Shingu river basin, located in Kii Peninsula of the Kinki area, Japan.*

The results shows that ensemble rainfall of NWP model produced better results compared with deterministic control run in terms of quantitative precipitation forecast (QPF), and flood forecasts driven by ensemble outputs showed that in general it has a large proportion of under and over predictions at short lead times and exhibited a negative bias at longer lead times. Despite the deficient performance for longer lead times, it was shown that the ensemble flood forecast provides additional information to the deterministic forecast.

3.1 Introduction

In early September, 2011, local heavy rainfalls due to season's 12th typhoon, "Talas" caused large flooding and enormous landslide disasters over the Kinki, Chugoku, Shikoku, and Tokai regions in Japan. It also caused unprecedented human damages, resulting in 78 dead and 16 missing persons. In these types of extreme events, it is essential to be able to provide as much advance warning as possible. This advance warning requires both quantitative precipitation forecasting (QPF) and quantitative flood forecasting (QFF). Numerical Weather Prediction (NWP) models are now becoming standard for short-range (1~2days) forecasts. NWP models use current weather conditions as input to atmospheric models to predict the evolution of weather systems. These models represent the atmosphere as a dynamic fluid and solve for its behavior through the use of mechanics and thermodynamics. The accuracy of weather forecasts has steadily improved over the years, due to advances in NWP techniques and increased computing power (Buizza et al., 1999; Demeritt et al., 2007).

The short-term Meso-Scale Model (MSM) of Japan Meteorological Agency (JMA) is now run operationally with a horizontal resolution of 5 km (Saito et al., 2006; Saito, 2012). During the Typhoon Talas event, the MSM generally predicted the typhoon track well in the early period. However, the predicted rainfall intensity was weaker than the observed radar rainfall, and the movement was also faster as the lead time was longer. As a result, the rainfall forecast pattern moved to the north-eastern part of the Kii peninsula quickly compared with the observed radar rainfall distribution.

One of the methods to overcome the forecast failure of deterministic predictions is to use ensemble outputs of NWP models. Ensemble outputs of NWP models have been generated since the early 1990s (e.g., ECMWF ensembles started in 1993) and

probabilistic weather forecasts have been used to express forecast uncertainty. It is believed that NWP ensemble prediction systems exhibit greater forecast skill than any single NWP model control run or deterministic model run (Buizza et al., 1999; Demeritt et al., 2007; Cuo et al., 2011).

Another method for an accuracy improvement of QPF and QFF areas can be achieved by increasing in the resolution of NWP models. In Japan, the JMA's operational one-week ensemble prediction has been developed to support typhoon track forecast and to provide probabilistic information with a horizontal resolution of 60 km and 51 ensemble members, and it used to be applied for hydrological applications. However, there is a limitation to use one-week ensemble prediction in respect of hydrological applications because one-week ensemble prediction has a coarse spatial resolution. With consideration for high-resolution and ensemble forecasts, the latest ensemble forecasts from NWP model with 30 hours forecast time and 2 km horizontal resolution has been experimentally generated by the Meteorological Research Institute (MRI) of the JMA. This ensemble forecast is still in research for an improvement in terms of the forecast accuracy, and it is expected that ensemble rainfall forecast can improve the forecast skill more than operational deterministic rainfall forecast.

In the context of flood management, it is important to integrate NWP model output and flood forecasting. It is possible to incorporate NWP model outputs directly into flood forecasting systems to obtain an extended lead time (Xuan et al., 2009). However, direct application of deterministic NWP model output can propagate uncertainties into the hydrologic domain. For this reason, the development of ensemble hydrological applications started in the late 1990s and is a field of ongoing research (De Roo et al., 2003; Gouweleeuw et al., 2005). Ensemble flood forecasting provides additional information to the deterministic flood forecast in the short forecast range, and provides a signal in terms of pre-warning and exceedance

probabilities for threshold values (e.g. critical discharge, levels causing inundation, and so on).

This chapter investigates the applicability of ensemble forecasts of NWP model for flood forecasting area based on the basic data of Chapter 2 and reviews the reasons why ensembles of NWP model are so attractive than deterministic model run. For ensemble rainfall forecasts during typhoon Talas event, 4 sets of ensemble prediction outputs with 30 hours forecast time and 2 km horizontal resolution are used. (1^{st} forecast: 2011/09/01 03:00 ~ 09/02 09:00 JST, 2^{nd} forecast: 2011/09/02 03:00 ~ 09/03 09:00 JST, 3^{rd} forecast: 2011/09/03 03:00 ~ 09/04 09:00 JST, 4^{th} forecast: 2011/09/04 03:00 ~ 09/05 09:00 JST; each forecast period of 2 km resolution is overlapped with 6 hours, Figure 3.1). For the comparison between ensemble and deterministic forecasts, the deterministic output with 15 hours forecast time and same initial time at 03:00 JST simulated by meso-scale model (MSM) is considered. However, it is difficult to compare fully with ensemble forecasts because the deterministic forecast by MSM, which has same initial time at 03:00 JST, forecasts up to 15 hours. Therefore, the control run of ensemble forecast, which has same initial condition (JMA non-hydrostatic 4DVAR (JNoVA)) and boundary condition (JMA's high-resolution (TL959L60) global spectral model (GSM)) with the meso-scale model is considered to deterministic forecast for the comparison with ensemble forecast. Figure 3.2 shows accumulated rainfall by control run and MSM forecast in 15 hours period during typhoon Talas event over Kinki region, Japan. This figure suggests that control run forecast is close to MSM forecast in terms of precipitation amount and spatial location. Then ensemble outputs are verified temporally and spatially whether they can produce suitable rainfall predictions or not compared with the deterministic control run output during the Typhoon Talas event. Finally, flood forecasting driven by ensemble and control run outputs is carried out over the Futatsuno (356.1 km^2) and Nanairo (182.1 km^2) dam catchments of Shingu river basin, located in Kii Peninsula of the Kinki area, Japan.

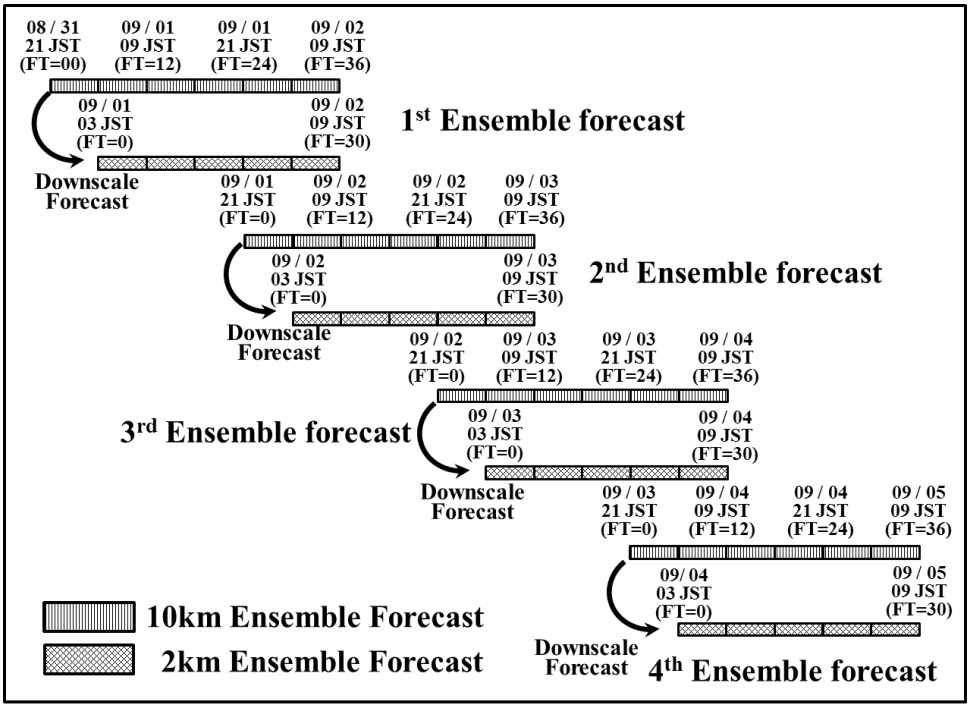

Figure 3.1 Schematic of 4 sets of forecast runs with 10 km and 2 km resolution

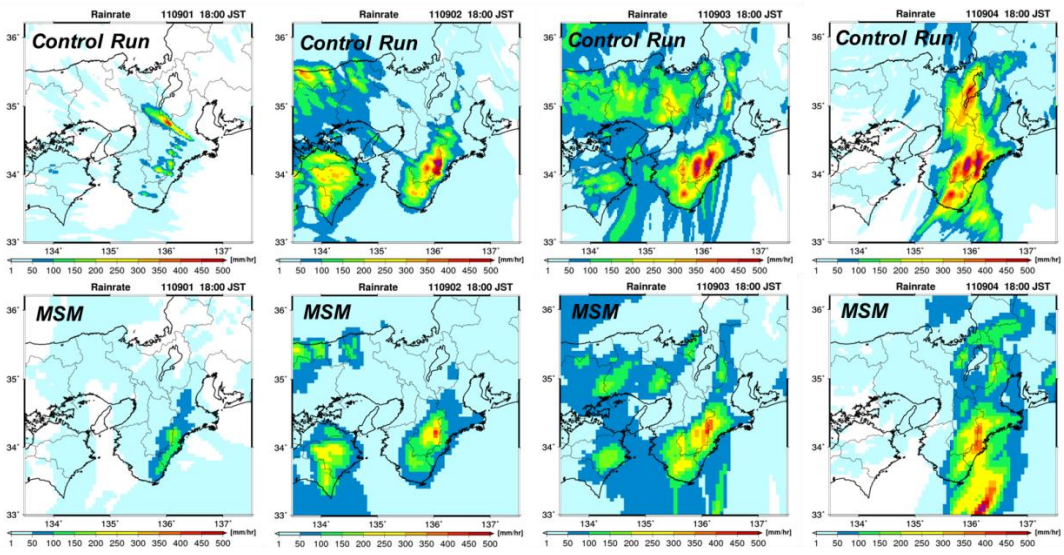

(a) 2011/09/01/03:00 ~ 18:00 (15 hours)

(b) 2011/09/02/03:00 ~ 18:00 (15 hours)

(c) 2011/09/03/03:00 ~ 18:00 (15 hours)

(d) 2011/09/04/03:00 ~ 18:00 (15 hours)

Figure 3.2 Accumulated rainfall by control run and MSM forecasts

3.2 Verification of Ensemble NWP rainfall

3.2.1 Temporal verification

For the purpose of temporal verification of QPF with ensemble NWP rainfall during the Talas event, the areal rainfall intensity of ensemble forecasts is compared with the Automated Meteorological Data Acquisition System (AMeDAS) over the Shingu River Basin. For comparison, the observed rainfall of AMeDAS (18 stations, 10min step) is interpolated using the Thiessen polygon spatial distribution method.

Figure 3.3 shows areal rainfall of ensemble forecast over the Shingu River Basin in the form of box plots plotted from 0 to 24 hours forecast time of ensemble forecast excluding overlapped forecast time (from 25 to 30 hours) compared with the areal rainfall of AMeDAS. In the 1st and 2nd forecast periods, the control run and ensemble forecast produced a suitable areal rainfall compared with the AMeDAS rainfall, but as shown in the 3rd forecast result, on which focused in this study, the control run forecast was well not matched and did not produce the rainfall intensity because the spatial pattern of raincells moved to the north-eastern part of Kii peninsula quickly by that the MSM failed to correctly forecast, as mentioned in the introduction section. On the other hand, the upper range of the ensemble forecast was able to produce considerable rainfall intensity, and the amounts of maximum rainfall intensity are also similar to AMeDAS rainfall. In 4th forecast period, the reason why rainfall intensities are overestimated can be explained by the fact that the last spatial rainfall pattern of the 3rd forecast moved to the north-eastern part of the Kii peninsula; however, it started the forecast again from the Kii peninsula in the 4th forecast. For this reason, rainfall intensities were very high in the 4th forecast period compared with AMeDAS.

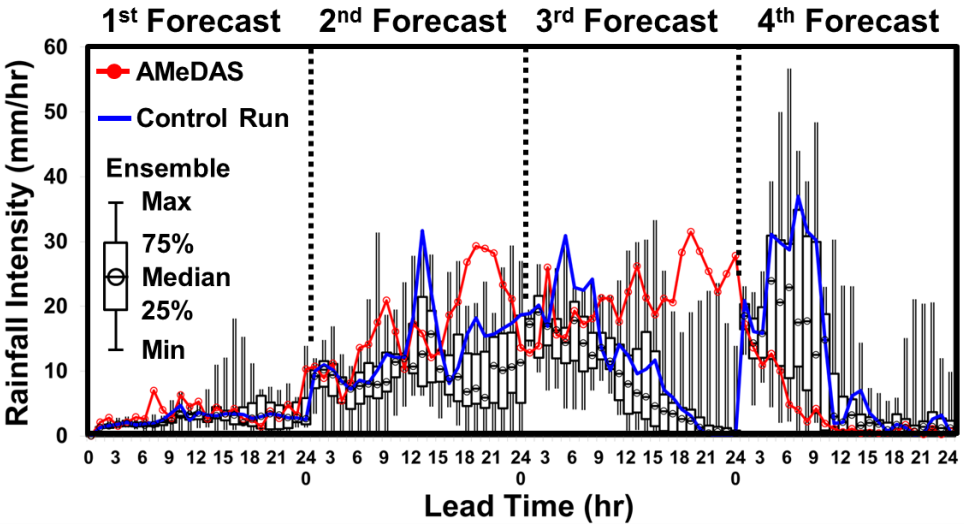

Figure 3.3 Areal rainfall of ensemble forecast in the form of box plots.

To evaluate the accuracy of the control run and ensemble forecast in terms of areal rainfall intensity, we calculated two error indexes. The first is the normalized root mean square error (RMSE), which is normalized by the mean value of the observations during the each forecast period (30 hours). The second is the log ratio bias, which a relative error and provides information about the total amount of rainfall. A log ratio bias value of zero indicates a perfect forecast; positive and negative values indicate underestimated and overestimated forecasts, respectively.

$$Nor.RMSE = \frac{\sqrt{\frac{1}{N}\sum_{t=1}^{N}\left(O_t - F_t\right)^2}}{\overline{O}} \tag{3.1}$$

$$\log\ ratio\ BIAS = \log\frac{\sum_{t=1}^{N} F_t}{\sum_{t=1}^{N} O_t} \tag{3.2}$$

where N is forecast time (30 hours) in each period, O_t and F_t are the observed and forecasted rainfall at time t.

In the index of normalized RMSE, the control run and ensemble mean have similar values from 1st to 3rd forecast period, but the best index of the ensemble spread could provide good value as compared with the deterministic control run. In the 4th forecast period, as mentioned above, the index of the control run and ensemble spread is relatively large, but the best index of the ensemble is estimated at 0.89 (the control run is 3.85). In the index of the log ratio bias, the best index of ensemble spread could cover zero value (perfect forecast), whereas the control run forecast was underestimated for the 1st, 2nd, and 3rd forecasts, and overestimated for the 4th forecast period.

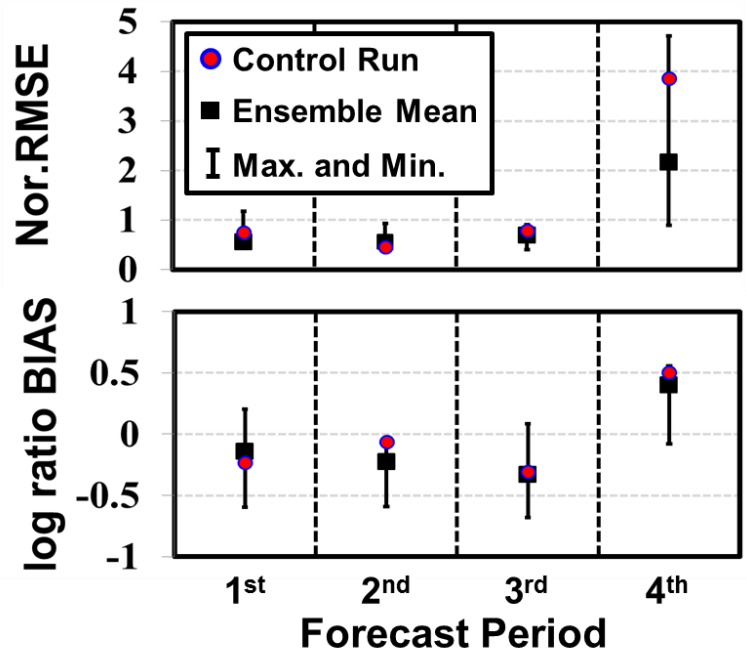

Figure 3.4 Verification results of areal rainfall with normalized RMSE and log ratio BIAS.

3.2.2 Spatial verification

The ensemble NWP rainfall forecast in this chapter have been verified spatially against the MLIT C-band composite radar data with 5 min interval and 1 km resolution, because their high spatial-temporal resolution is suitable to capture the spatial variability of rainfall. The ensemble forecast was expressed as probabilities of exceeding selected rainfall thresholds (1.0 and 5.0 mm/h). A contingency table can be constructed with a spatial comparison, in which each area with more than selected rainfall threshold is defined as "yes," and other areas are defined as "no" for both forecasted and observed rainfall fields. In this chapter, two indexes are considered for spatial verification of ensemble forecast in the Kinki region (Figure 3.5). First index is critical success index (CSI), which is also called the “threat score” and its range is 0 to 1, with a value of 1 indicating a perfect forecast. It takes into account both false alarms and missed events. And second one is BIAS, which has range with 0 to ∞. CSI and BIAS are given by:

$$CSI = \frac{hits}{hits + misses + false\ alarms} \tag{3.3}$$

$$BIAS = \frac{hits + false\ alarms}{hits + misses} \tag{3.4}$$

where hits are the number of correct forecasts over the threshold (i.e. rainfall is forecast and also observed), and misses are the number of times rainfall is not forecast, but is observed. False alarms are the number of times rainfall is forecast but is not observed.

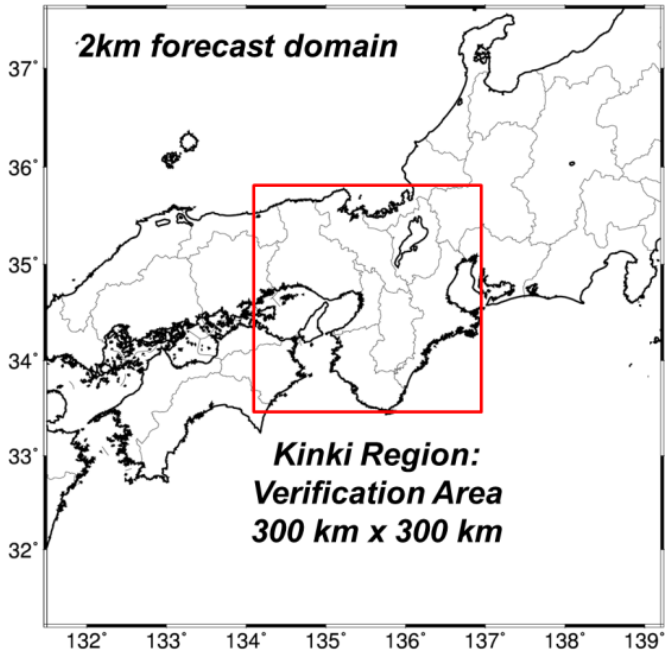

Figure 3.5 Spatial verification area

Figure 3.6 shows the results of CSI and BIAS in a comparison of radar data and ensemble forecasts with selected rainfall thresholds (1.0 and 5.0 mm/h) during the 1st, 2nd, 3rd and 4th forecast period. In the 1st forecast period of CSI with 1.0 mm/h threshold value, ensemble spread could provide better results than deterministic control run after 17 hours forecast time, whereas the CSI of control run is close to the ensemble mean value. In the 2nd forecast period, although the CSI of control run are better than ensemble mean, the best index of the ensemble spread outperformed than the control run. In the 3rd forecast period, as stated above, the spatial pattern of raincells moved to the north-eastern part of Kii peninsula quickly, so the CSI of control run decreased as lead time increased, whereas the best value of ensemble spread could provide the better result than the control run. In the 4th forecast period, the control run was close to the ensemble mean, and ensemble spread could cover the control run.

In the 3rd forecast period with 1.0 and 5.0 mm/h threshold value, on which focused in this study, the BIAS decreased quickly as lead time increased. However, the best values of the ensemble spread could maintain higher forecast accuracy compared to the control run forecast. It showed that ensemble forecasts have an advantage in terms of spatial accuracy, although lower value of ensemble forecasts exists in each forecast period as lead time increases.

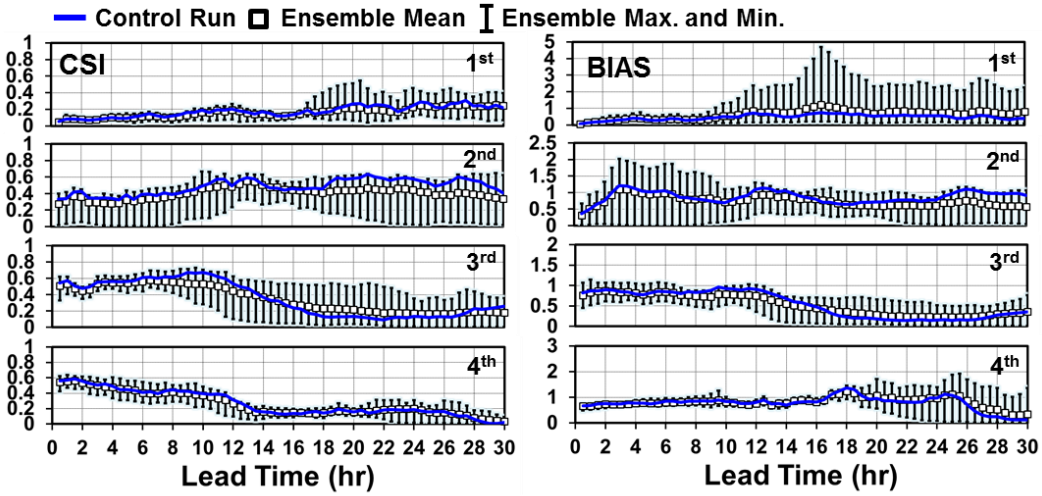

(a) CSI and BIAS with 1 mm/h threshold value

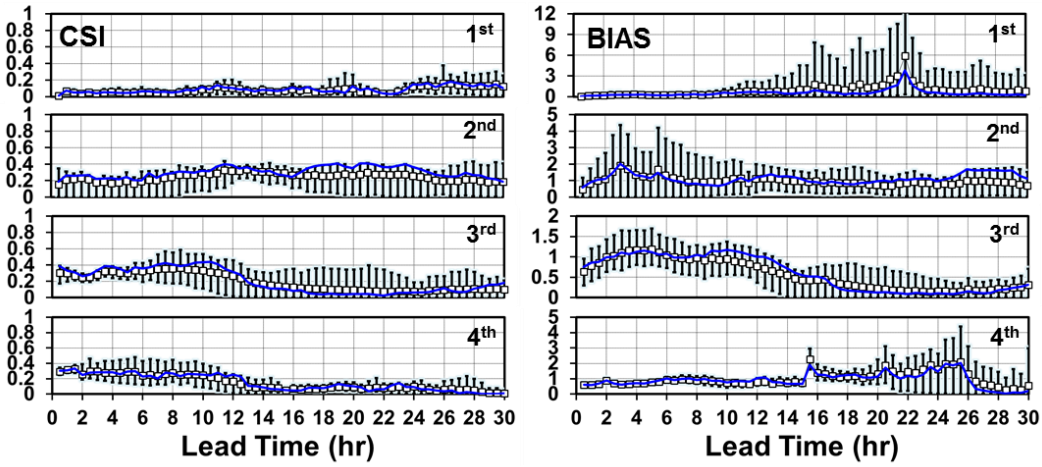

(b) CSI and BIAS with 5 mm/h threshold value

Figure 3.6 CSI and BIAS with threshold values in verification area.

3.3 Ensemble Flood Forecasting

As state above, we considered two dams located in the Shingu River Basin: Futatsuno (356.1 km^2) and Nanairo (182.1 km^2) dam catchments, for an assessment of the ensemble flood forecast driven by ensemble NWP rainfall. Simulated discharge from the observed radar rainfall used the as the initial condition for the ensemble flood forecast in each forecast period. Figures 3.7 (a) and (b) show the results of the 30 hours ensemble flood forecast from 1st to 4th forecast periods over the Futatsuno and Nanairo dam catchments for Typhoon Talas event.

As shown in Figures 3.7 (a) and (b), the 1st and 2nd forecast (rising limbs) of both the control run and ensemble forecast produced a suitable discharge, but were lower than the true value from 20 to 30hr lead times of the 2nd forecast period over the Futatsuno dam catchment, caused by the underestimation of the rainfall forecast. In the 3rd forecast period of peak discharge, the control run forecast was typically lower than the observed discharge, caused by its shift from the correct spatial position. The majority of ensemble members were also lower than the observed discharge, but a few ensemble members exceeded the control run forecast, and were close to the observed discharge in both the Futatsuno and Nanairo dam catchments. In the 4th forecast period (falling limb), both the control run and ensemble forecast were overestimated because the over-estimation in rainfall forecast (4th forecast of Figure 3.3) triggered a runoff over-estimation. From the results of ensemble flood forecast over the Futatsuno and Nanairo dam catchments, flood forecasts driven by ensemble outputs produced more suitable results compared with deterministic control run, but showed that in general it has a large proportion of under and over predictions at low lead times and exhibit a negative bias at longer lead times.

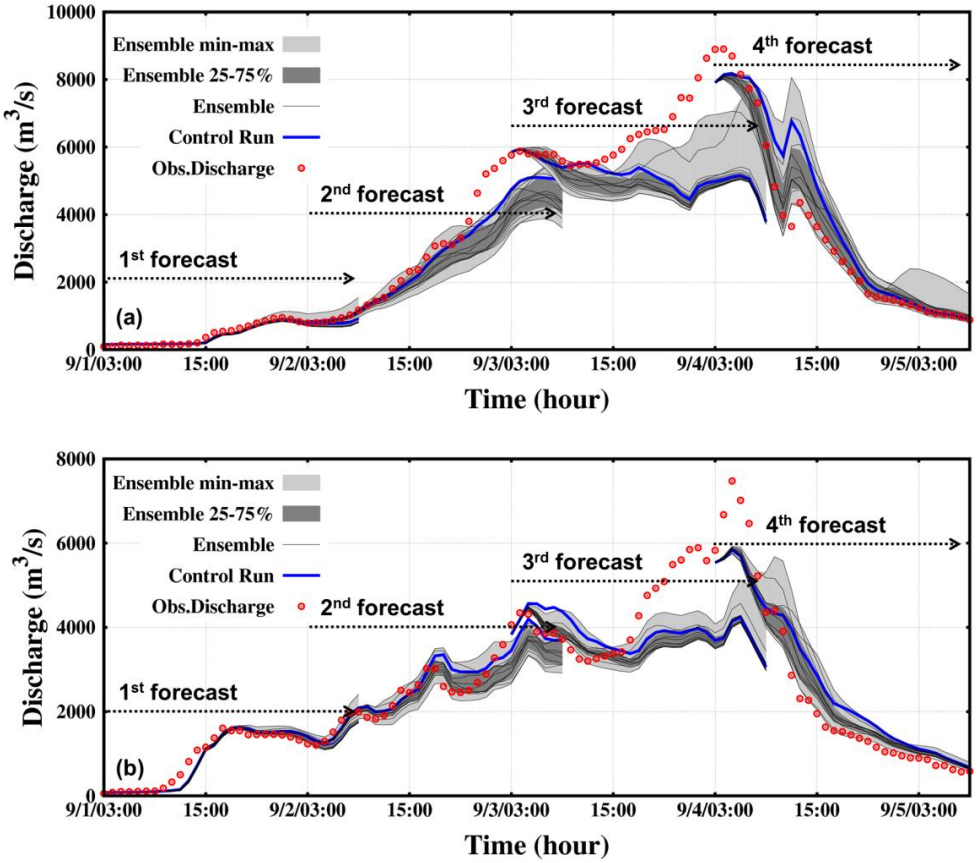

Figure 3.7 30 hours ensemble flood forecast results over (a) Futatsuno dam catchment and (b) Nanairo dam catchment

The scatter plots of Futatsuno and Nanairo dam catchments show that the ensemble forecasts had better results than the control run forecast in terms of the coefficient of determination (also called the "R-squared") which is used to describe how well a regression line fits a set of observed data (Figure 3.8). In these results, the ensemble flood forecasts provided additional information (e.g. the indication of the possibility of an extreme event) that were not present in the deterministic forecast. And in the index of normalized RMSE and log ratio BIAS, the best index of the ensemble spread could provide good value as compared with the deterministic control run in each forecast period (Figure 3.9), and this additional information of ensemble forecast could be used for real-time flood forecast, dam inflow forecast, and dam release support considering forecast uncertainty.

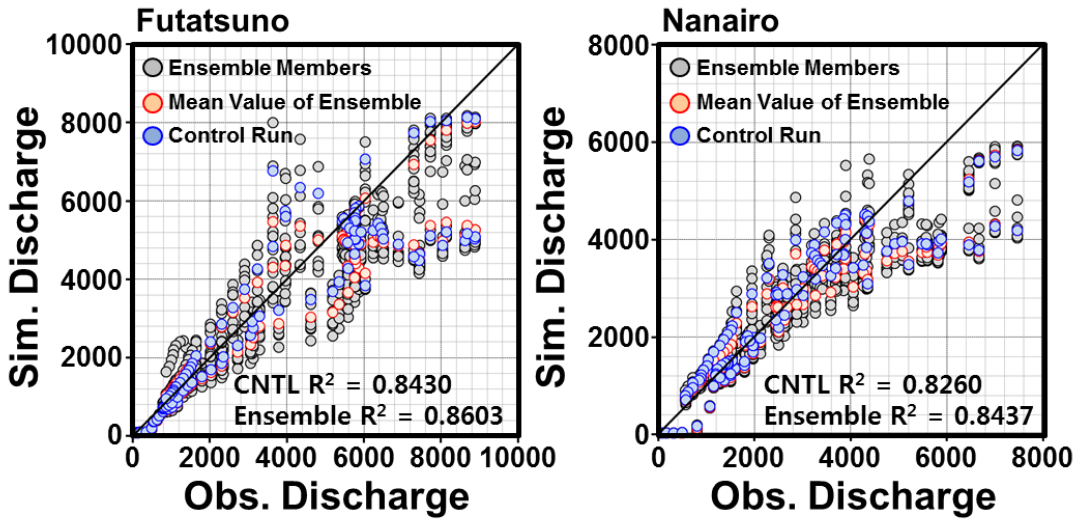

Figure 3.8 Scatter plot of 30hr ensemble flood forecast over Futatsuno and Nanairo dam catchments

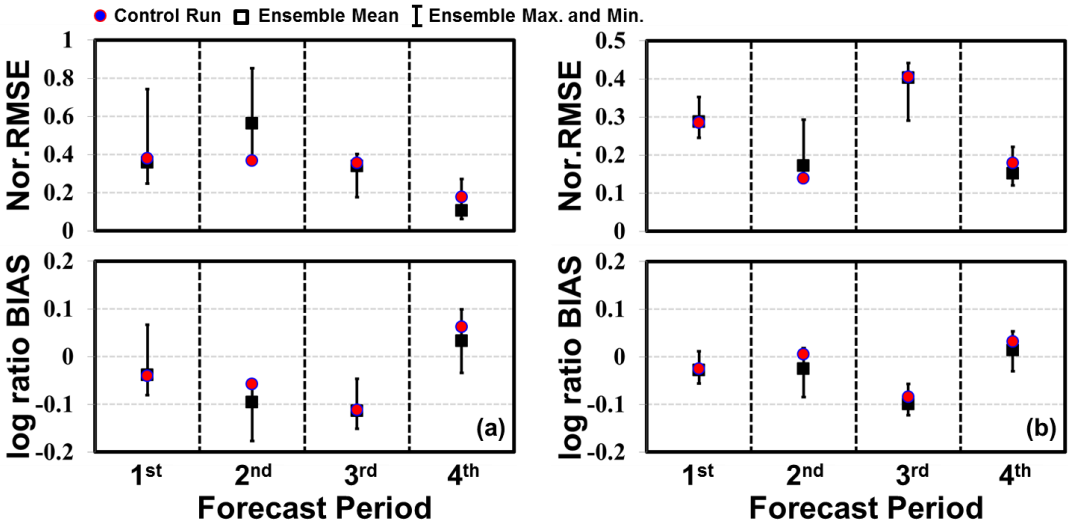

Figure 3.9 Verification results of flood forecast with normalized RMSE and log ratio BIAS over (a) Futatsuno and (b) Nanairo dam catchments.

3.4 Summary and Discussion

This chapter investigated the applicability of ensemble forecasts of numerical weather prediction (NWP) model for flood forecasting. At first, ensemble outputs are verified temporally and spatially with observed radar rainfall during the typhoon Talas event. Then flood forecasting driven by ensemble outputs was carried out over the Futatsuno (356.1 km^2) and Nanairo (182.1 km^2) dam catchments. Major findings from this chapter lead to the following conclusions.

Although ensemble forecast could catch the rainfall pattern and produced more suitable results compared with deterministic control run in terms of quantitative precipitation forecast (QPF), the uncertainty of ensemble NWP rainfall was also significant at longer lead times. Flood forecasts driven by ensemble outputs showed that in general it has a large proportion of under and over predictions at short lead times and exhibited a negative bias at longer lead times. Despite the deficient performance for longer lead times, it was shown that the ensemble flood forecast provides additional information to the deterministic forecast.

From these results, although ensemble forecast is an attractive product for flood forecasting systems with an extended lead time and better quantify predictability than deterministic one, ensemble forecast also needs to be improved to provide reliable hydrologic prediction. It means that some kind of pre-processing (e.g. QPF location error correction, bias correction, blended and/or hybrid products) is required. Therefore, in order to use ensemble forecasts of NWP model for flood forecasting effectively, it is important to establish methodologies to improve the ensemble flood forecasting.

Chapter 4

Assessment of Uncertainty Propagation of Ensemble NWP Rainfall to Flood Forecast with Catchment Scale

Abstract *This chapter presents the uncertainty propagation of rainfall forecast into hydrological response with catchment scale through distributed rainfall-runoff modeling based on the forecasted results of Chapter 3. The research questions that this chapter address is: How does rainfall forecast error translate to the flood forecast error, and how does flood forecast uncertainty propagate as a function of catchment scale dependency. It assumed that contributions to the uncertainty of predicted discharge come from the uncertainty of rainfall forecast, which is the difference between predicted and observed rainfall, so pay no attention to hydrological model uncertainties, which are classified into model parameter and structure errors.*

At first, forecast rainfall error based on the BIAS is compared with flood forecast error to assess the error propagation. Second, the variability of flood forecast uncertainty according to catchment scale is discussed using ensemble spread. Then we also assess the flood forecast uncertainty, which has the assumption that forecasted ensemble rainfall has not errors compared with observed radar rainfall, with catchment scale using an estimation regression equation between ensemble rainfall BIAS and discharge BIAS. Finally, the flood forecast uncertainty with RMSE using specific discharge in catchment scale is discussed.

4.1 Introduction

Advanced ensemble flood forecast systems include the combined use of meteorological NWP and hydrological models. The coupled use of NWP rainfall output and hydrologic flood forecasting requires an assessment of uncertainty through hydrological response. One of the biggest sources of uncertainty in flood forecasting comes from forecast rainfall. Due to the uncertainty of rainfall forecasts, flood forecasts are also uncertain. And the grid size in NWP models is often larger than the sub-catchment size in hydrological models, which results in the forecast rainfall data not being at the appropriate resolution required for flood forecasting. In addition, even small errors in the location of weather systems by NWP models may result in forecast rainfall for the catchment concerned being significantly wrong (Leahy et al., 2007; Ebert, 2001).

The biases and uncertainties of rainfall forecast may be amplified when cascaded through the hydrological system, and small uncertainties in rainfall forecast may translate into larger errors in flood forecasting. As an example, Komma et al. (2007) showed that an uncertainty range of 70% in terms of NWP rainfall translated into an uncertainty range of 200% in terms of runoff for a lead time of 48 hours. They presented this to the nonlinearity of the catchment responses, but uncertainties such as forecast rainfall, parameter, and structure of a hydrologic model may contribute to the amplification of the uncertainty in terms of flood forecasting. In the context of flood forecasts, it is therefore important to assess the forecast rainfall uncertainty in terms of the effect on runoff. And uncertainties based on spatial scale are also important by means of the information for real-time flood forecast and the possible amount of flow to the reservoir and exceeding its capacity to optimize the water volume to be released. Therefore, uncertainty related to spatial scale must be assessed.

In general, errors are usually classified into input errors (e.g., forecast rainfall and measurement rainfall), model errors (e.g., model parameter and structure), and output errors (Figure 4.1). It is difficult to understand the full range and interaction of uncertainties in flood forecasting. Uncertainty related to model parameters tends to decrease with time as more recorded runoff data is available to adjust the model parameters (Leahy et al., 2007). This study is carried out under the assumption that model parameter and structure errors do not contribute to uncertainty of flood forecasting to remove the focus from forecast rainfall error. As a result, a distributed hydrologic model is considered to be the appropriate tool to assess rainfall forecast quality and to understand how uncertainty in the rainfall forecasts field may propagate throughout the watershed. Further, the integration of the rainfall forecast into runoff simulation at multiple locations in a catchment allows the investigation of the effects of catchment scale on the propagation of rainfall forecast errors in a flood forecast.

The main objective of this chapter is to assess the error and uncertainty propagation due to NWP rainfall uncertainty on hydrological response through a distributed hydrologic model depending on catchment scale. The research question is as follows: How does ensemble NWP rainfall error translate into flood forecast, and how does flood forecast uncertainty propagate as a function of catchment scale dependency? To our knowledge, there exists research about rainfall uncertainty's direct propagation into the hydrological domain, but the spatial scale dependency of uncertainty propagation of ensemble NWP rainfall into hydrological predictions has not been fully addressed. First, we compared forecast rainfall error based on the BIAS, which is used to measure error amplification, to flood forecast error driven by ensemble NWP forecast outputs to assess error propagation. Second, we discussed the variability of flood forecast uncertainty according to catchment scale using ensemble spread, which is driven by ensemble NWP rainfall through a distributed hydrologic model. We also assessed flood forecast uncertainty, which is under the

condition that ensemble NWP rainfall has not BIAS compared with observed radar rainfall and catchment scale using an estimation regression equation between ensemble NWP rainfall and discharge based on the BIAS. Finally, we assessed flood forecast uncertainty with RMSE using specific discharge in catchment scale. Note that we focused not only on the quantitative error propagation of rainfall forecast into flood forecast but also the variability of flood forecast uncertainty with catchment scale.

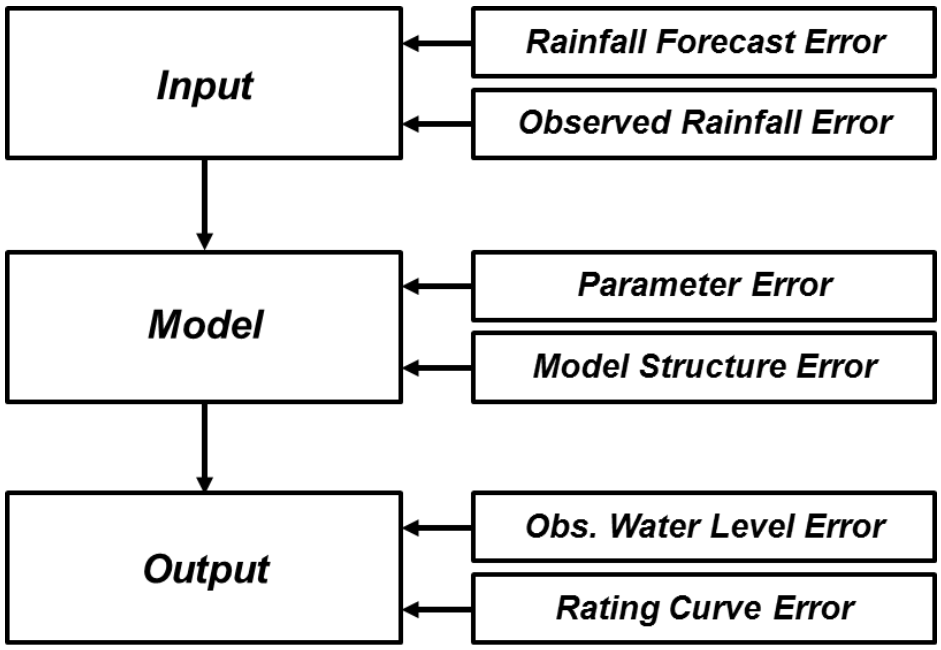

Figure 4.1 Error framework for rainfall-runoff modeling used in flood forecasting.

4.2 Data and Methodology

Ensemble rainfall forecast outputs of the NWP model introduced in chapter 3 are used as forcing data to hydrologic model to assess rainfall forecast uncertainty and to understand how uncertainty in the rainfall forecast may propagate throughout the watershed. Therefore, 4 sets of ensemble outputs with 30 hours of forecast time and 2 km resolution during the typhoon Talas event are used (1st forecast, 2011/09/01 03:00 ~ 09/02 09:00; 2nd forecast, 2011/09/02 03:00 ~ 09/03 09:00; 3rd forecast, 2011/09/03 03:00 ~ 09/04 09:00; 4th forecast, 2011/09/04 03:00 ~ 09/05 09:00) (Chapter 3, Figure 3.1).

The Shingu river basin was selected as the target area; the left and right sides exhibit different characteristics. The left side is the Totsukawa basin, and the right side is the Kitayamakawa basin. Their characteristics are completely different. The elevation of Totsukawa is higher than that of Kitayamakawa. And Kitayamakawa has a lower level in the channel. We first divided the Shingu river basin into 33 sub-catchments from 54.24 ~ 2245 km^2 (Figure 4.2, Table 4.1), including 6 gauged (5 dams and 1 gauge station) and 27 ungauged locations, for the assessment of uncertainty of ensemble NWP rainfall into flood forecast with catchment scale. We also specified 33 sub-catchments into 3 types, small catchment (< 200 km^2), medium catchment (200 ~ 1000 km^2), and large catchment (> 1000 km^2) to evaluate the variability with catchment scale. We also divided catchment characteristics into 2 types, mountainous area (> 800 m) and flat area (< 800 m) considering average elevation (800 m) of the 33 sub-catchments.

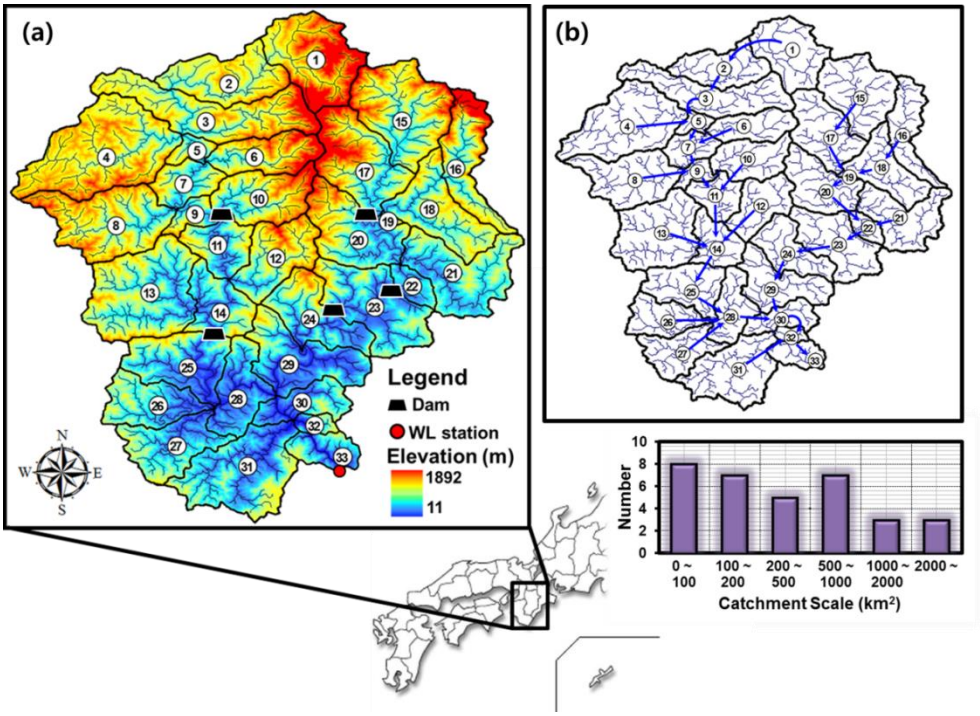

Figure 4.2 33 sub-catchments and connections with flow directions.

Table 4.1 Sub-catchment area at gauged and ungauged points.

Catchment	Area (km^2)	Catchment	Area (km^2)
1	92.2	18	141.56
2	165.99	19	347.35
3	279.78	20	429.07
4	150.56	21	94.23
5	444.04	22 (Nanairo dam)	529.49
6	54.24	23 (Komori dam)	633.22
7	533.73	24	700.49
8	105.72	25	1090.92
9 (Kazeya dam)	656.08	26	56.68
10	65.97	27	65.20
11	766.19	28	1268.03
12	65.04	29	783.85
13	130.74	30	2091.38
14 (Futatsuno dam)	1012.15	31	110.92
15	112.13	32	2212.24
16	72.65	33 (Ouga station)	2245.56
17 (Ikehara dam)	203.27		

There was no observed discharge data in sub-catchments, except in 5 dams and 1 gauge station. For that reason, the parameter optimization of the hydrologic model was conducted using the MLIT C-band composite radar data, which has high spatial-temporal resolution to capture the spatial variability of rainfall. The Shuffled Complex Evolution (SCE) global optimization method (Duan et al., 1994) was used for the parameter optimization of the hydrologic model using MLIT composite radar rainfall to acquire the reference data of each sub-catchment. In this study, the SCE optimization method was modified to minimize the objective function between observed inflows and simulated results for all 5 dams and 1 gauge station at the same time (Equation 4.1). Figure 4.3 shows the results of multi-calibration using the SCE optimization method and minimizing the objective function of 6 observation points.

$$Minimize\ \ OF = \sum_{basin=1}^{n} RMSE_{Basin} \tag{4.1}$$

Observed radar data and its simulated discharge were used as reference data to compare the ensemble NWP rainfall forecast and flood forecast for the assessment of error propagation. Although the simulated discharge from observed radar rainfall does not specifically represent the true discharge, the simulated discharge from the observed radar data is nevertheless set as reference data for comparison with the discharge from ensemble prediction data.

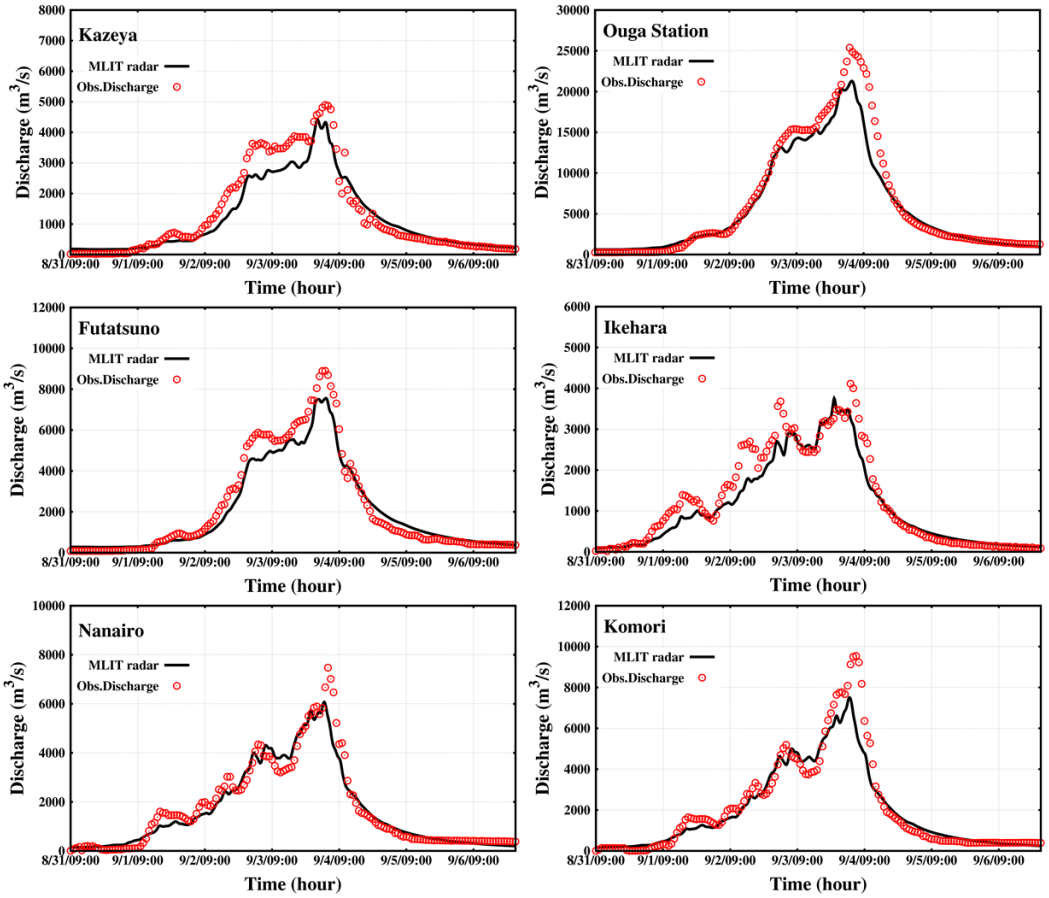

Figure 4.3 Multi-calibration using SCE optimization method and minimizing the objective function of 6 observation points.

4.3 Results and Discussion

4.3.1 Uncertainty Propagation of NWP Rainfall Forecast to Flood Forecast

As stated above, rainfall forecast error of ensemble outputs from the NWP model is compared with the flood forecast error driven by those rainfall forecasts to assess the error propagation. It is important, however, to quantify error propagation from rainfall forecast to flood forecast using statistical measures that appropriately capture forecast deviations. For this reason, the BIAS was used to compare the mean conditions in the forecast and observation in terms of rainfall and flood forecast and to measure error amplification. Note that the BIAS of the basin-mean rainfall is directly compared with the discharge BIAS, and the BIAS is used for an average value of 30 hours of forecast time of rainfall and flood forecast results. Furthermore, the results are classified according to the forecast period of ensemble rainfall from the NWP model.

$$\mathrm{BIAS}_i = \frac{\sum_{t=1}^{N} F_{i,t}}{\sum_{t=1}^{N} O_t} \tag{4.2}$$

where N is the forecast time of each forecast period (30 hours); O_t and F_t are the observed and forecasted rainfall and discharge at time t, respectively; and i is each ensemble forecast (11 ensemble members).

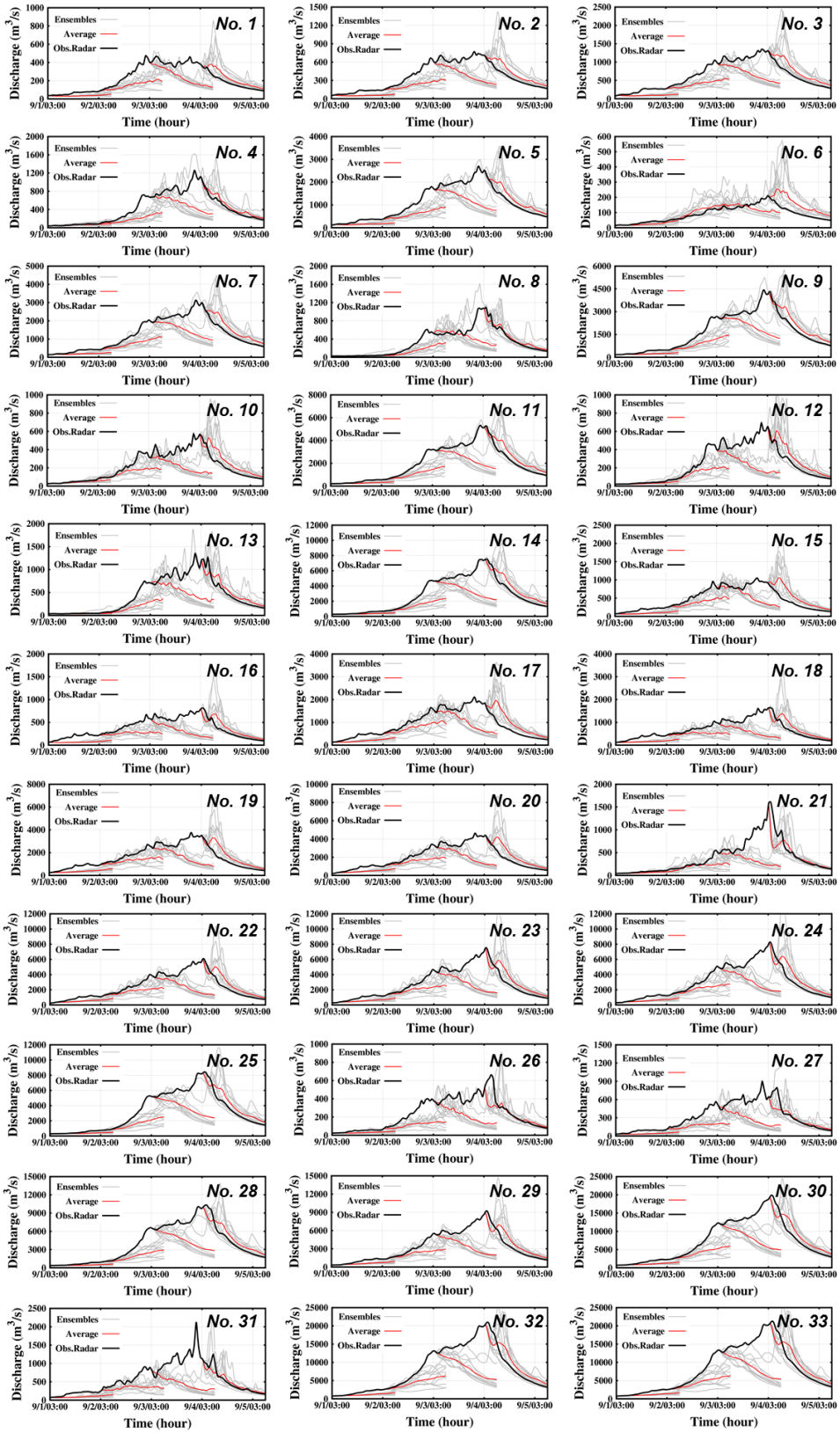

Figure 4.4 Flood forecast results over 33 sub-catchments.

Figure 4.5 presents a comparison of rainfall and flood forecast errors from the first to the fourth forecast periods with linear regression equations based on a statistical measure, the BIAS, for 33 sub-catchments of the Shingu river basin represented in Figure 4.4. In the first and fourth forecast periods of Figure 4.5, rainfall forecast errors lead to proportional flood forecast errors with linear regression equations. The discharge BIAS is varies based on the same rainfall BIAS, so the discharge BIAS is different based on catchment scale. For small catchments, rainfall errors from forecast location error occur sensitively due to rainfall pixels of NWP model, which does not cover the small catchment exactly. For larger catchments, many rainfall pixels contribute to the rainfall forecast error propagation in the flood forecast. Therefore, the variability of flood forecast uncertainty according to catchment scale should be investigated.

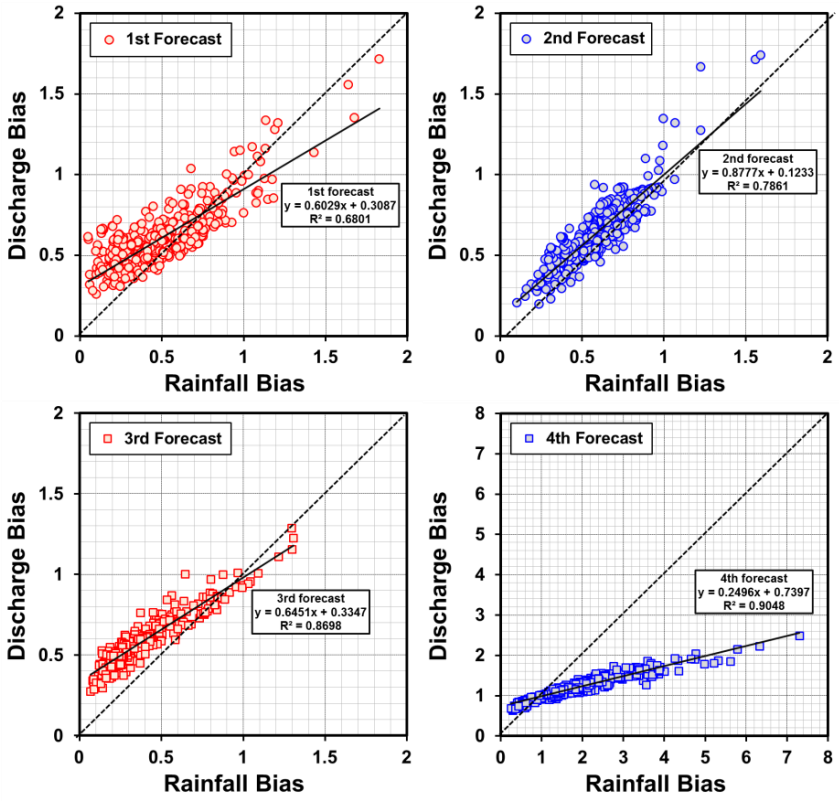

Figure 4.5 Propagation of rainfall forecast errors to flood forecast errors

4.3.2 Flood Forecast Uncertainty with Catchment Scale

As mentioned above, the Shingu river basin is divided into 33 sub-catchments from 54.24 to 2245 km^2, including 6 gauged and 27 ungauged locations, for the assessment of uncertainty of ensemble NWP rainfall into flood forecast with catchment scale. The Shingu river basin has 3 types (small, medium, and large catchments) and 2 characteristics (mountainous and flat area) for evaluation of the variability with catchment scale.

First, for the evaluation of the variability of flood forecast uncertainty according to catchment scale, the mean value of the coefficient of variation (CV), which is a normalized measure of dispersion of a probability distribution or frequency distribution, was used (Equation 4.3). It is defined as the ratio of the standard deviation to the mean. The absolute value of the CV is sometimes known as relative standard deviation (RSD), which is expressed as a percentage. The coefficient of variation determines the risk.

$$\text{Ave. CV}_i = \frac{\sum_{t=1}^{N} \frac{\sigma_{i,t}}{\mu_{i,t}}}{N} \tag{4.3}$$

where N is the forecast time of each forecast period (30 hours), and $\sigma_{i,t}$ and $\mu_{i,t}$ are the standard deviation to the mean value of the flood forecast at each ensemble i and time t, respectively.

Figure 4.6 shows the flood forecast variability expressed by coefficient of variation using ensemble spread of the flood forecasting with catchment scale and characteristic. Each CV value refers to the average value from the first to the fourth forecast period. It is evident from Figure 4.6 that the coefficient of variation in medium and large catchments is close to 0.25, and this is maintained as the catchment increases. For small catchments, however, there is a larger variability than for medium and large catchments, and small catchments have a high coefficient of variation (> 0.3). This result suggests that uncertainty variability occurs sensitively and diversely at the same time in different catchments, and small catchments have more sensitive variability in uncertainty. Therefore, flood forecasting in small catchment requires care due to the large variability of uncertainty. On the other hand, in medium and large catchments, there is less uncertainty than with small catchments, and the coefficient of variation converges into a uniform value.

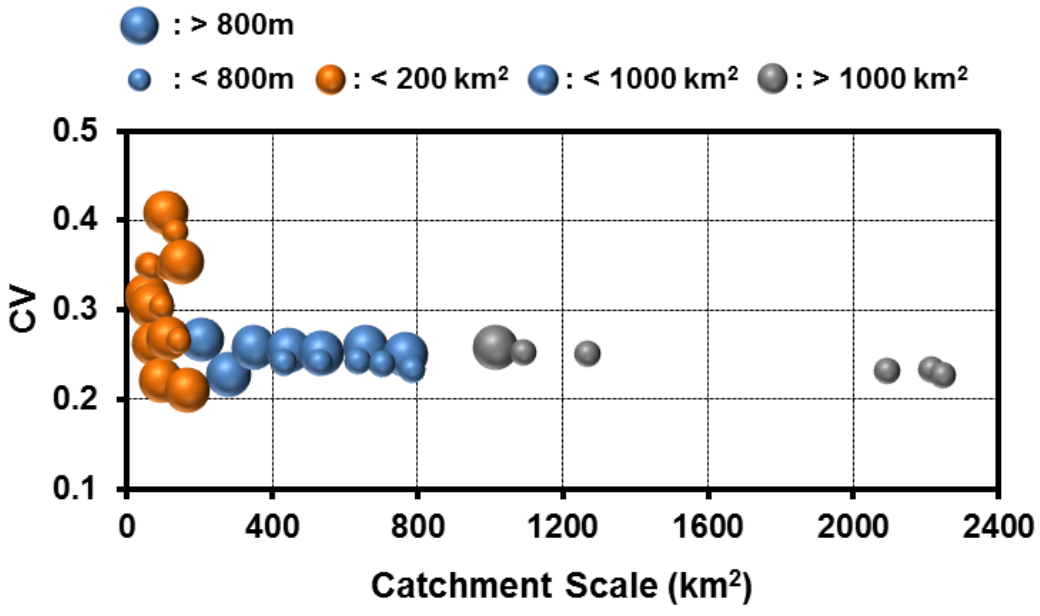

Figure 4.6 Flood forecast variability expressed by coefficient of variation with catchment scale and characteristic.

Flood forecast uncertainty (it is assumed that rainfall forecast has no errors compared to the observed radar rainfall) focuses on the discharge uncertainty with catchment scale and was assessed when rainfall BIAS was 1, using an estimated linear regression equation between each ensemble rainfall BIAS and discharge BIAS of 33 sub-catchments. Figure 4.7 compares the rainfall BIAS of ensemble members and discharge BIAS driven by those rainfall forecasts in each sub-catchment and linear regression equation. From Figure 4.7, the relationship between rainfall forecast errors and flood forecast errors is proportional in ensemble members to the linear regression equation, and is different with catchment scale. And as a result of separation of the forecast BIAS by each sub-catchment, we obtain 132 linear regression equations for 33 sub-catchments and 4 forecast periods. Then we calculate the discharge BIAS when rainfall BIAS is 1 using a linear regression equation for each sub-catchment to focus on the discharge BIAS with catchment scale.

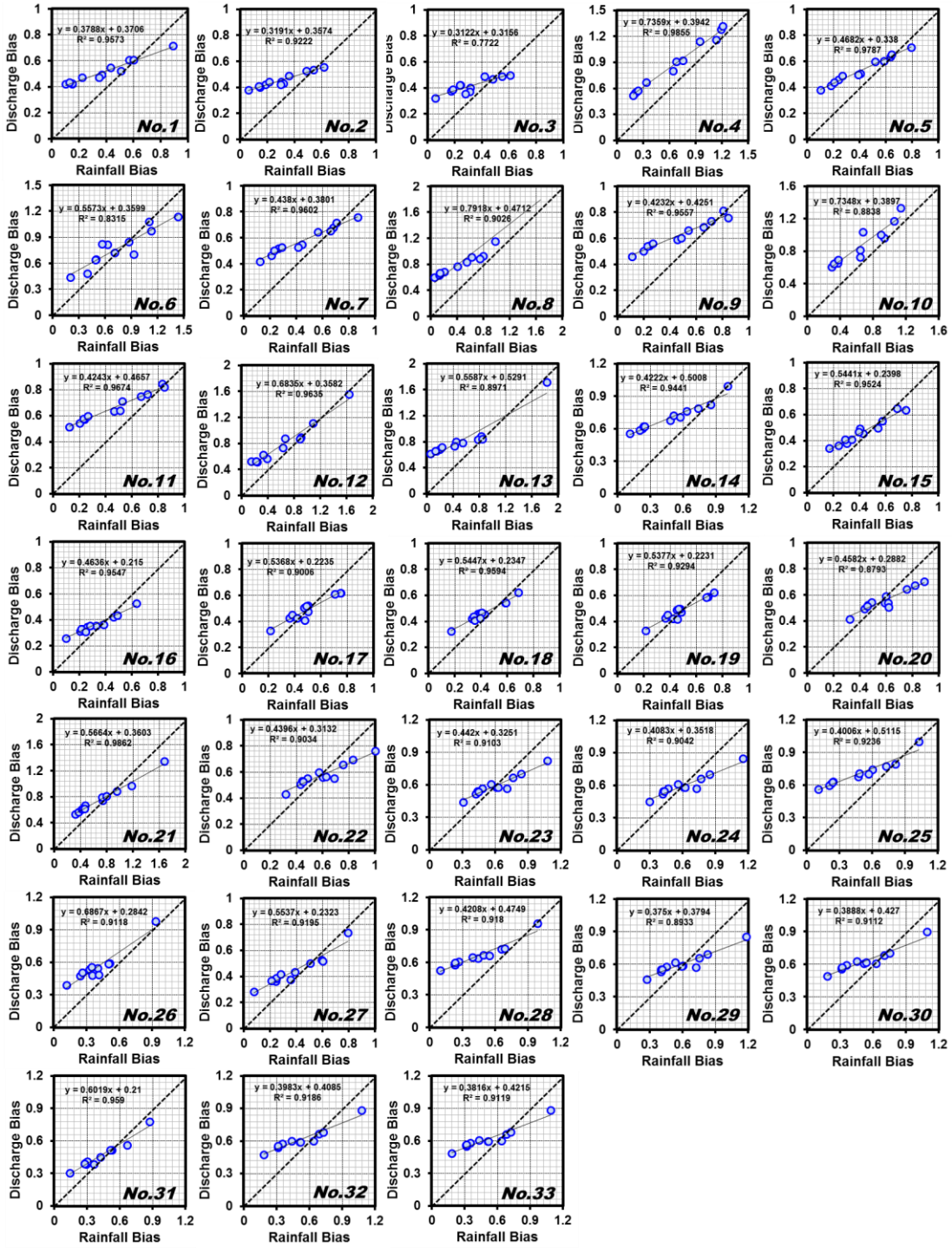

Figure 4.7 Comparison of rainfall and discharge BIAS of ensemble members in each sub-catchment and linear regression equation.

Figure 4.8 represents the discharge BIAS. It is assumed that rainfall forecast has no error compared to observed radar rainfall (rainfall BIAS is 1 using the linear regression equation) with catchment scale and characteristic. Figure 4.8 shows that there is a discharge BIAS in all of small, medium and large catchments even though rainfall forecast has no errors compared to observed radar rainfall. This is due to the spatial variability of rainfall, even though basin-mean rainfall is similar to the observed radar rainfall. As an example, Lee et al. (2008) showed that input uncertainty is due to spatial variability of rainfall on catchment responses in rainfall-runoff modeling. As stated above, however, we focused not only on the quantitative error propagation of rainfall forecast into flood forecast but also the variability of flood forecast uncertainty with catchment scale. The discharge BIAS in medium and large catchments has properties similar to those of the coefficient of variation in Figure 4.5. The small catchments indicate large variability of discharge BIAS.

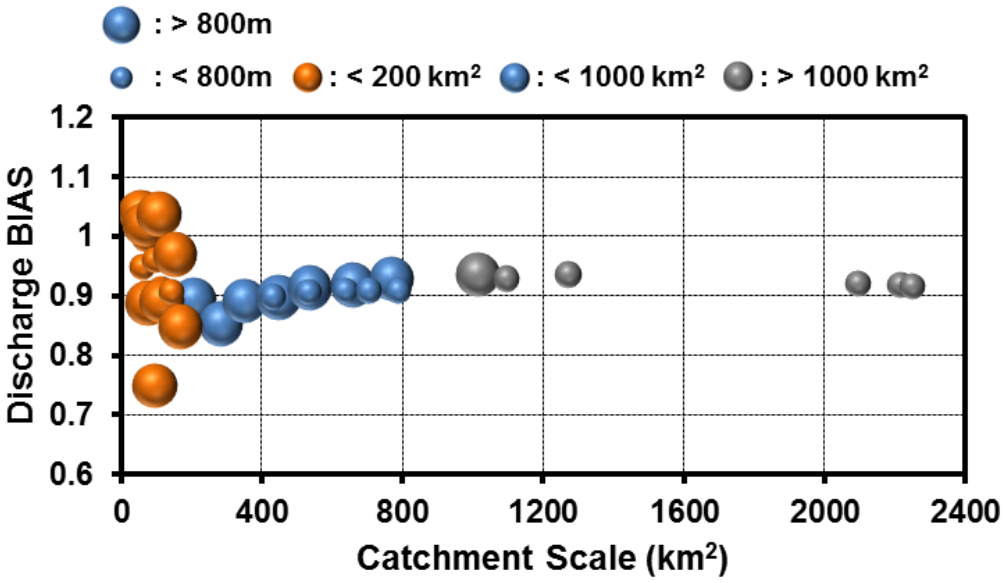

Figure 4.8 Flood forecast variability expressed by BIAS with catchment scale and characteristic.

Figure 4.9 represents the flood forecast uncertainty with root mean square error (RMSE) using specific discharge (discharge/catchment scale) of outlets with catchment scale. Figure 4.9 demonstrates properties similar to those resulting from the coefficient of variation and BIAS in Figures 4.6 and 4.8, respectively. In medium catchments, however, there are two types of characteristics in forecast uncertainty variability. In mountainous areas, discharge RMSE is less than that in flat areas, and this characteristic is also seen in Totsukawa and Kitayamaka, the left and right sides of the Shingu river basin, respectively.

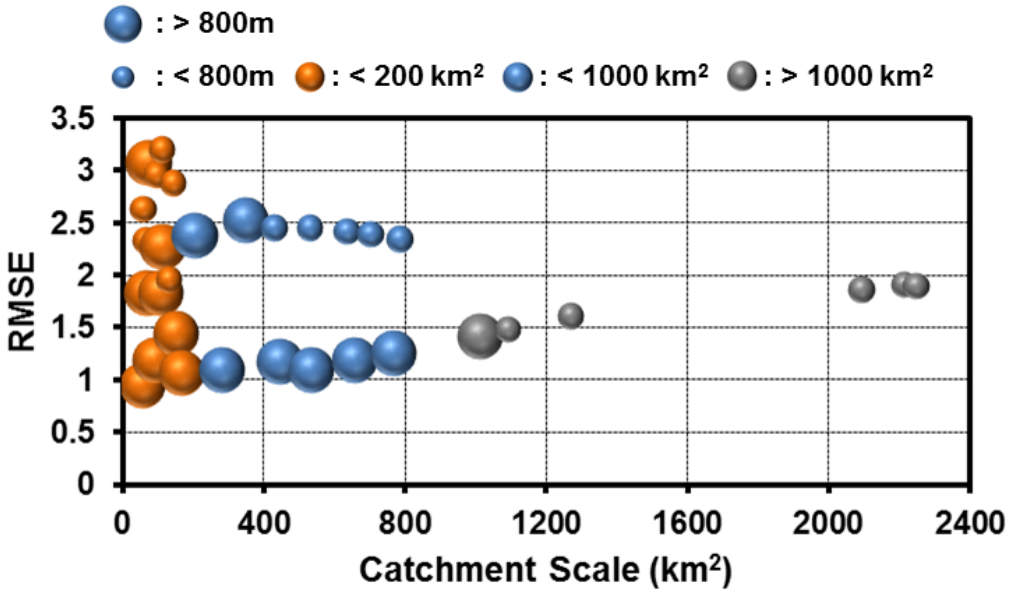

Figure 4.9 Flood forecast variability expressed by RMSE with catchment scale and characteristic.

4.4 Summary

This chapter aimed to investigate the uncertain propagation of rainfall forecast into a hydrological response with a catchment scale through distributed rainfall-runoff modeling based on the forecasted results of Chapter 3. The research questions that this chapter addresses are as follows: How does rainfall forecast error translate into flood forecast error, and how does flood forecast uncertainty propagate as a function of catchment scale dependency? Forecast rainfall error based on the BIAS was compared with flood forecast error to assess error propagation. Second, the variability of flood forecast uncertainty according to catchment scale was discussed using ensemble spread. Then we assessed the flood forecast uncertainty with catchment scale using discharge BIAS and RMSE. This chapter demonstrates that uncertainty variability occurs sensitively and diversely at the same time in different catchments, and small catchments have sensitive variability of uncertainty. Therefore, flood forecasting in small catchment should be careful due to the large variability of uncertainty. On the other hand, in medium and large catchments, there is less uncertainty than in small catchments.

Chapter 5

Accuracy Improvement of Flood Forecasting using Pre-processing of Ensemble NWP Rainfall Fields

Abstract *This chapter proposes pre-processing methodologies with consideration of appropriate ensemble members and a spatial shift of ensemble NWP rainfall fields, in order to improve the accuracy of the ensemble flood forecasting. First, the selection of appropriate members is investigated by comparison of spatial distributions between observed radar rainfall and forecasted ensemble rainfall. And selected ensemble information is applied into the next forecast period to assess the accuracy improvement of flood forecasting. Second, as an approach for the accuracy improvement of the flood forecasting, transposition method, which is spatial shift of ensemble rainfall distributions considering the correction of misplaced predicted rainfall distributions, is introduced. Finally, above two methods are integrated in order to use advantages of characteristics of each method at the same time and apply into the next forecast period to confirm the accuracy improvement of the flood forecast skill. Through the Chapter 5, the analysis shows that appropriate ensemble members of NWP rainfall improves the accuracy of the mean value when ensemble forecasting a flood, whereas the transposition of NWP rainfall fields has a more suitable impact on the accuracy of the best values.*

5.1 Introduction

Flood forecasting is an important technique to reduce damages from flood disasters. The accuracy of weather forecasts has improved over the years, due to advances in NWP techniques and increased computing power. Thus, it is now possible to generate high-resolution rainfall forecasts at the catchment scale and to integrate quantitative precipitation forecasting (QPF) into flood forecasting systems with extended lead time (Demeritt et al., 2007; Cuo et al., 2011).

At the same time, one of the rising research themes in the flood forecasting area is the development of ensemble prediction systems (EPSs). EPSs have been used to account for uncertainties and have resulted in better quantitative predictability for the same location and time. Several authors have utilized and investigated EPS, and found that ensembles increase forecast accuracy and allow for skillful predictions with lead time (Buizza et al., 1999; Bartholmes and Todini, 2005; Gouweleeuw et al., 2005; Roulin and Vannitsem, 2005; Komma et al., 2007; Palmer and Buizza, 2007; Xuan et al., 2009; Velazquez et al., 2011; Hsiao et al., 2013; Yu et al., 2013, 2014).

However, in many cases, the potential of forecasting with EPS is described alongside more cautious approaches to the considerable variability and uncertainty in operational flood forecasting. First, the time/spatial scale of the hydrological model is still much finer than that of the meteorological model. Although the NWP-based QPF can generally catch the rainfall pattern, the uncertainties of rainfall to the catchment scale were always significant. Schaake et al. (2004) analyzed the statistical properties of the prediction outcomes from the US National Centers for Environmental Prediction (NCEP) during 1997 and 1999 over the continental US. They stated that ensemble forecasts contain biases that must be removed before they are used as an input for hydrologic models. Second, NWP models have challenges with misplacement of the forecasting rainband, which means that the intensity and

shape of the forecasted storm cell may be correct, but the location of the storm cell is wrong. Errors in the location of a weather system in an NWP model depend on how it is being forced. If the weather system is moving freely across the forecast domain, the error might be expected to increase at around 6 to 8 km per hour (WMO, 2011). And Ebert and McBride (2000) stated that QPF quality needs to be improved, in order to provide reliable hydrologic prediction, and errors in location misplacement, timing, and intensity hampered the direct application of QPF from the NWP into hydrologic prediction models

Given the current issue with ensemble forecasting methods, meteorological characteristics (e.g., spatial shift and rather coarse resolution) and proper pre-processing should be considered carefully, in order to use EPS effectively in flood forecasting systems on a small catchment scale. The aim of this chapter is to address the uncertainties in ensemble hydrological forecasting driven by ensemble NWP rainfall and to explore an accuracy improvement of flood forecasting by pre-processing ensemble NWP rainfall fields. For these objectives, we considered two different methods to apply into flood forecasting. First, we investigated the appropriate ensemble members of NWP rainfall during the current period to apply into the next target period of flood forecasting. Second, we examined transposition and considered the implications of the spatial variability of NWP rainfall fields in a current period to correct the misplaced spatial position and evaluate the continuity of transposition behavior from the current period to the next target period. Finally, we integrated the above two methods, in order to consider the forecast characteristics of each method at the same time and apply them into the next forecasting period to confirm their flood forecast ability. The flood forecasting results of these two methods on ensemble NWP rainfall prediction were compared with the results of original ensemble flood forecasting, which was carried out by Yu et al. (2013) using the Typhoon Talas event of 2011.

The ensemble surface precipitation (Psrf) from 2 km-downscaled NWP data with 30 h forecast time was utilized as input data into a hydrologic model. The analysis was utilized the 2 sets of ensemble prediction outputs (1st forecast: 2011/09/02 03:00 ~ 09/03 09:00 JST, 30 hours; 2nd forecast: 2011/09/03 03:00 ~ 09/04 09:00 JST, 30 hours). In Shingu river basin, we focused on two sub-catchments, which are Futatsuno (356.1km^2) and Nanairo (182.1km^2) dam catchments, and performed separately for the rising limb and peak discharge periods because these two periods are most important phases of real-time flood forecasting.

5.2 Flood Forecasting using Selected Ensemble Members of NWP Rainfall

For the purpose of accuracy improvement in flood forecasting, the ensemble NWP rainfall in rising limb of flood period (2011/9/2 3:00 ~ 9/3 9:00; 30 hours forecast time with 30 min intervals) have been verified spatially with C-band composite radar data from the Ministry of Land, Infrastructure, Transport and Tourism (MLIT) at a resolution of 1 km and 5 min in the verification area (Figure 5.1) to investigate the appropriate ensemble members. For this reason, we calculated two error indexes: the root mean square error (RMSE) and critical success index (CSI) with forecast time. We then selected the best 3 members using the 24 hours average RMSE and CSI values of each ensemble member because ensemble NWP rainfall is newly forecasted after 24 hours.

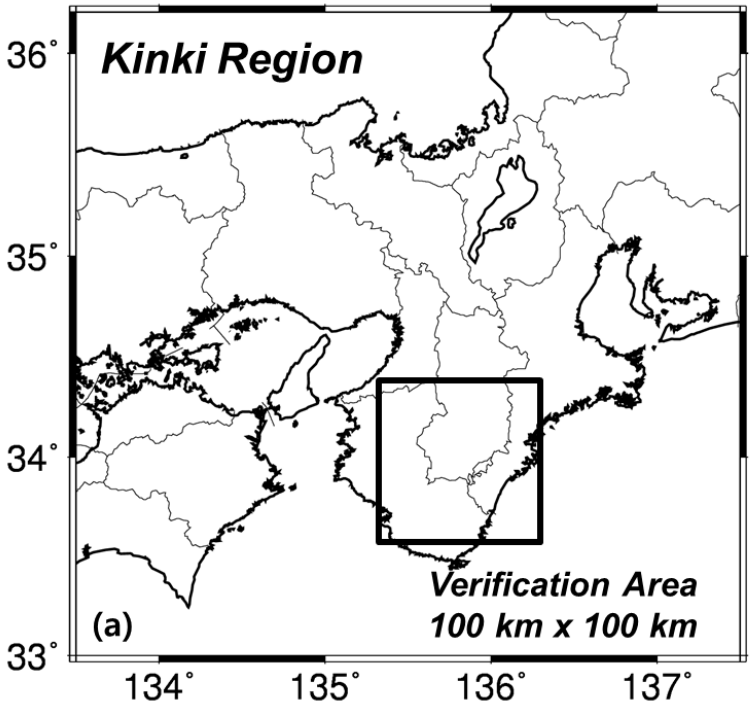

Figure 5.1 Verification area for calculation of RMSE and CSI value.

In the CSI analysis, the ensemble forecasts were expressed as probabilities of exceeding a selected rainfall threshold (10mm/h), which were used to compare an obvious spatial distribution of observed MLIT radar data with forecasted NWP rainfall. A contingency table can be constructed with a spatial comparison, in which each area with more than 10mm/h is defined as "yes," and other areas are defined as "no" for both forecasted and observed rainfall fields.

$$RMSE = \sqrt{\frac{1}{N}\sum_{t=1}^{N}\left(O_t - F_t\right)^2} \tag{5.1}$$

$$CSI = \frac{hits}{hits + misses + false\,alarms} \tag{5.2}$$

where N is the total grid cells (100 × 100), O_t and F_t are the observed and forecasted rainfall at time t, hits are the number of correct forecasts over the threshold (i.e., when the rainfall that is forecasted is also observed), and misses are the number of times rainfall is not forecasted, but is observed. False alarms are the number of times rainfall is forecasted, but not observed.

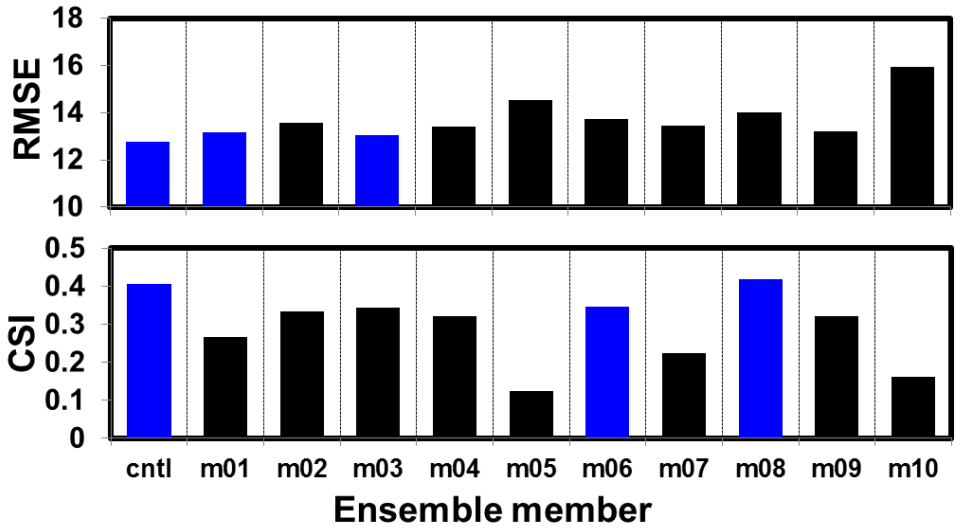

Figure 5.2 RMSE and CSI values of each ensemble NWP rainfall and the selected members (blue color) in rising limb periods

Figure 5.2 shows the results of the average RMSE and the average CSI of 24hr in a comparison of observed radar data and forecasted ensemble NWP rainfall during the rising limb period. As shown in Figure 5.2, we selected the best 3 values (blue color) for both RMSE and CSI value and applied them to the next peak discharge period of the flood forecasting (2011/09/03 3:00 ~ 09/04 9:00; 30h forecast time). Using the selected five members (cntl, m01, m03, m06 and m08) of ensemble NWP rainfall for the rising limb period, we first examined the ensemble flood forecasting in a rising limb period and applied the members into the flood forecasting for the next peak discharge period, which focused on in this study, to assess the accuracy improvement. Base on the simulated results in the rising limb and peak discharge

period, we compared the accuracy improvement with the results of the original ensemble flood forecasting for the former study (Yu et al., 2013) using the mean absolute error (MAE), which is a quantity used to measure how close each forecast was to the observation.

Figure 5.3 shows the results of the 30 hours ensemble flood forecasting using the original and five selected ensemble members during rising limb and peak discharge periods over the Futatsuno dam catchment. The comparative results are reflected in Table 5.1, which shows the flood forecast skill of the original and five selected ensemble members, in terms of ensemble mean and best value of flood forecasting. First, as shown in Table 5.1, the accuracy of the mean value of the Futatsuno catchment from five selected ensemble members was improved, compared to the original ensemble's skill, because the ensemble members, which have low efficiency criteria in the RMSE and CSI values, were excluded from the selection of appropriate ensemble members (Figure 5.2). The best member in the rising limb period (m08) also provided the best MAE value in peak discharge period, with the same MAE value as the original ensemble skill. Second, in the case of the Nanairo catchment, the accuracy of the mean value from the five selected ensemble members was also improved, compared to the original ensemble skill. The best member was m03, which provided the best MAE value in the rising limb period, but the best member was m08 in the peak discharge period. The best MAE values were the same between the original and five selected members because m03 and m08 were included in the five selected ensemble members. Thus, one of five selected ensemble members in the rising limb period was also represented in the peak discharge period as the best index. Based on these results, using the selected ensemble members can improve the accuracy of the mean value, while conserving the best value between the original and selected ensemble members in flood forecasting.

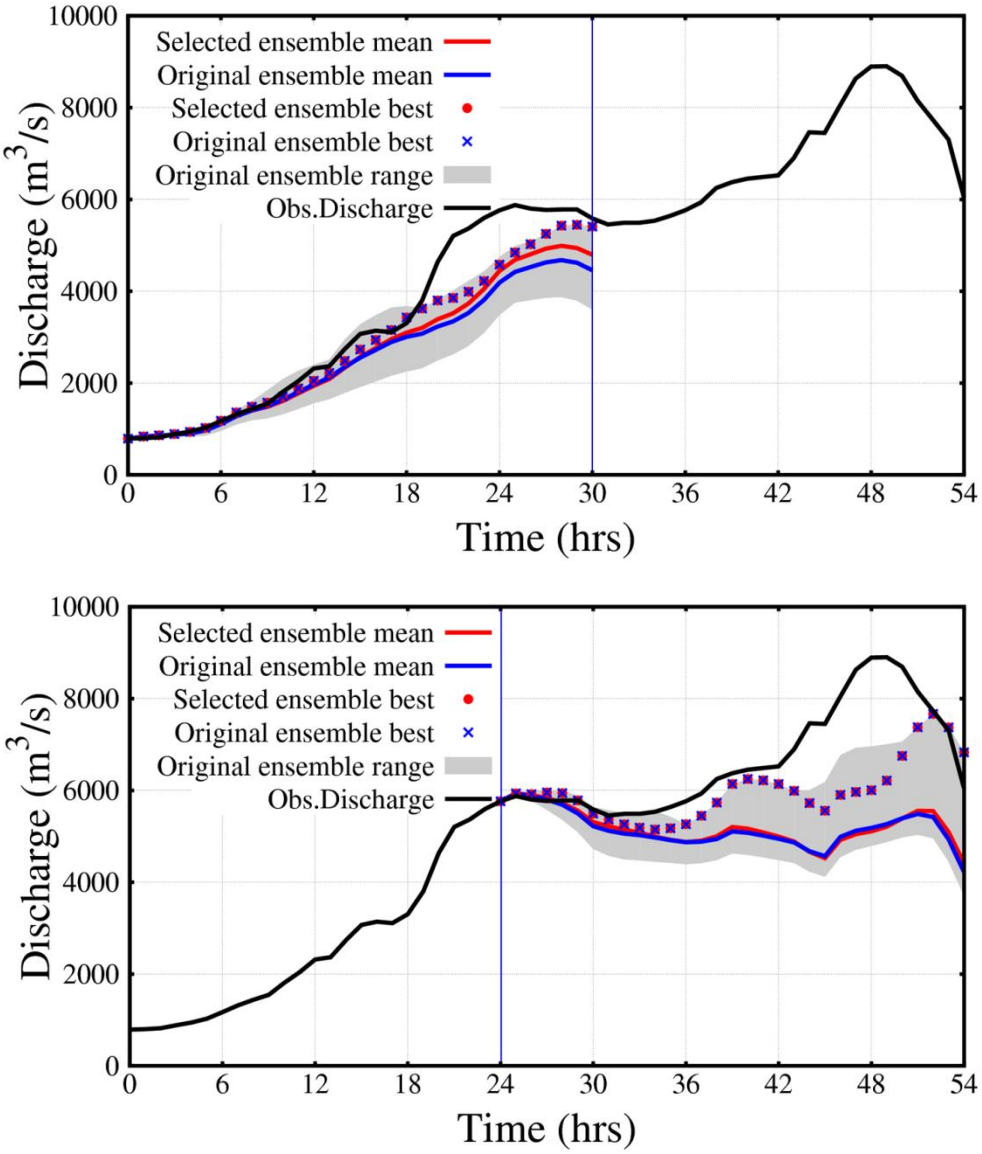

Figure 5.3 Ensemble flood forecasting using the five selected ensemble members during a rising limb period: upper and lower figures are the results of the rising limb and peak discharge period over the Futatsuno dam catchment.

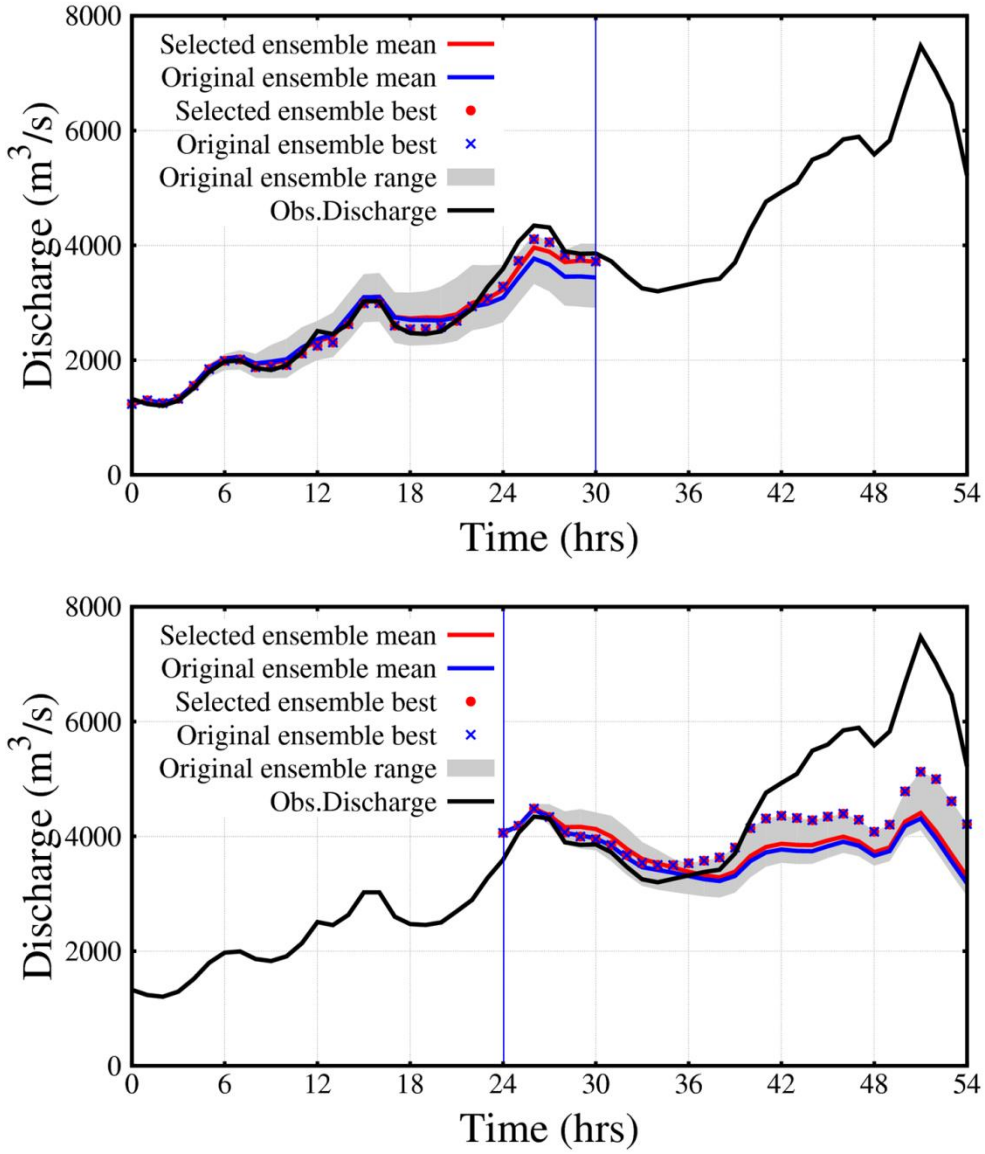

Figure 5.4 Ensemble flood forecasting using the five selected ensemble members during a rising limb period: upper and lower figures are the results of the rising limb and peak discharge period over the Nanairo dam catchment.

Table 5.1 Comparisons between the original and five selected ensemble results in flood forecast skill: A bold red color indicates a better result, and members in parentheses refer to the member with the best flood forecast skill.

Catchment	**Forecast Period**	**Type**	**MAE**	
			Mean	**Best**
Futatsuno	Rising limb	Original ensemble	655.7	378.3 (m08)
		Five Selected ensemble	**555.0**	378.3 (m08)
	Peak period	Original ensemble	1548.0	774.3 (m08)
		Five Selected ensemble	**1513.9**	774.3 (m08)
Nanairo	Rising limb	Original ensemble	270.8	206.2 (m03)
		Five Selected ensemble	**220.9**	206.2 (m03)
	Peak period	Original ensemble	1125.3	784.9 (m08)
		Five Selected ensemble	**1106.9**	784.9 (m08)

5.3 Flood Forecasting using Transposition of Ensemble NWP Rainfall Fields

We examined the transposition of ensemble rainfall fields and considered the misplacement from the original spatial position, in order to improve the flood forecast skill. For the transposition of ensemble rainfall fields, the catchment mask (100 km × 100 km) moved within the forecast domain with a maximum distance in the x and y directions of each at about 40 km with 5 km intervals (from L5 to L40), in 8 directions from the right side rotating in a counter-clockwise direction with 45° intervals (from D1 to D8) (Figure 5.5).

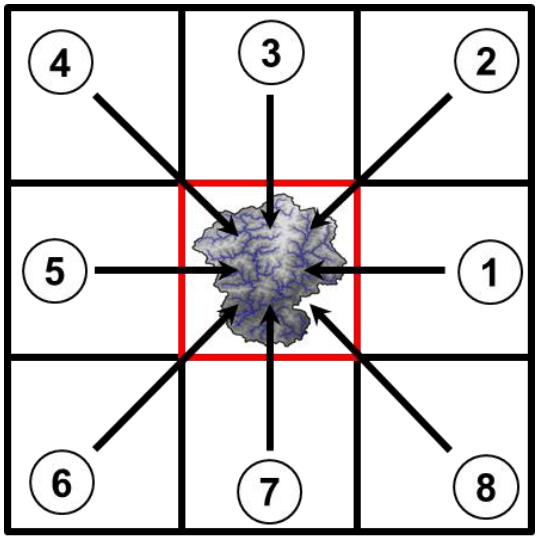

Figure 5.5 A schematic diagram representing the of transposition of rainfall fields

Therefore, we constructed 704 transposition members (11 ensemble members × 8 distances × 8 directions) and compared the error indexes (RMSE and CSI) to assess the performance of the transposition method. We considered the top 10% transposition locations, which have high efficiency criteria for each RMSE and CSI value, of each ensemble member during the rising limb period (Table 5.2), in order to apply them to the flood forecasting of the peak discharge period and improve

accuracy. Table 5.2 shows the top 10% transposition locations during the rising limb period using the RMSE and the CSI values, respectively. To evaluate the continuity of transposition behavior, the top 10% transposition locations were compared with the top 10% during the peak discharge period. The yellow color marks in Table 5.2 indicate the transposition locations that are continually satisfied during the two periods, and the percentage of transposition locations was recorded by a 50% and a 30.3%, respectively, for the RMSE and CSI values.

Table 5.2 The top 10% transposition locations of each ensemble member from RMSE and CSI in the rising limb period (D: direction, L: length (km))

Rank / Ensemble	Root Mean Square Error (RMSE)					
	1	**2**	**3**	**4**	**5**	**6**
cntl	D7L5	D6L5	D5L5	D3L5	D2L5	D1L5
m01	D6L5	D5L5	D7L5	D3L10	D6L10	D3L5
m02	D7L5	D8L5	D1L5	D7L10	D2L5	D6L5
m03	D6L5	D5L5	D7L5	D6L10	D5L10	D3L5
m04	D5L5	D7L5	D6L5	D3L5	D1L5	D5L10
m05	D5L5	D4L5	D6L5	D3L5	D5L10	D3L10
m06	D7L5	D6L5	D6L30	D6L25	D6L35	D5L5
m07	D5L5	D6L5	D7L5	D3L5	D5L10	D4L5
m08	D2L20	D2L25	D6L5	D7L5	D5L5	D2L30
m09	D6L5	D5L5	D7L5	D5L10	D3L5	D6L10
m10	D6L35	D6L40	D6L30	D7L5	D6L25	D6L5

Rank / Ensemble	Critical Success Index (CSI)					
	1	**2**	**3**	**4**	**5**	**6**
cntl	D7L5	D6L5	D5L5	D1L5	D2L5	D3L5
m01	D6L5	D5L5	D7L5	D6L10	D5L10	D3L5
m02	D7L5	D1L5	D8L5	D2L5	D1L10	D2L20
m03	D7L5	D6L5	D5L5	D3L5	D1L5	D8L5
m04	D5L5	D6L5	D7L5	D3L5	D4L5	D5L10
m05	D3L5	D4L5	D5L5	D3L10	D6L5	D3L15
m06	D7L5	D6L5	D5L5	D1L5	D8L5	D7L10
m07	D5L5	D6L5	D7L5	D5L10	D3L5	D4L5
m08	D7L5	D6L5	D5L5	D2L5	D3L5	D1L5
m09	D6L5	D5L5	D7L5	D3L5	D5L10	D2L5
m10	D2L25	D7L5	D2L20	D5L5	D3L5	D2L5

Figure 5.6 indicates the results of the 30 hours ensemble flood forecast over the Futatsuno dam catchments during the rising limb and peak discharge periods using the top 10% transposition locations of the ensemble rainfall fields. Table 5.3 compares the forecast skill of the original and transposition ensembles using the mean and best values of the flood forecasting. As shown in Figure 5.6 and Table 5.3, the mean and best values during the peak discharge period for the Futatsuno dam catchment improved. The top 10% of transposition locations during the rising limb period and the transposition ensemble range were closer to the observed discharge than the original ensemble range, as represented in Figure 5.6.

In the case of the Nanairo dam catchment (Figure 5.7 and Table 5.3), the best values also improved during the rising limb and peak discharge periods. On the other hand, the mean values show that the original ensemble provided more the suitable results than the transposition ensemble because smaller catchments indicate a larger uncertainty in the flood forecast; also, the ensemble members with low values for the RMSE and CSI values (see Figure 5.2) were not chosen, which affected the results of the ensemble flood forecasting. Based on these results, we determined that the other members, which were not selected for the appropriate ensemble, have the potential to provide the best value to flood forecasting skill when using the transposition method. Second, flood forecasting using the transposition of ensemble rainfall fields improved the accuracy for the under-predicted areas, and had better values than flood forecasting using the original and selected ensemble members.

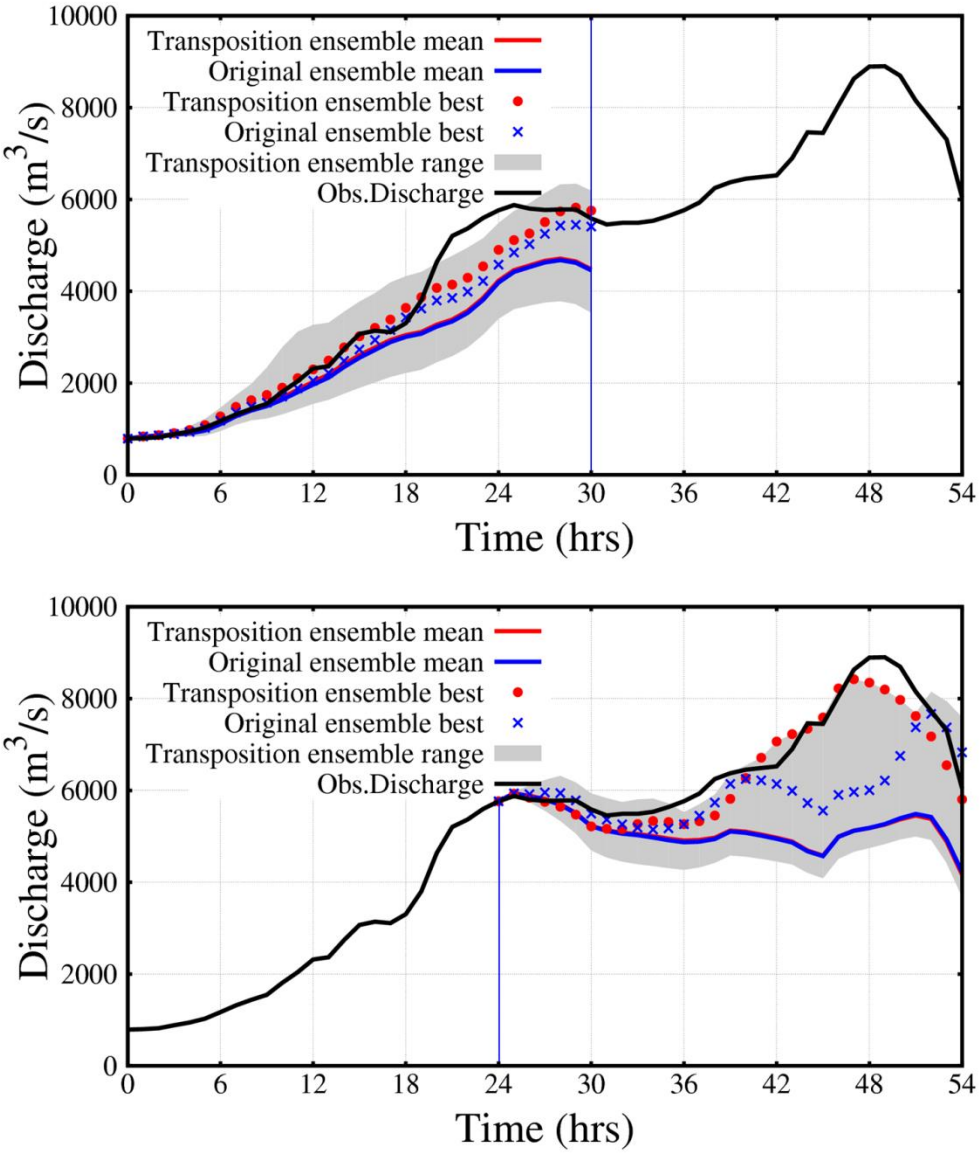

Figure 5.6 Ensemble flood forecasting using the transposition of ensemble rainfall fields during a rising limb period: upper and lower figures are the results of the rising limb and peak discharge period over the Futatsuno dam catchment.

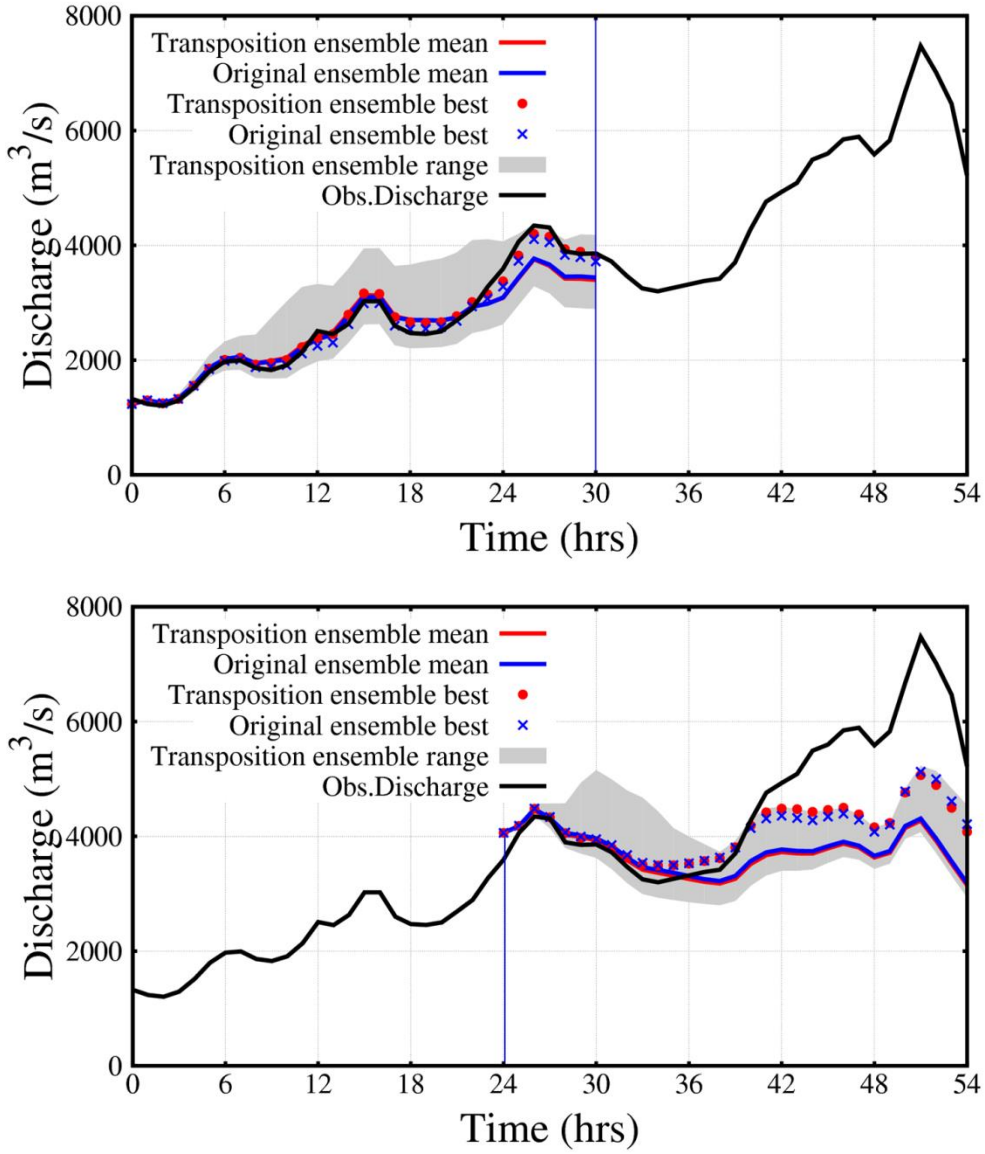

Figure 5.7 Ensemble flood forecasting using the transposition of ensemble rainfall fields during a rising limb period: upper and lower figures are the results of the rising limb and peak discharge period over the Nanairo dam catchment.

Table 5.3 Comparisons of the original and transposition ensemble results in flood forecast skill: The bold red color indicates the better result, and members in parentheses refer to the member with the best flood forecast skill.

Catchment	**Forecast Period**	**Type**	**MAE**	
			Mean	**Best**
Futatsuno	Rising limb	Original Ensemble	655.7	378.3 (m08)
		Transposition	**622.8**	**280.0** (D2L5 of m08)
	Peak period	Original Ensemble	1548.0	774.3 (m08)
		Transposition	**1542.9**	**357.4** (D5L10 of m07)
Nanairo	Rising limb	Original Ensemble	**270.8**	206.2 (m03)
		Transposition	274.5	**196.3** (D3L5 of m03)
	Peak period	Original Ensemble	**1125.3**	784.9 (m08)
		Transposition	1138.7	**758.5** (D1L5 of m08)

5.4 Flood Forecasting using a Combination of Selected and Transposition Methods

We also assessed the integrated method of considering the forecast characteristics of the above two methods simultaneously. We used the five selected ensemble members and the transposition locations of each ensemble member in Figure 5.2 and Table 5.2, respectively. Finally, we applied the constructed ensemble rainfall set from the rising limb period into the flood forecasting for the peak discharge period to assess the accuracy improvement and the applicability of combining the selected and transposition methods.

As shown in Figure 5.8, 5.9 and Table 5.4, the ensemble mean improved when integrating the selection and transposition methods over the two catchments, rather than using only the transposition method, because of the consideration of the five selected ensemble members, even though their mean values (Table 5.1) have higher-quality accuracy. The integrated method also provided better results than typical ensemble forecasting. Based on these results, combining selection and transposition methods could improve the accuracy of flood forecasting, particularly the mean and best values in small catchments.

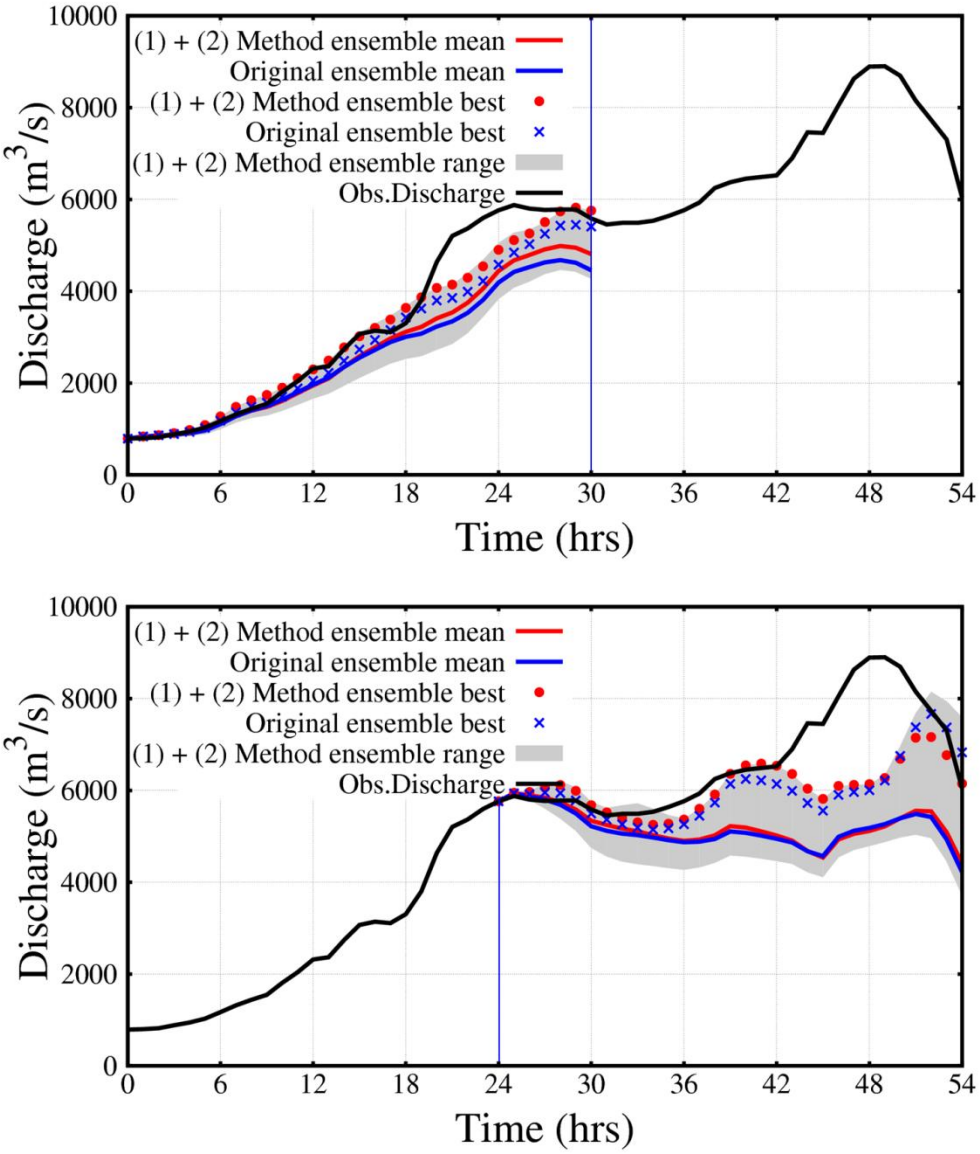

Figure 5.8 Ensemble flood forecasting with the combination of selected ensemble members and the transposition method during a rising limb period: upper and lower figures are the results of the rising limb and peak discharge period over the Futatsuno dam catchment.

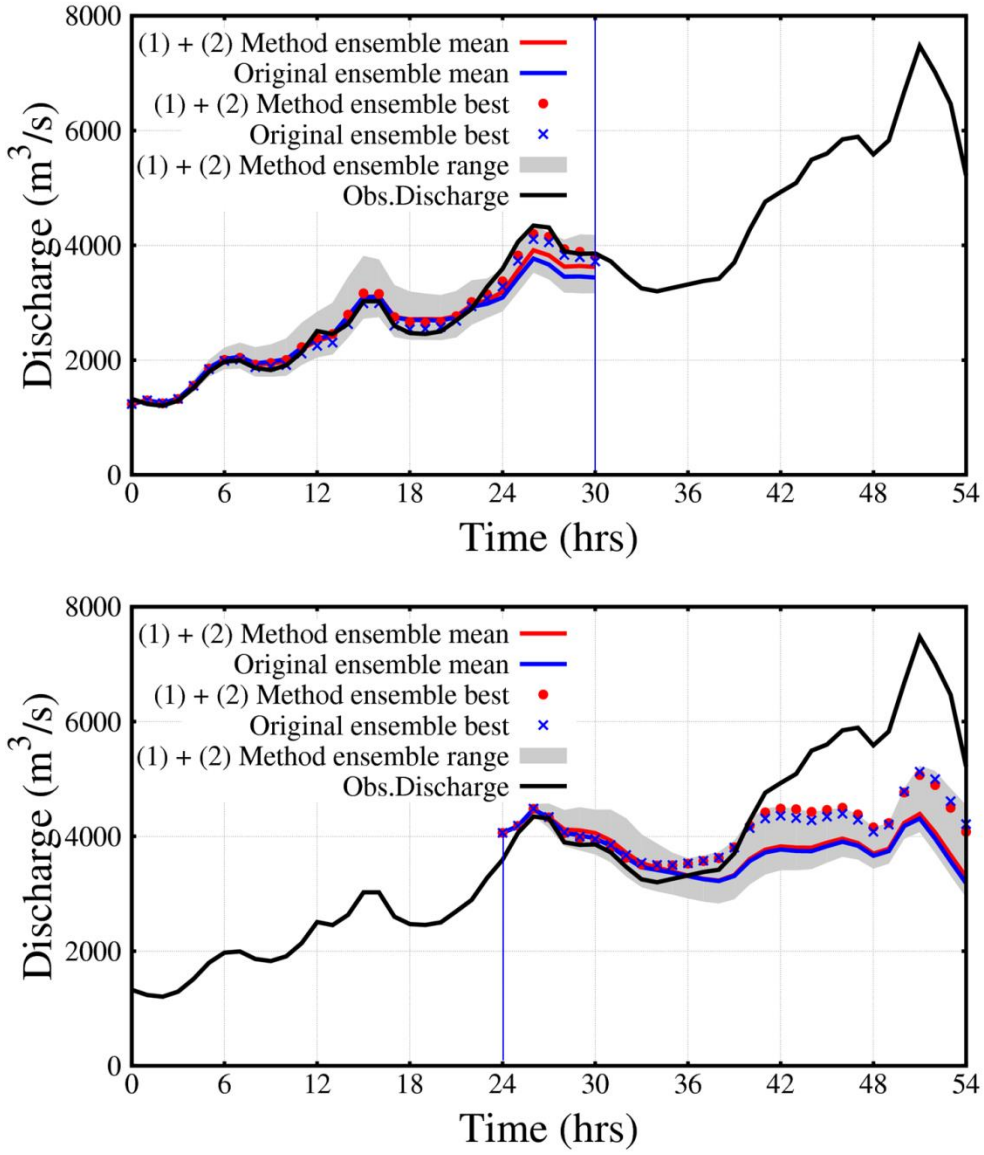

Figure 5.9 Ensemble flood forecasting with the combination of selected ensemble members and the transposition method during a rising limb period: upper and lower figures are the results of the rising limb and peak discharge period over the Nanairo dam catchment.

Table 5.4 Comparisons of flood forecast skill between the original and combination of the two methods. A bold red color indicates the better result, and members in parentheses refer to the member with best flood forecast skill.

Catchment	Forecast Period	Type	MAE	
			Mean	Best
Futatsuno	Rising limb	Original Ensemble	655.7	378.3 (m08)
		Combination	**548.9**	**280.0** (D2L5 of m08)
	Peak period	Original Ensemble	1548.0	774.3 (m08)
		Combination	**1499.3**	**703.8** (D5L5 of m08)
Nanairo	Rising limb	Original Ensemble	270.8	206.2 (m08)
		Combination	**236.6**	**196.3** (D3L5 of m03)
	Peak period	Original Ensemble	1125.3	784.9 (m08)
		Combination	**1110.6**	**758.5** (D1L5 of m08)

5.5 Summary

This chapter investigated the accuracy improvement of flood forecasting in the Futatsuno and the Nanairo dam catchments when driven by three methods: with selected ensemble members, transposition of rainfall fields, and a combination of these methods using the spatial verification of the RMSE and CSI values. The selected ensemble members and the transposition locations for the rising limb period were adopted into flood forecasting for the peak discharge period to evaluate the continuity of behavior patterns and improvement in accuracy.

In the flood forecast using selected ensemble members, this method can improve the accuracy of the mean value while conserving the best value between the original and selected ensemble members over two catchments. And the ensemble flood

forecasting using transposition of NWP rainfall fields produced better results than the original and selected ensemble members, in terms of the best values of flood forecast skill in all periods over the two catchments. Finally, the integration of the selected and transposition methods recovered the accuracy of the mean values for two periods over the Nanairo catchment, compared with the use of the transposition method alone, although the mean values from using the selected ensemble method have outstanding accuracy.

In this chapter 5, we assessed the pre-processing method separately for the rising limb and peak discharge periods because they are the most important phases of real-time flood forecasting. However, it is very important to divide the periods, including the rising limb and peak discharge periods, when applying this method to an actual operation. Therefore, in further research, we need to consider the methodology required to divide the periods and to verify the applicability of these methods through a number of case studies.

Chapter 6

Real-time Updating of Flood Forecasting using Transposition of Ensemble NWP Rainfall Fields considering Orographic Rainfall

Abstract *This chapter enhances the transposition method proposed in Chapter 5 and suggests real-time updating of flood forecasts using transposition of ensemble rainfall distributions that consider orographic rainfall for accuracy improvement. In the first step of the proposed method, ensemble forecast rainfalls from a numerical weather prediction (NWP) model are separated into orographic and non-orographic rainfall fields using atmospheric variables (e.g., air temperature, horizontal wind and relative humidity) and the extraction of topographic effect. Then the non-orographic rainfall fields are examined by the transposition scheme to produce additional ensemble information and new ensemble NWP rainfall fields are calculated by recombining the transposition results of non-orographic rain fields with separated orographic rainfall fields for a generation of place-corrected ensemble information. Then, the additional ensemble information is applied into a hydrologic model for post-flood forecasting with a 6-hour interval and shows improvement in the accuracy of flood forecasting with the proposed update method.*

6.1 Introduction

The accuracy of weather forecasts has steadily improved over the years, due to advances in Numerical Weather Prediction (NWP) techniques and increased computing power. These NWP models represent the atmosphere as a dynamic fluid, solve for its behavior through the use of mechanics and thermodynamics, and use current weather conditions as input to atmospheric models to predict the evolution of weather systems.

However, meteorological forecasting is difficult because the atmosphere is a nonlinear and chaotic system (Lorenz, 1969). A slight change in the initial and boundary layer conditions of a circulation system could result in unpredictable outcomes. Presently, one of the main alternatives is an ensemble NWP system with various initial and boundary conditions. It is believed that ensemble NWP systems exhibit greater forecast skill than any single NWP model control run or deterministic model run (Buizza et al., 1999; Demeritt et al., 2007). These recent advances in weather measurement and forecasting have created opportunities to improve flood forecasts (Cuo et al., 2011).

At the same time, operational and research flood forecasting systems are increasingly moving towards using NWP model ensembles, known as ensemble prediction systems (EPSs), rather than single deterministic forecasts. EPSs in flood forecasting are now widely regarded as the state-of-the-art technique in forecasting science, following on the success of the use of ensembles for weather forecasting (Buizza et al., 2005; Gneiting and Raftery, 2005). EPSs have been used to account for uncertainties and make an attractive product for flood forecasting systems with the potential to extend lead time and better quantify predictability than any single deterministic run for the same location and time (Palmer and Buizza, 2007). Several authors also have utilized and investigated EPSs and have found that ensemble

forecasts in hydrological fields increase accuracy and allow for skillful predictions with extended lead time (Xuan et al., 2009; Roulin and Vannitsem, 2005; Yu et al., 2013, 2014).

However, in many cases, the potential of flood forecasting with EPS is described alongside cautious notes regarding variability and uncertainty of ensemble information. Several authors agreed that, compared to traditional deterministic forecasting, the additional information provided by EPS should help improve forecasting quality and provide flood forecasts with valuable information, but were less clear about exactly what that information was or how useful it might be for their operational purposes (Palmer, 2002; Legg and Mylne, 2004; Hlavcova et al., 2006). And, in some cases of medium-range meteorological forecasts, ensemble gave a clear flood signal up to 4 days in advance, but it has a restricted application for using EPSs effectively in flood forecasting systems on a small catchment scale because it needs localized higher accuracy in terms of rainfall prediction. As a result, EPSs with NWP models do not capture true rainfall distributions, in some cases, for short-range flood forecasting on a small catchment scale.

EPSs with NWP models also have challenges with misplacement of spatial rain distributions, which means the intensity and shape of a rainfall pattern may be correct but the location of spatial storm distribution deviates from the true rainfall distributions. As a result, the misplacement of rain distributions demonstrates the poor reliability of quantitative precipitation forecasts. Ebert and McBride (2000) also stated that QPF quality needs to be improved in order to provide reliable hydrologic prediction, and errors in location misplacement, timing, and intensity hampered the direct application of QPF from the NWP into hydrologic prediction models.

Given the current issue and problem with EPSs with NWP models, a proper pre-processing that deals with spatial misplacement of rainfall distributions should be

considered carefully in order to use EPSs effectively in flood forecasting systems on a small catchment scale. Yu et al. (2014) have utilized and investigated this ensemble NWP rainfall forecast for flood forecasting and proposed a spatial shift (hereafter, transposition) of ensemble rain distributions to improve the accuracy of flood forecasts. However, in cases of the transposition of rain distributions in mountainous areas, the problem arises that the orographic rain patterns also move to non-mountain areas with the transposition scheme. As a result, it results in a great loss of the physical meaning of orographic rainfall. To prevent the problem of orographic rainfall shifting, we modified Yu et al. (2014)'s method of separating ensemble NWP rainfalls into orographic and non-orographic rain fields by solving physically based equations that included the atmospheric variables in advance of the transposition scheme.

This chapter enhances the transposition method proposed in Chapter 5 and suggests a post-processing ensemble flood forecasting method for real-time updating and the accuracy improvement of flood forecasts that considers two points: the separation of the orographic rainfall and the correction of misplaced rain distributions using additional ensemble information through the transposition of rain distributions. Figure 6.1 shows a flowchart of the proposed process in chapter 6 for the real-time updating of flood forecasts using transposition of rainfall fields that considers orographic rainfall. The newly proposed method is comprised of 5 steps. The first step is the separation of ensemble NWP rainfalls into orographic and non-orographic rain fields using the extraction of topography effect. Then, the non-orographic rainfall fields are examined by the transposition scheme to produce additional ensemble information (step 2), and ensemble NWP rainfall fields are calculated by recombining the transposition results of non-orographic rain fields with those of orographic rainfall fields in order to generate place-corrected ensemble information (step 3). The recombined ensemble rain fields are spatially verified by C-band composite radar data from the Ministry of Land, Infrastructure, Transport and

Tourism (MLIT) of Japan for the previous 6 hours with error indexes—namely, the critical success index (CSI) and the root mean square error (RMSE)—to find out the appropriate ensembles and transposed locations (step 4). The best ensemble members and transposed locations give information to hydrologic models for real-time updating of post-flood forecasting within a 6-hour interval (Step 5) in the Typhoon Talas event of 2011. In this chapter, the results of ensemble prediction with 2 km horizontal resolution utilize the two sets of ensemble prediction outputs (1st forecast: 2011/09/02 03:00–09/03 09:00 JST, 30 hours; 2nd forecast: 2011/09/03 03:00–09/04 09:00 JST, 30 hours). Total analysis time is 54 hours with an overlap of 6 hours between the output sets, and 2 km ensemble rainfall prediction outputs are used as input data into a hydrologic model.

This chapter has been organized in the following manner. After the introduction, Section 6.2 introduces the methodology for the calculation of orographic rainfall and transposition scheme for making ensemble information and section 6.3 addresses the results of real-time updating of flood forecasts. Finally, we summarize our major conclusions in section 6.4.

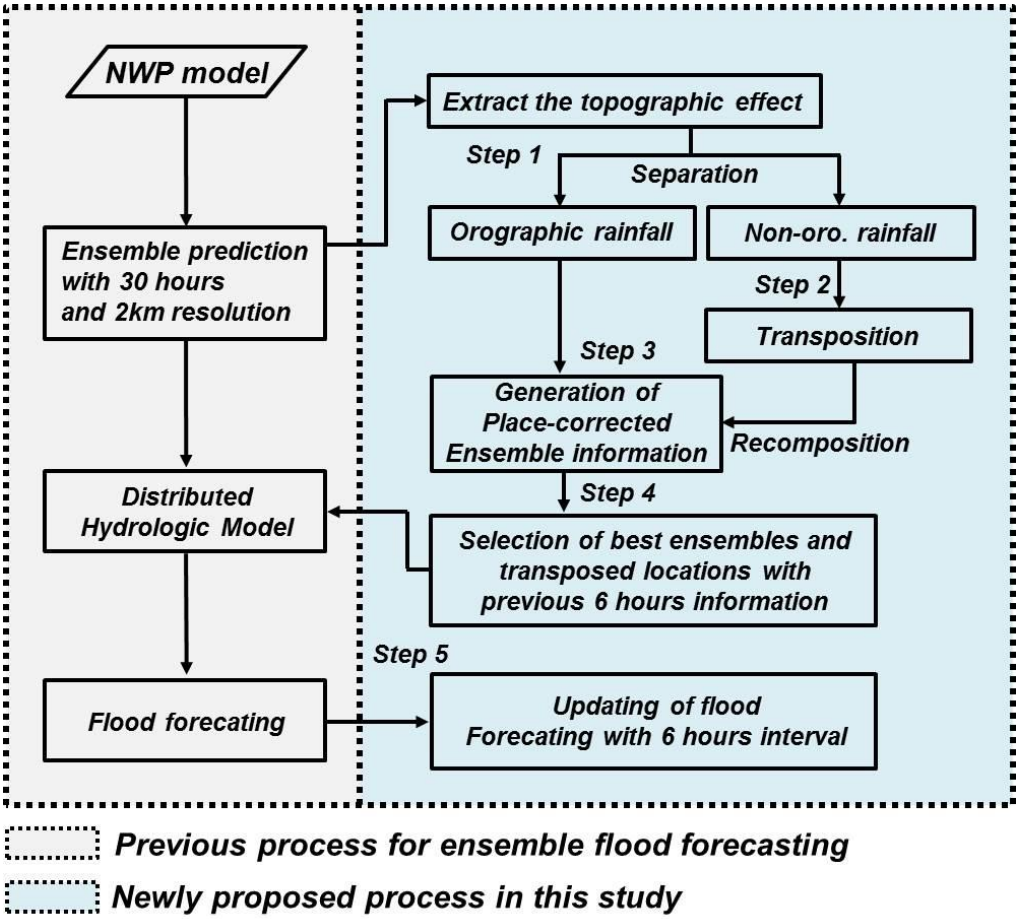

Figure 6.1 Flowchart of the proposed process for the real-time updating of flood forecasts using the transposition of ensemble NWP rainfall fields and considering orographic rainfall.

6.2 Methodology

6.2.1 Physically based Method for Orographic Rainfall

Tatehira (1976) proposed a physically based method for calculating orographic and non-orographic rainfall fields from observed radar rainfall measurements. Many studies have applied and verified this method in a variety of hydrologic applications,

that have shown that this method was effective and adequate to consider orographic and non-orographic rainfall (Nakakita and Terazono, 2008; Nakakita et al., 2012). However, they used radar rainfall measurements to separate the orographic and non-orographic rainfall in a previous study, whereas our approach applies this method into the ensemble NWP rainfall as mentioned previously.

In this method, the orographic effect is calculated based on the seeder-feeder mechanism. The precipitation droplets or ice particles fall from an upper-level precipitating cloud (seeder) and collect cloud water as they pass through a lower-level orographic stratus cloud (feeder) by collision and coalescence, thus producing greater precipitation on the mountainous area under the cap cloud than on the nearby flat regions. The availability of the process depends on sufficiently strong low-level moist flow to maintain the cloud water content in the orographic feeder cloud and the continuing effectiveness of precipitation particles from the seeder cloud. The strong rain bands that stagnate near the mountaintop (orographic rainfall) are estimated using additional atmospheric variables. The flux of cloud water content L (g/m3) in a rising air parcel, along with wind, is calculated by equation (6.1).

$$\frac{dL}{dt} = -cL - a(L - L_c) + WG - WL\left(\frac{\partial \ln \rho_v}{\partial z}\right) \tag{6.1}$$

where ρ_v is the density of water vapor (g/m^3), c is the ratio of cloud drops captured by seeder hydrometeors of an upper level, a is the ratio of precipitation particles to cloud drops, L_c is the threshold amount of water content before conversion into precipitation (g/m^3) and G is the amount of saturated water vapor ρ_s increased by a rising saturated air parcel (g/m^4) (i.e., $-d\rho_s/dz$). Finally, W is the vertical wind velocity (m/s), which is estimated by an inner product of horizontal wind and gradient of topographic height using DEM.

These atmospheric variables (air temperature, horizontal wind, relative humidity) are estimated by the use of Grid Point Value (GPV) data from Japan Meteorological Agency (JMA) and are solved in a seven-layer model at heights of 200, 400, 1000, 2000, 3000, 4000, and 5000 m in a σ-vertical coordinate system using the method of Nakakita et al. (1996). In equation (6.1), the first and second terms on the right-hand side are related with that the amount of water content is decreased. The third term shows the water vapor condensing as the air parcel ascends with a unit distance. The last term expresses the influence of atmospheric compressibility, and can be ignored because its order is less than that of the other terms. The amounts of cloud water content in an inflow and outflow mesh (L_{in} and L_{out}) can be calculated by the integral of equation (6.1) with respect to time t.

$$L_{out} = \frac{WG + aL_c}{c + a} + \left(L_{in} - \frac{WG + aL_c}{c + a} \right) e^{-(c+a)\Delta t} \tag{6.2}$$

In this chapter, the ensemble NWP rainfall (RNWP) is interpreted to be the summation of orographic rainfall (Ro) and non-orographic rainfall (Rn) (Equation (6.3)). Nakakita and Terazono (2008) suggested equation (6.4) for orographic rainfall intensity Ro (mm/h) and assumed that the ratio c of cloud drops captured by raindrops is estimated by equation (6.5). Finally, the orographic rainfall is supposed to be a function of non-orographic rainfall and is calculated by solving simultaneous equations (6.2) ~ (6.5) in multi-atmospheric layers

$$R_{NWP} = R_o + R_n \tag{6.3}$$

$$R_o = \frac{L_{in} + WG\Delta t - L_{out}}{\Delta t} \times 3.6 \times H \tag{6.4}$$

$$c = 0.6778 R_N^{\,0.731} \times 10^{-3} \tag{6.5}$$

where L_{in} and L_{out} are amounts of cloud water content (g/m^3) in an inflow and outflow side mesh, respectively. Δt is a timescale (s) during which an air parcel passes through one mesh, and H is the thickness of each layer (m).

Figure 6.2 shows the procedure for the separation of orographic and non-orographic rainfall. First, cloud water content is calculated from atmospheric variables of grid mesh in each layer vertically, and the ensemble NWP rainfall (RNWP) is assumed to be that of the lowest layer (200 m height). It is separated into orographic (Ro1) and non-orographic (Rn1) rainfall by solving equations (6.2) ~ (6.5). It is supposed that the non-orographic rainfall (Rn1) is expressed as the sum of the orographic rainfall (Ro2) and non-orographic rainfall (Rn2) in the upper layer. In this way, orographic rainfall and non-orographic rainfall in each layer can be repeatedly separated from the lowest to the highest layer. Then, the non-orographic rainfall field of highest layer is utilized as an input domain for the transposition scheme to make additional ensemble information and the total orographic rainfall in each layer gives the value by recombining the transposition results of the non-orographic rainfall field.

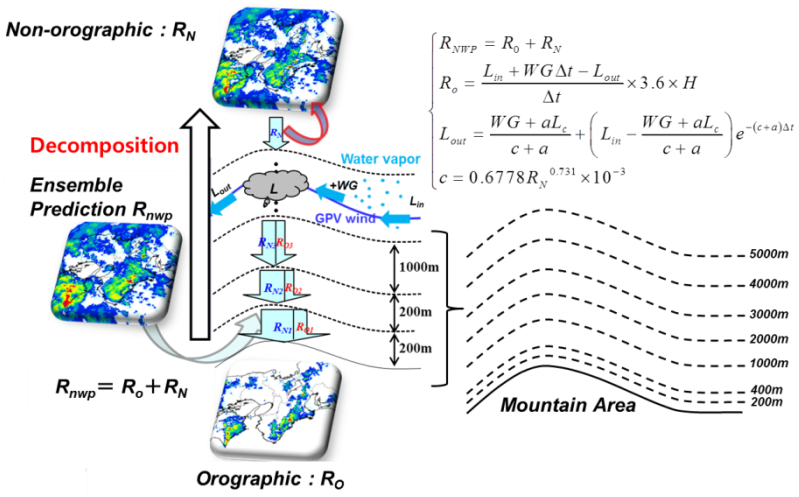

Figure 6.2 Procedure for a calculating orographic and non-orographic rainfall.

6.2.2 Transposition of Non-orographic Rainfall Fields

As previously stated, we examined the transposition scheme of non-orographic rainfall fields in order to produce additional ensemble information and consider the misplacement from the original spatial position. Many EPSs are based on a Monte Carlo framework of an NWP model with one realization starting from a central analysis (the control forecast) and others generated by perturbing the initial and/or boundary conditions (the perturbed forecasts) (Cloke and Pappenberger, 2009). In this chapter, we also used ensemble NWP rainfall created by perturbation of initial and boundary conditions, and we took into consideration the transposition scheme for additional ensembles. The technique for making additional ensemble information is fairly straightforward in this chapter: we utilized spatial transposition of each separate non-orographic rain field.

Figure 6.3 shows a schematic of transposition that uses non-orographic rainfall fields and recombines them with the total orographic rainfall in each vertical layer. For the transposition with separated non-orographic rainfall fields from the established ensemble prediction, the transposed catchment mask (100 km × 100 km) moved into the original forecast domain from location 1 to location 80 with a maximum distance in the x and y directions of each at about 20 km with a 5 km interval in order to produce additional ensemble information. We finally constructed an additional 891 transposed ensemble domains (existing 11 ensemble members × 80 locations + 11 original locations of established ensemble members). Then, the final place-corrected ensemble rainfall fields are estimated by integrating the transposed non-orographic rain fields with the total orographic rainfall, which is calculated in each vertical layer.

In previous research, Yu et al. (2014) have also utilized the transposition method to address the uncertainties in ensemble hydrological forecasting and to improve the

accuracy of flood forecasts. They investigated the appropriate transposed locations of ensemble rainfall fields during the current period to apply the transposed information into the next target period of flood forecasting and then evaluated the continuity of misplacement behavior of ensemble rainfall from the current period to the next target period. Our approach agrees with that of Yu et al. (2014) in terms of the accuracy improvement of flood forecasting skill, but differs from the previous approach in two main aspects. The first is that our approach considered the separation of rainfall distribution into orographic and non-orographic rainfall as mentioned above. Secondly, our approach took into account the transposed information with a 6-hour interval and applied it to flood forecasts for real-time updating, whereas Yu et al. (2014) considered 30 hours of the current period to find out the appropriate transposed locations and separately applied the 30 hours of the next target period. Our approach in this paper mainly focuses on the real-time updating of flood forecasts using a transposed ensemble approach with a 6-hour interval.

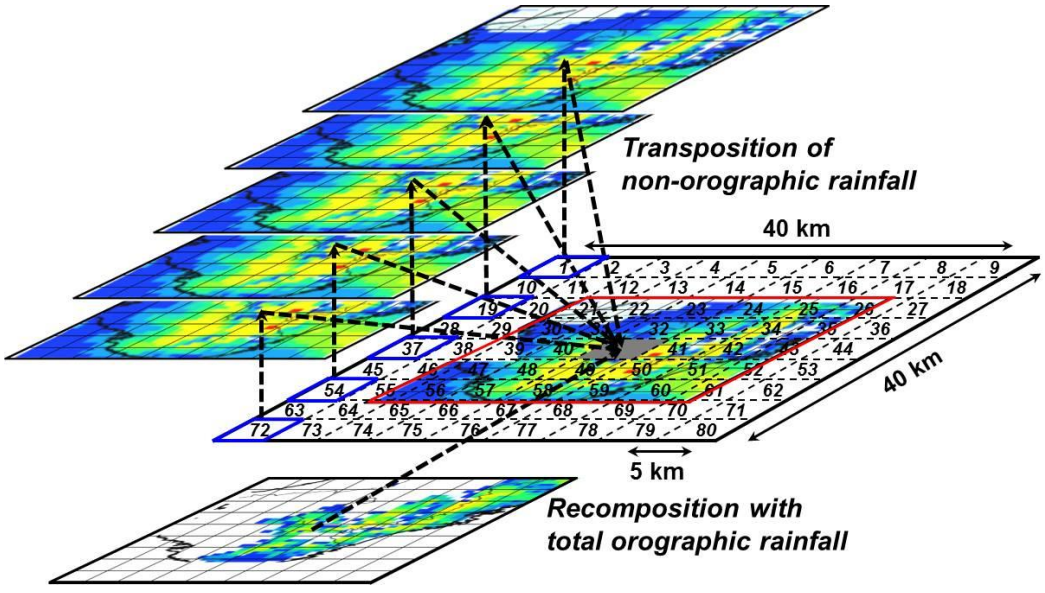

Figure 6.3 A schematic of transposition scheme that uses non-orographic rainfall fields and recombines them with the total orographic rainfall in each vertical layer.

6.3 Results and Discussion

6.3.1 Transposition Considering Misplaced Spatial Location

As stated above, we separated the established 11 ensemble rainfall fields into orographic and non-orographic rainfall using a physically based method to take advantage of the non-orographic rainfall as part of a transposition scheme for additional ensemble information. Based on the results of separated orographic and non-orographic rainfall, we investigated how the orographic rainfall comprised and dominated the total rainfall over the verification area.

Figure 6.4 shows the accumulated orographic and non-orographic rainfall by control run forecast and comprises the proportion of accumulated orographic rainfall in total rainfall during the 30 hours of the 1st forecast period. The comprising ratio of the orographic rainfall is calculated as follows:

$$ratio_{i,j} = \frac{R_{o,i,j}}{R_{total,i,j}} \tag{6.6}$$

where $R_{o,i,j}$ and $R_{total,i,j}$ are the accumulated orographic and total rainfall of each grid cell.

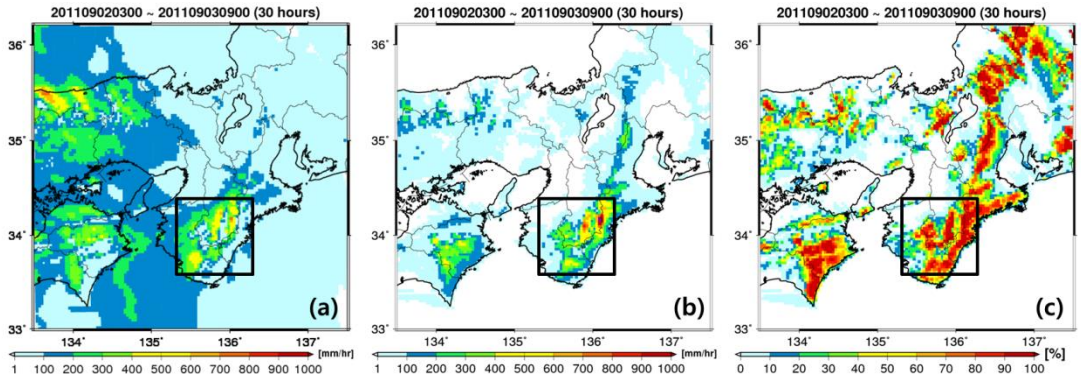

Figure 6.4 (a) Accumulated non-orographic rainfall by control forecast, (b) accumulated orographic rainfall, and (c) its comprising ratio in total rainfall (Figure 2.3(c)). The rectangle inside the domain denotes the verification area.

From Figure 6.4, note that there is an abundance of non-orographic rainfall in a non-mountainous area, whereas orographic rainfall was predominant in the verification area, which is a mountainous region. Moreover, the ratio of orographic to non-orographic rainfall in the verification area exceeded 50 percent and the maximum percentage is 99.8 percent. From these results, it is apparent that orographic and non-orographic rainfall should be separated and that only non-orographic rain fields should be utilized for spatial transposition because orographic rain patterns also move to non-mountainous areas with the transposition scheme if they are not separated.

We also visualized the orographic and non-orographic rainfall patterns separated from 11 established ensemble members with mean areal rain rates of the Shingu river basin during 54 hours and 2 forecast periods. Figure 6.5 shows comparisons of orographic (circle) and non-orographic (square) rainfall during the forecasted ensemble NWP rainfall in two forecast periods (1st forecast: 2011/09/02 03:00–09/03 09:00 JST (30 hours), 2nd forecast: 2011/09/03 03:00 ~ 09/04 09:00 JST). Mean areal rain rates (mm/h) over the Shingu river basin are shown in the plot. Through Figure 6.5, areal orographic rainfall rates are dominant over non-orographic

rainfall until 20 mm/h, whereas the component ratio of the orographic rainfall decreases with a two-dimensional trend line over 20 mm/h.

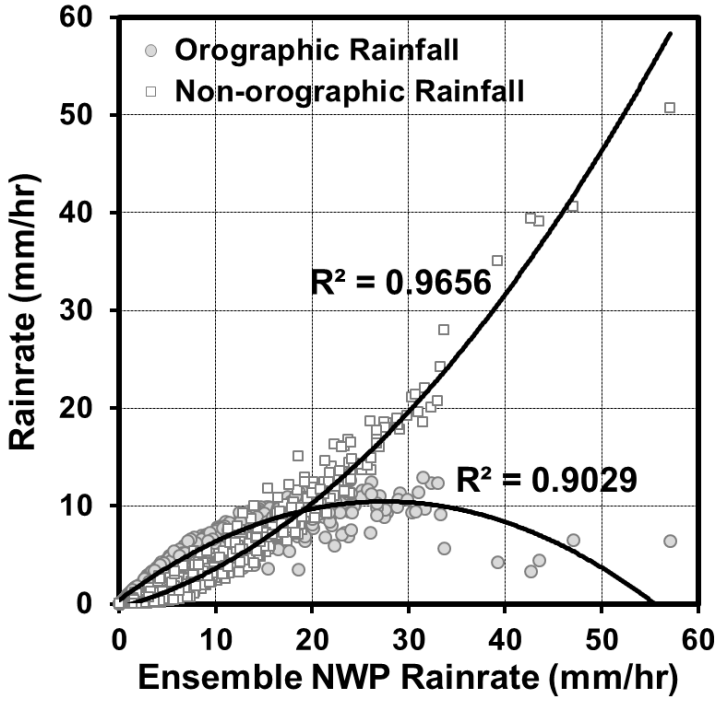

Figure 6.5 Comparisons of orographic (circle) and non-orographic (square) rainfall during the forecast time of the ensemble NWP rainfall.

Then, as stated above, we constructed 891 transposed ensemble domains by integrating the transposed non-orographic rain fields with the orographic rain fields in order to produce additional ensembles and investigate the misplaced spatial locations. Transposed ensemble domains have been verified spatially with MLIT observed radar rain data in the verification area to investigate the appropriate ensemble members and transposition locations, which have high efficiency criteria during the previous 6-hour interval for updating flood forecasts. We used two popular indices to evaluate transposed ensemble domains: critical success index (CSI) for qualitative verification and root mean square error (RMSE) for quantitative verification, expressed as follows:

$$CSI = \frac{H}{H + M + FA} \tag{6.7}$$

$$RMSE = \sqrt{\frac{1}{N}\sum_{i,j=1}^{N}\left(O_{i,j} - F_{i,j}\right)^2} \tag{6.8}$$

where N is the total grid cells (100 × 100) in the verification area, $O_{i,j}$ and $F_{i,j}$ are the observed and forecasted rainfall of each grid cell at forecast time t, H is the number of correct forecasts over the threshold (i.e., when the forecast rainfall is also observed), and M is the number of times rainfall is not forecast, but is observed. FA is the number of times rainfall is forecast, but not observed.

For the calculation of CSI value, the ensemble forecasts were expressed as probabilities of exceeding a selected rainfall threshold (10 mm/h), which were used to compare an obvious spatial distribution of observed MLIT radar data with forecasted NWP rainfall. A contingency table can be constructed with a spatial comparison, in which each area with more than 10mm/h threshold is defined as "yes," and other areas are defined as "no" for both forecasted and observed rainfall fields (Table 6.1).

Table 6.1 A contingency table showing the frequencies of predicted and/or observed events determined by threshold (T)

		Predicted	
		rain < T	rain > T
Observed	rain < T	zeroes (Z)	false alarms (FA)
	rain > T	misses (M)	hits (H)

Figure 6.6 shows the results of the average CSI and RMSE of the previous 6 hours (2011/09/02 03:00–09:00) in a comparison of observed radar rainfall and each transposed NWP rainfall domain during the first forecast period. Each grid value represents the average CSI and RMSE when a transposed mask dominated each grid as the center moved to an original domain within zero points of the x and y locations.

Based on comparison of observed radar domain and each transposed output, most CSI values provided a well-matched spatial pattern in case of transposition from central and left grid points to an original domain, whereas members 1 and 5 were close to zero value in overall grid points. From the CSI results, the forecast rainfall patterns moved slowly compared with real rainfall patterns because the rainfall's direction of progress was from left to right. On the other hand, the RMSE value (Figure 6.6(b)) showed well-matched values in the middle areas. Figure 6.7 also shows the results of the average CSI and RMSE from 6 to 12 hours (2011/09/02 09:00–15:00). From the results of Figures 6.6 and 6.7, we confirmed that spatial distribution patterns of the CSI and RMSE comparison results during the first 6 hours and next 6 hours were similar, and it can be said that misplacement behaviors of rainfall distribution have the continuity of transposition locations in each spatial distribution pattern.

Furthermore, we considered the top 10% transposition locations, which have high efficiency criteria for each RMSE and CSI value, of a total 891 additional ensemble members during the 6-hour interval, in order to apply them to post-flood forecasting and assess the accuracy improvement for the application assessment of real-time updating of flood forecasts. As stated above, the real-time updating of flood forecasts with a 6-hour interval starts with the assumption that misplacement behaviors of rainfall distribution have continuity between 0 and 6 hours and from 6 to 12 hours of transposition locations. Therefore, a verification measure using correlation coefficients was adopted to conduct a continuity assessment of misplacement

behaviors of rainfall distribution with critical success index (CSI) in each 6-hour update step. The correlation coefficient has been computed as follows:

$$corr = \frac{\mathrm{cov}(A,B)}{\sigma_A \sigma_B} = \frac{N\sum_{i=1}^{N} A_i B_i - \sum_{i=1}^{N} A_i \sum_{i=1}^{N} B_i}{\sqrt{\left[N\sum_{i=1}^{N} A_i^2 - \left(\sum_{i=1}^{N} A_i\right)^2\right]\left[N\sum_{i=1}^{N} B_i^2 - \left(\sum_{i=1}^{N} B_i\right)^2\right]}} \quad (6.9)$$

where A is the average CSI results of each ensemble member from 0 to 6 hours (i.e., Figure 6.6(a)), B represents the average CSI results of each ensemble member from 6 to 12 hours (i.e., Figure 6.7(a)), *cov* is the covariance of average CSI results between 0 to 6 hours and 6 to 12 hours of transposition locations, and σ_A and σ_B are the standard deviations of average CSI results from 0 to 6 hours and from 6 to 12 hours, respectively.

Table 6.2 shows the continuity assessment of transposition behaviors of forecasted rainfall distribution using the correlation coefficient of the critical success index (CSI) in each 6-hour update step for real-time updating of flood forecasts, and the correlation coefficient with CSI distribution was recorded over 0.42 to 0.95. It means that the transposition scheme is continually satisfied during the two 6-hour update steps and is appropriate for real-time updating of flood forecasts.

Table 6.2 Continuity assessment of transposition behaviors of rainfall distribution using correlation coefficients in each 6-hour update step.

Period		**Correlation Coefficient**
1st forecast	0 ~ 6 h with 6 ~ 12 h	0.949
	6 ~ 12 h with 12 ~ 18 h	0.531
	12 ~ 18 h with 18 ~ 24 h	0.829
	18 ~ 24 h with 24 ~ 30 h	0.418
2nd Forecast	0 ~ 6 h with 6 ~ 12 h	0.504
	6 ~ 12 h with 12 ~ 18 h	0.619
	12 ~ 18 h with 18 ~ 24 h	0.842
	18 ~ 24 h with 24 ~ 30 h	0.834

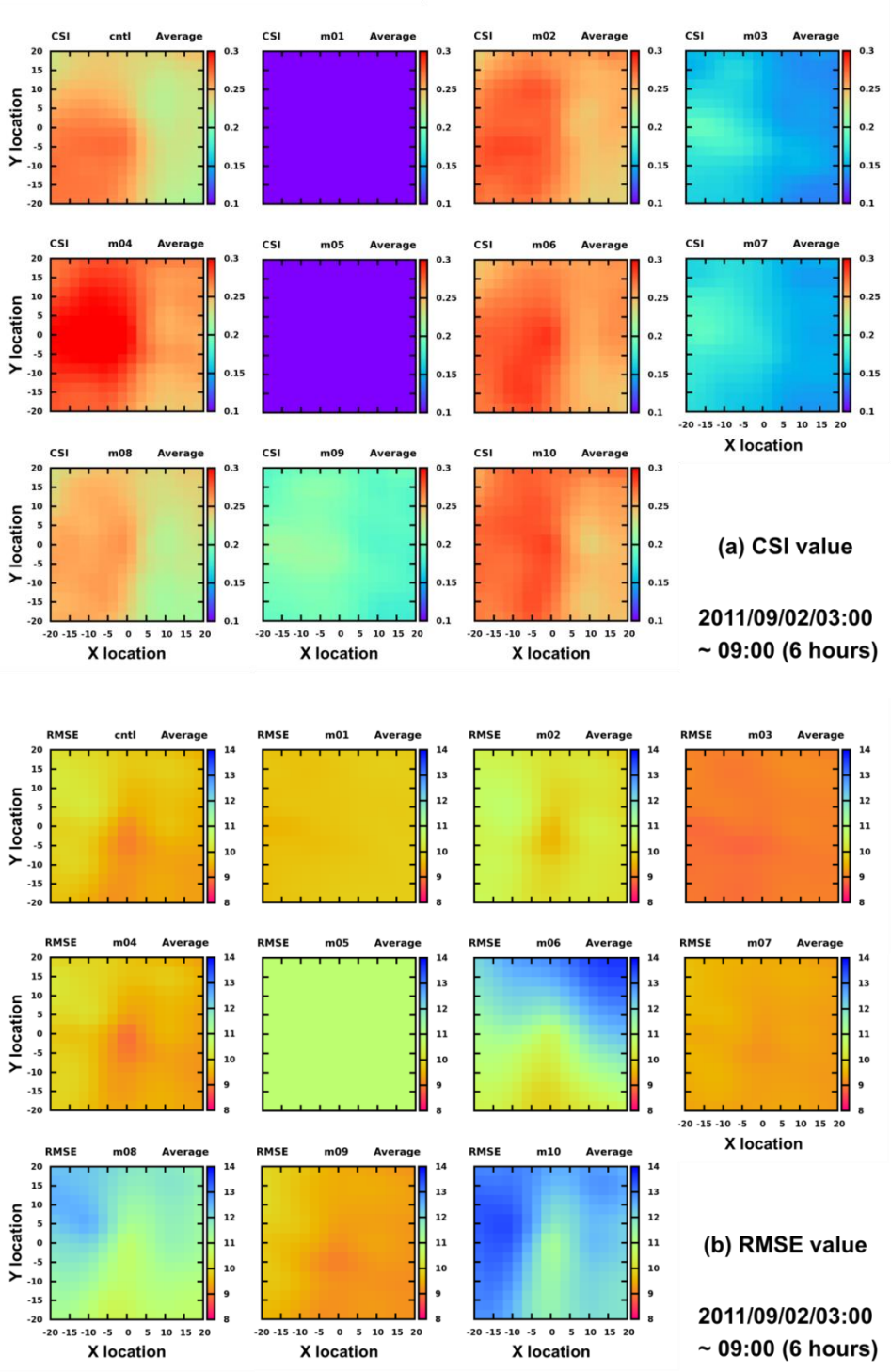

Figure 6.6 Average CSI and RMSE results over 6 hours (2011/09/02 03:00 ~ 09:00) in a comparison of observed radar rainfall and each transposed NWP rainfall domain during the first forecast period.

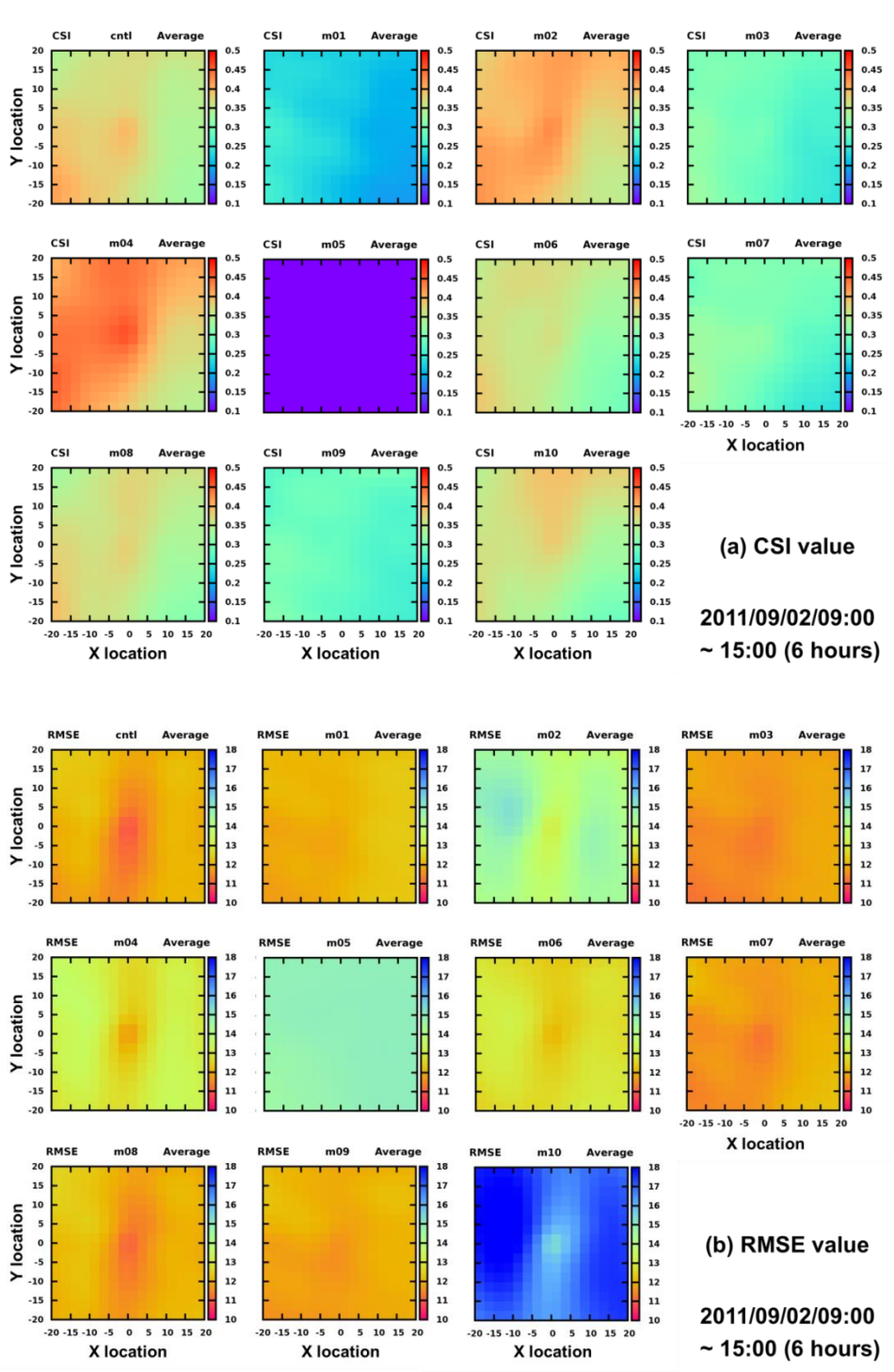

Figure 6.7 Average CSI and RMSE results over 6 hours (2011/09/02 09:00 ~ 15:00) in a comparison of observed radar rainfall and each transposed NWP rainfall domain during the first forecast period.

6.3.2 Real-time Updating of Post-Flood Forecasts

The proposed approach has been tested in the Futatsuno and Nanairo dam catchments of the Shingu river basin for the real-time updating of flood forecasts for the largest flood event of 2011, which was caused by Typhoon Talas. Figures 6.8 and 6.9 show the ensemble flood forecasts using the original 11 ensemble members in the first and second forecast periods and corresponding post-flood forecasts after 6, 12, 18 and 24 hours by transposition updating over the Futatsuno and Nanairo dam catchments, respectively. Each figure illustrates a complete set of the forecast discharge for the ensemble range (grey range), the top 10% ensemble members (180 ensembles, dark grey curve), the ensemble mean (blue curve), the simulation result using observed radar rainfall (black curve) and the observed discharge data of outlet point (red point) for each dam catchment.

At first, in the 1st forecast period (rising limb period, left side of Figure 6.8) over the Futatusno dam catchment, the ensemble spread of the original ensemble forecasting provided a well-matched hydrograph temporal pattern during 0 to 18 lead times, which were lower and less predictable than the true value from 18 to 30 lead times over the Futatsuno dam catchment; this was caused by an underestimation of the rainfall forecast. After updating using the transposition scheme, the ensemble spread of the flood forecast is close to peak discharge in the rising limb period and is maintained through the updating, at 6-hour intervals, of the transposition information. In the second forecast period (peak discharge period, right side of Figure 6.8), the ensemble spread of the original ensemble forecasting could not represent the peak discharge, whereas an additional ensemble spread of updated flood forecasts, using a transposition scheme, provided the accuracy improvement of ensemble mean value and covered the observed discharge in the peak discharge period.

Second, in the first forecast period (rising limb period, left side of Figure 6.9) over the Nanairo dam catchment, additional ensemble spread of flood forecasting using a transposition scheme with a 6-hour update interval could cover the overall observed discharge during the update periods. Meanwhile, in the second forecast period (peak discharge period, right side of Figure 6.9), although the ensemble spread from updated flood forecasts via the transposition method was under-predicted compared with the observed discharge, the accuracy of the ensemble spread and mean value improved with a 6-hour update interval during the peak discharge period over the Nanairo dam catchment.

We also used the index to evaluate accuracy improvement with the results of the original ensemble flood forecasts and post-flood forecasting using the RMSE, which is a quantity used to measure how close each forecast was to the observation. Table 6.3 shows the RMSE comparisons of ensemble mean value from updated flood forecasting, by transposition scheme, in each update period. Each value represents the RMSE in each update period, and the bold percentages in parentheses indicate the improvement ratio compared to the RMSE of prior updated flood forecasting in the same period. As Table 6.3 shows, our newly proposed method for real-time flood forecast updating could enhance the accuracy of post-flood forecasts with a 6-hour update interval, although post-flood forecasting after 12 hours in the rising limb period over the Nanairo dam catchment indicated a decrease (-9.6%) in accuracy due to a slight over-prediction compared to post-flood forecasting after 6 hours, but ensemble spread could cover the observed discharge. Finally, from the results of real-time updating of post-flood forecasts, QPF location correction using a transposition scheme that considers orographic rainfall could improve the accuracy of flood forecasts, but exhibited a negative bias of ensemble mean value as lead time increased.

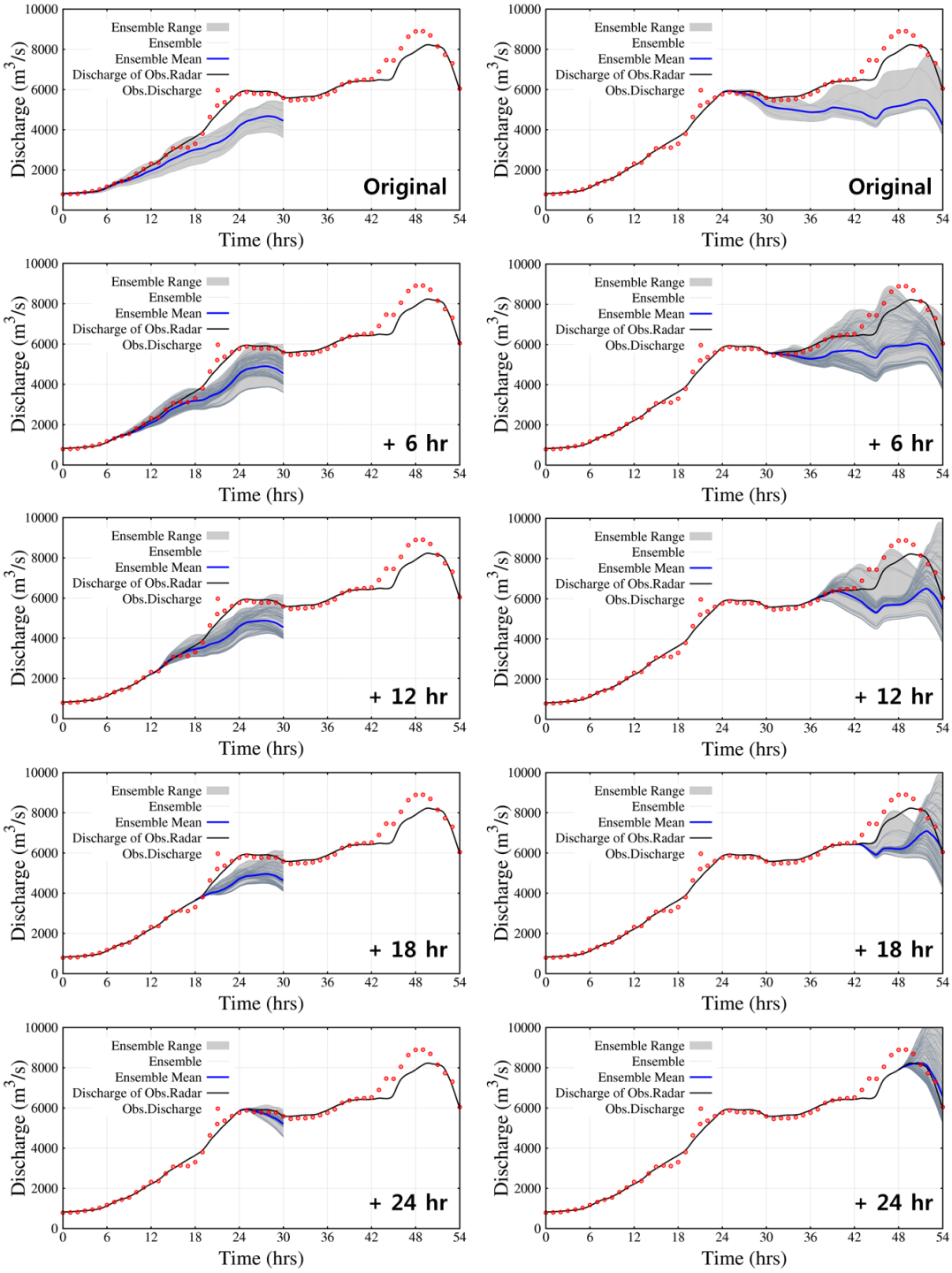

Figure 6.8 Ensemble flood forecasting using the original 11 ensemble members in the first and second forecast period and corresponding post-flood forecasting after 6, 12, 18 and 24 hours via transposition updating over the Futatsuno dam catchment.

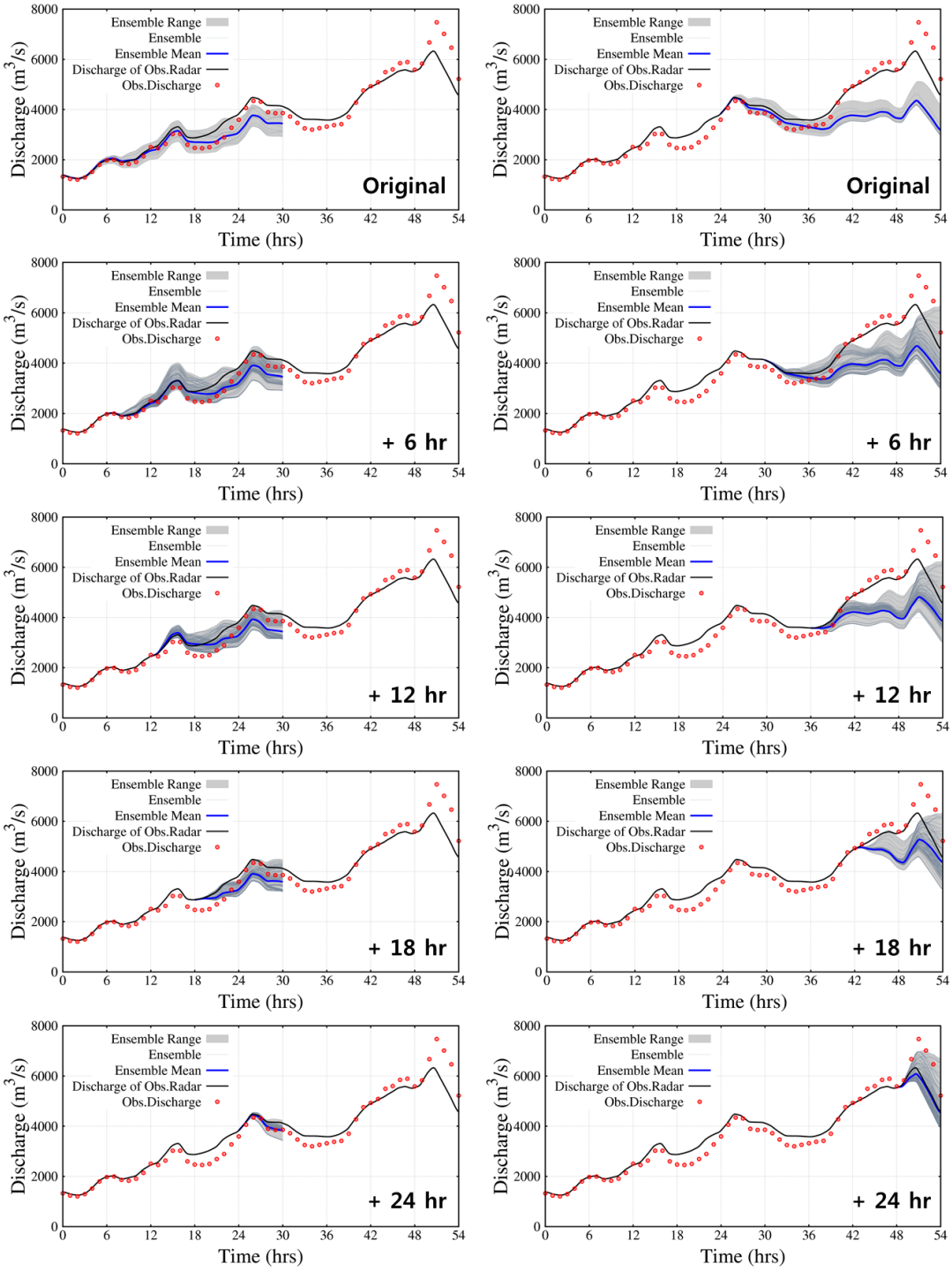

Figure 6.9 Ensemble flood forecasting using the original 11 ensemble members in the first and second forecast period and corresponding post-flood forecasting after 6, 12, 18 and 24 hours via transposition updating over the Nanairo dam catchment.

Table 6.3 RMSE comparisons of updated flood forecasting results.

Catchment	Forecast Period	Original Forecast	Transposition Updating			
			+ 6 h	**+ 12 h**	**+ 18 h**	**+ 24 h**
Futatsuno	1st forecast	940.2	876.8 **(+16.6%)**	915 **(+9.2%)**	962.3 **(+13.3%)**	190.5 **(+79.8%)**
	2nd forecast	1978.7	1695.1 **(+23.2%)**	1881.8 **(+3.5%)**	1810.3 **(+20.6%)**	712.8 **(+59.1%)**
Nanairo	1st forecast	316.2	336.9 **(+3.9%)**	418.7 **(-9.6%)**	406.9 **(+7.4%)**	110.8 **(+75.1%)**
	2nd forecast	1485.9	1460.2 **(+11.9%)**	1529.6 **(+8.8%)**	1378.2 **(+6.6%)**	895.8 **(+48.1%)**

6.4 Summary

This chapter aimed to enhance the transposition method proposed in Chapter 5 and to propose a new real-time updating method for flood forecasting using transposition of ensemble rainfall distributions considering orographic rainfall. At first, ensemble forecast rainfalls from the NWP model are separated into orographic and non-orographic rainfall fields using atmospheric variables of GPV data and extraction of the topography effect. Then the non-orographic rainfall fields are shifted by the transposition scheme to produce additional ensemble information and new ensemble rainfall fields are calculated by recombining the transposition results of non-orographic rainfall fields with separated orographic rainfall. Then, the additional ensemble information is applied into a hydrologic model for post-flood forecasting with a 6-hour interval. Major findings from this chapter led to the following conclusions.

Orographic rainfall was dominant in the Shingu river basin, which is located in a mountainous region; the percentage of orographic rainfall in the verification area exceeded 50 percent and its maximum proportion of total rainfall is 99.8 percent. From the continuity assessment of transposition behaviors of forecasted rainfall distribution using a correlation coefficient in each 6-hour update step, the transposition scheme is continually satisfied during both update steps and has continuity for misplaced locations in the spatial distribution pattern. Thus, our newly proposed method for updating flood forecasts in real time could enhance the under-predicted part of the original ensemble flood forecast method and improve the accuracy of post-flood forecasting with 6-hour update intervals.

In Chapter 6, our transposition scheme focuses on QPF location error correction considering orographic rainfall but not predicted bias correction, which is a quantitative correction that uses the difference between observed and predicted rainfall. For this reason, it is possible to be vulnerable when forecasted rainfall intensity is under-predicted and suitable spatial distribution fails compared with observed reference data. Therefore, bias correction and/or hybrid products with radar-based prediction are required to achieve more reliable hydrologic predictions; bias correction and blending method for accuracy improvement will be addressed in Chapter 7.

Chapter 7

Hybrid Flood Forecasting blending Ensemble NWP Rainfall and Radar-based Prediction considering Orographic Rainfall and Error Field Scheme

Abstract *This chapter proposes hybrid system blending ensemble information from radar-based prediction and numerical weather prediction (NWP) to improve the accuracy of rainfall and flood forecasting. First, an improved radar image extrapolation method proposed by Nakakita et al. (2012), which is comprised of the orographic rainfall identification and the error ensemble scheme, is introduced. Then, ensemble outputs of NWP model are updated based on two different methods. The first one is a bias correction method using mean bias of error fields proposed by Kim et al. (2009). The second one is transposition update method considering orographic rainfall introduced in Chapter 6. Finally, the improved radar-based prediction and updated ensemble NWP rainfall are blended dynamically with changing weight functions, which are computed from the expected skill of each radar prediction and updated NWP rainfall with 3 hrs lead time.*

The proposed method is verified temporally and spatially through a target event and is applied to the hybrid flood forecasting for updating with 1-hr intervals. The newly proposed method based on bias correction shows sufficient reproducibility in peak discharge value compared with the result based on QPF location correction in updated flood forecasting, whereas the blending based on transposition scheme could reduce the width of ensemble spread, which is expressed as the uncertainty, in the flood forecasting.

7.1 Introduction

The quantitative precipitation forecast (QPF) integration is particularly needed in small- and medium-sized mountainous basins where, given the short response time of the watershed, a precipitation forecast is necessary for an extension of the lead time of the flood warning (Toth et al., 2000). For the very short-term and short-term QPF, different methodologies have been developed over several decades. One of them can be achieved through the extrapolation of radar reflectivity field, another one would be the mesoscale Numerical Weather Prediction (NWP) model.

Many basins in Japan are characterized by steep mountainous regions, generating orographic rainfall events. Orographic rainfall may cause localized heavy rainfall to induce flash floods and sediment disasters. However, the accuracy of radar-based rainfall prediction was not enough because of the complex geographical pattern of the mountainous areas. In order to prevent flood disasters and reduce damage due to localized heavy rainfall, characteristics of orographic rainfall must be identified and the characteristics should be considered in a short-term rainfall prediction procedure. For this reason, Nakakita et al. (2012) proposed an improved radar image extrapolation method by combining orographic rainfall identification scheme and the error-field scheme considering error structure. This method improved prediction accuracy in mountainous areas by separating radar rainfall into orographic and non-orographic rain fields, and also considered future prediction error using characteristics of current prediction error with error-field scheme (Nakakita and Terazono, 2008; Kim et al., 2009; Nakakita et al., 2012).

The accuracy of radar-based rainfall prediction performs best for very short lead time, but the accuracy of radar prediction rapidly decreases with increasing lead times. As an alternative to radar prediction, QPFs can also be produced by numerical weather prediction (NWP) models. NWP models simulate the dynamics and physics

of the atmosphere, and therefore they produce more reliable forecasts over longer lead times compared with radar-based prediction (Golding, 2009).

The combination of radar-based prediction with outputs of an NWP model, which is used in short-lead-time forecast, has also provided a considerable advance in science, allowing the prediction of cell development and decay, as well as trajectory. Blending is the merging of rainfall prediction outputs through radar image extrapolation method with outputs of an NWP model. Hybrid blending system of radar-based prediction with NWP rainfall could potentially produce more skillful forecasts than either NWP forecast or radar prediction alone. Several authors have attempted and investigated the blending approaches using two different data sources to improve the accuracy of rainfall prediction in a few hrs (Golding, 1998; Pierce et al., 2001; Lin et al., 2005; Bowler et al., 2006; Atencia et al., 2010). However, to our knowledge, there is research about the merging of two different data sources with NWP and radar directly, but the accuracy improvement of each prediction method with NWP and radar prior to blending technique has not been addressed well in previous research.

The main objective of this chapter is to blend the advantages of ensemble information of radar-based prediction with NWP rainfall for the accuracy improvement of rainfall and flood forecasting in viewpoint of the hybrid forecast. At first, the accuracy of radar image extrapolation method is improved considering orographic rainfall identification and the error-field scheme proposed by Nakakita et al. (2012). And the mesoscale ensemble NWP is also updated using two different methods. The first method is the NWP updating with error-field scheme considering bias correction with future prediction error characteristics proposed by Kim et al. (2009). The second one is the NWP updating with the transposition scheme of rainfall fields considering QPF location correction with the separation of orographic and non-orographic rainfall introduced in Chapter 6. Finally, improved radar-based

prediction and updated ensemble NWP rainfall forecast by two different methods are merged with changing weight function through CSI and RMSE indexes of the previous 3 hrs lead time. The proposed blending method is verified through 2011's largest rainfall event for Typhoon Talas and is applied to the hybrid flood forecasting on two sub-catchments, which are Futatsuno (356.1km^2) and Nanairo (182.1km^2) dam catchments. Figure 7.1 shows a flowchart of the proposed process for the flood-forecasting-blending-improved radar-based prediction and updated ensemble NWP rainfall forecast.

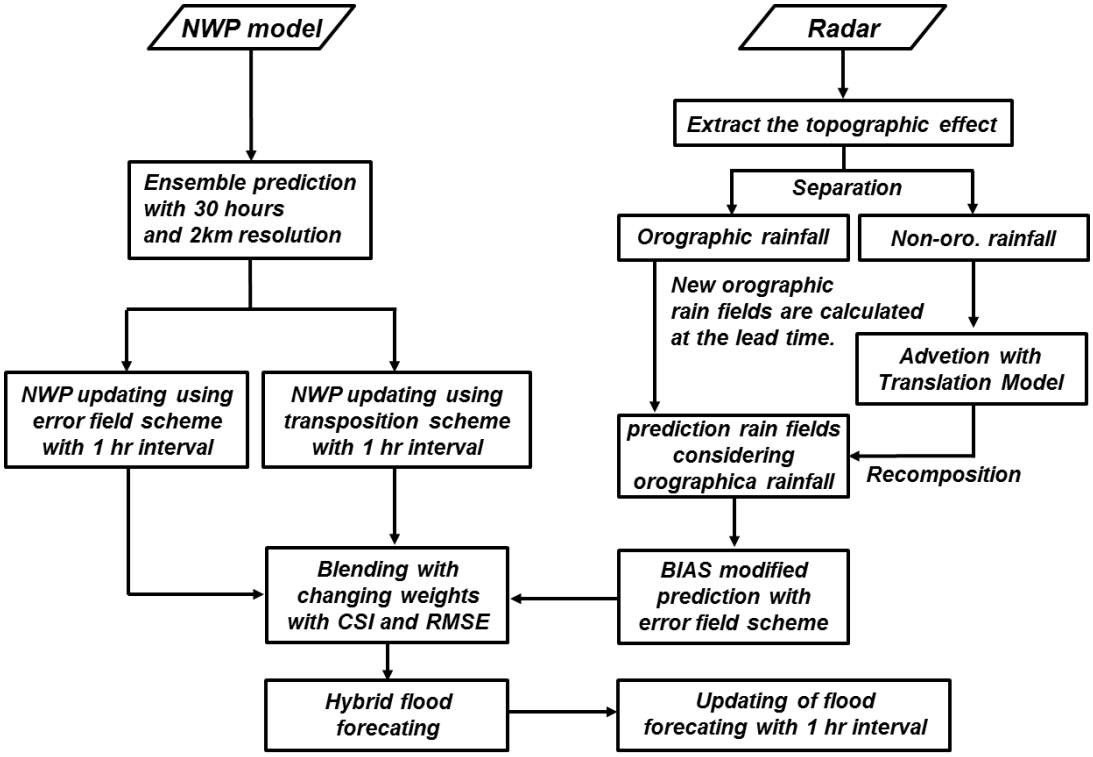

Figure 7.1 Flowchart of the proposed process for flood forecasting blending improved radar-based prediction and updated ensemble NWP rainfall forecasts.

7.2 Data and Methodology

7.2.1 Meteorological Input Data and a Hydrologic Model

The radar data come from the C-band composite radar, provided by Japan's MLIT at a resolution of 1 km and 5 min, and topology data come from the DEM produced by Japan's Geospatial Information Authority at a resolution of 1 km. The target area for radar rainfall prediction is the Kinki region of Japan (Figure 7.2). The datasets are projected onto 123 × 123 grid cells (369 × 369 km with 3 km resolution). Atmospheric variables (e.g., air temperature, horizontal wind, relative humidity) for the separation of orographic and non-orographic rainfall are estimated by the use of GPV data from JMA.

In case of the short-term ensemble NWP rainfall forecast, ensemble prediction with a horizontal resolution of 2 km and 30 hrs forecast time implemented by the MRI is used. The analysis utilizes the 2 sets of ensemble prediction outputs (1^{st} forecast: 2011/09/02 03:00 ~ 09/03 09:00 JST, 30 hrs; 2^{nd} forecast: 2011/09/03 03:00 ~ 09/04 09:00 JST, 30 hrs). And a distributed hydrologic model based on "Object-oriented Hydrological Modelling System" (OHyMoS) is used for flood forecasting by blending improved radar-based prediction and updated ensemble NWP rainfall forecasts in viewpoint of the hybrid forecast. In this model, the one-dimensional kinematic wave method is applied to each grid-cell for subsurface and surface flow simulation. A digital elevation model (DEM) with 250 m resolution is used to calculate the flow direction and to delineate a sub-catchment for each river segment.

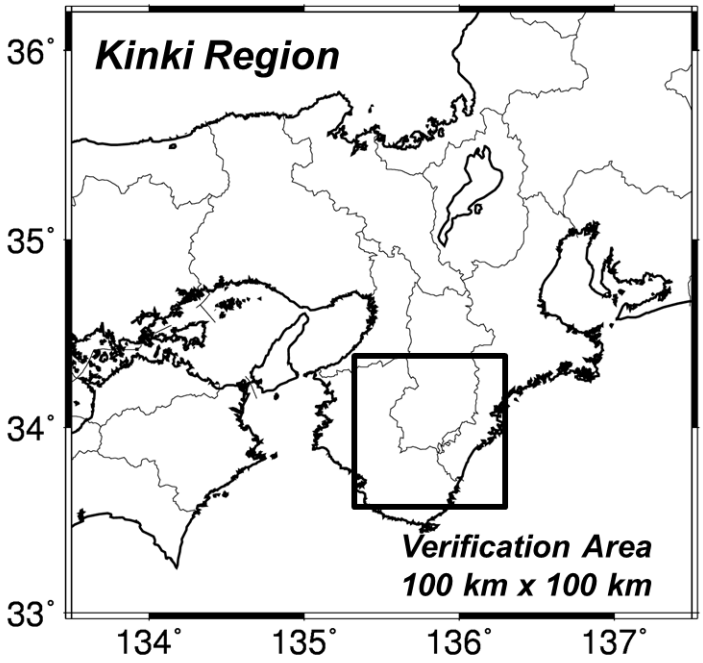

Figure 7.2 Target area for radar rainfall prediction and verification area for CSI and RMSE calculation

7.2.2 Improved Radar Image Extrapolation Method

Many methods for short-term rainfall prediction based on radar data have been proposed. Golding (1998) highlighted that radar-based prediction techniques are able to capture the initial precipitation state. However, as the forecast's lead time increases, the skill of the forecasts rapidly decreases, mainly due to the fact that growth and decay precipitation processes are not taken into account. Nakakita et al. (2012) described a short-term rainfall prediction method using a radar image extrapolation method by combining orographic rainfall identification and the error-field scheme considering error structure. The proposed prediction scheme not only improved the prediction accuracy of the original image extrapolation method by considering the orographic rainfall but also analyzed the prediction error structure by mean bias of error fields spatially and temporally.

Introduction of Translation Model

The translation model by Shiiba et al. (1984) is used for short-term radar rainfall prediction. In this model, the horizontal rainfall intensity distribution, $R(x, y)$ with the spatial coordinate (x, y) at time t is defined as follows:

$$\frac{\partial R(x,y)}{\partial t} + u_r(x,y)\frac{\partial R(x,y)}{\partial x} + v_r(x,y)\frac{\partial R(x,y)}{\partial y} = \delta(x,y) \tag{7.1}$$

where $u_r(x, y)$ and $v_r(x, y)$ are advection velocities along (x, y), respectively, and $\delta(x, y)$ is the rainfall growth-decay rate with lead time. As with other similar equations for the rainfall intensity distribution, characteristics of the translation model are defined by the vectors $u_r(x, y)$, $v_r(x, y)$, and $\delta(x, y)$, which are specified on each grid as follows:

$$u_r(x,y) = c_1 x + c_2 y + c_3 \tag{7.2}$$

$$v_r(x,y) = c_4 x + c_5 y + c_6 \tag{7.3}$$

$$\delta(x,y) = c_7 x + c_8 y + c_9 \tag{7.4}$$

The advection velocities can express the patterns of the non-uniform movement of rainfall, such as rotation and sheer strain (Takasao et al., 1994). In order to optimize the parameters c_1 ~ c_9 using observed radar rainfall data, equations (7.2) ~ (7.4) are approximated by the central difference scheme on the rectangular horizontal area with $\Delta x \times \Delta y$ (e.g. 3×3 km) grid size and Δt (e.g. 5 min) time resolution.

$$
\begin{aligned}
x_i &= \left(i - \frac{1}{2}\right)\Delta x, && i = 1, \cdots, M \\
y_i &= \left(j - \frac{1}{2}\right)\Delta y, && j = 1, \cdots, N \\
t_k &= k\Delta t, && k = -(k-1), \cdots, 0
\end{aligned}
\tag{7.5}
$$

Here, M and N are the number of grids along the x and y-axis, respectively, and K is the number of rainfall patterns used for the optimization. The parameters $c_1 \sim c_9$ are optimized sequentially using the square root information filter and rainfall observations.

$$
J_c = \sum_{k=-K}^{-1} \sum_{i=2}^{M-1} \sum_{j=2}^{N-1} v_{ijk}^2 \tag{7.6}
$$

where

$$
v_{ijk} = \left[\frac{\Delta z}{\Delta t}\right]_{ijk} + (c_1 x_i + c_2 y_j + c_3)\left[\frac{\Delta z}{\Delta x}\right]_{ijk} + (c_4 x_i + c_5 y_j + c_6)\left[\frac{\Delta z}{\Delta y}\right]_{ijk} - (c_7 x_i + c_8 y_j + c_9)
$$

The translation model provides expected rainfall movement under an assumption that the vectors $u_r(x, y)$ and $v_r(x, y)$ are time invariant for the next several hrs. It further assumes that there is no growth-decay of rainfall during that time (i.e., $\delta(x, y) = 0$ for all x and y).

Translation Model considering Orographic Rainfall

Figure 7.3 shows the procedure for short-term radar rainfall prediction using the translation model with consideration of orographic rainfall. This procedure is composed of 4 steps. First, cloud water content is calculated using atmospheric variables from GPV data in each layer and grid. Supposing that the observed radar rainfall (R_{radar}) is that of the lowest layer (200 m height), it is separated into orographic (R_{o1}) and non-orographic (R_{n1}) rainfall by solving equations (6.2) ~ (6.5) in Chapter 6 and using the extraction of topography effect. And it is assumed that the non-orographic rainfall (R_{n1}) can be expressed as the sum of the orographic rainfall (R_{o2}) and non-orographic rainfall (R_{n2}) in the upper layer at height of 200 m. In this way, orographic rainfall of each layer can be calculated from the lowest to the highest layer at heights of 200, 400, 1000, 2000, 3000, 4000, and 5000 m repeatedly. The separation of orographic and non-orographic rain fields agrees with previous separation method based on seeder-feeder mechanism using NWP rainfall fields in Chapter 6, but shot-term radar rainfall prediction method in this chapter needs the composition scheme after advection procedure of non-orographic rainfall. Second, under the assumption that non-orographic rainfalls are not affected by orographic effects, only the separated non-orographic rain fields in the highest layer at heights of 5000 m are advected with translation model up to 3 hrs lead time. At the specific lead time, newly atmospheric variables are calculated from GPV data because atmospheric variables, such as water vapor and wind, are expected to change, even if orographic rain fields are stagnant for several hours. Supposing that the advected non-orographic rain fields are of the top layer at the specific lead time, new orographic rain fields are calculated by solving equations (6.2) ~ (6.5) in Chapter 6 from the top layer to the lower layer. Lastly, prediction rain fields are calculated by combining the orographic and non-orographic rain fields.

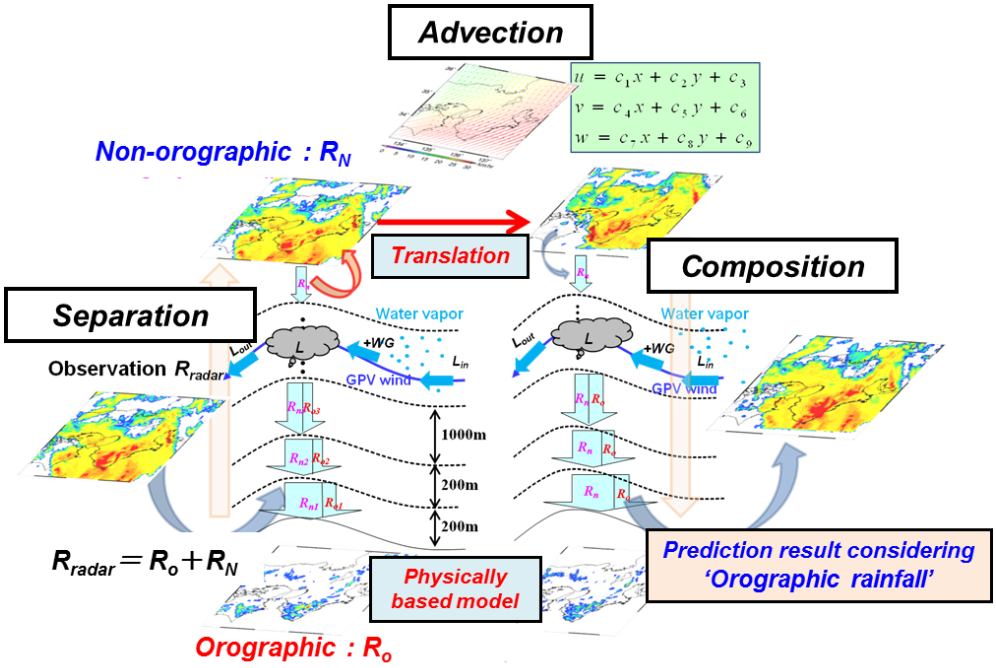

Figure 7.3 Procedure for short-term radar rainfall prediction with translation model considering orographic rainfall (Nakakita et al., 2012)

Ensemble Forecasting Method using Prediction Error Field

Kim et al. (2009) introduced a stochastic prediction method considering the spatial distributions of error in prior prediction rain fields in the translation model, and the extended prediction fields not only improved the accuracy of the original prediction by the translation model but also gave reliability with variant form of rainfall fields. This error-field scheme, which employs a stochastic approach, represents the uncertainty affecting the forecasting of motion and evolution of the rainfall field. The proposed scheme for a stochastic error field simulation uses a certain time length of previous prediction error data to simulate future prediction errors as shown in Figure 7.4, and Nakakita et al. (2012) integrated radar rainfall prediction method considering orographic rainfall with the stochastic prediction method of Kim et al. (2009).

The stochastic prediction method has the assumption that a temporal persistence of the error characteristics continues from the current time (t_o) to the prediction target time. In Figure 7.4, the observed rainfall fields, the deterministic prediction fields, and the prediction error fields are sequentially illustrated until the current time. The spatial distribution of an absolute prediction error (E_k) was considered with the forms:

$$E_k = R_{o,k} - R_{p,k} \qquad (k = 1, 2, ..., n) \tag{7.7}$$

where $R_{o,k}$ is an observed radar rainfall field, $R_{p,k}$ is a predicted rainfall field using the Translation Model, and n is the number of error fields.

The absolute prediction error fields are calculated and statistically analyzed. The calculation in equation (7.7) is conducted for each corresponding grid cell of $R_{o,k}$ and $R_{p,k}$. For the calculation of error fields, total 11 consecutive previous radar prediction results (previous 60 min with 5 min interval) are calculated. The current characteristic of the prediction error through total 11 consecutive previous radar observation and prediction results can be presented by basic statistic fields such as the ensemble mean field $\bar{E}$. It assumed that if the spatio-temporal characteristics of the prediction error are maintained for several hrs, the statistical characteristics of the error on the prediction lead time $t_0 + \Delta T$ are similar to the characteristics of the current error. Finally, the bias-modified prediction field ($R_{p,0}$) is calculated by adding the ensemble mean field $\bar{E}$ to the prediction field (R_p) at time $t_0 + \Delta T$:

$$R_{p,0} = R_p + \bar{E} \tag{7.8}$$

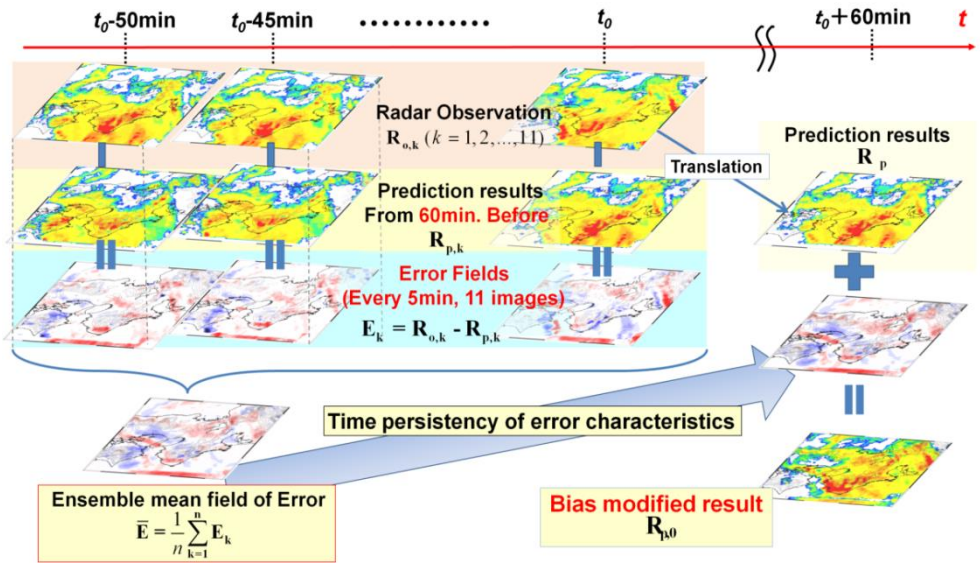

Figure 7.4 Schematic drawing of the error-ensemble prediction algorithm (Kim et al., 2009).

7.2.3 Mesoscale NWP updating Method

NWP Updating with Error-Field Scheme

For the purpose of NWP updating with forecast time interval, the error-field scheme considering the spatial distributions of error in forecasted rain fields, which is the same method as the error-field scheme of improved radar image extrapolation method, is implemented. At first, ensemble NWP rainfall with 11 members and 2 km horizontal resolution is forecasted up to 30 hrs. After 3 hrs, the mean bias of error fields is calculated using 6 consecutive previous observed radar images and original ensemble NWP rainfall outputs (previous 3 hrs with 30 min interval). And then mean bias of 3 hrs error fields gives the information to post ensemble NWP rainfall forecasting (Figure 7.5). These updated 3 hrs in ensemble NWP rainfall are then used to run the blending method, which merges with radar rainfall prediction from improved radar image extrapolation method.

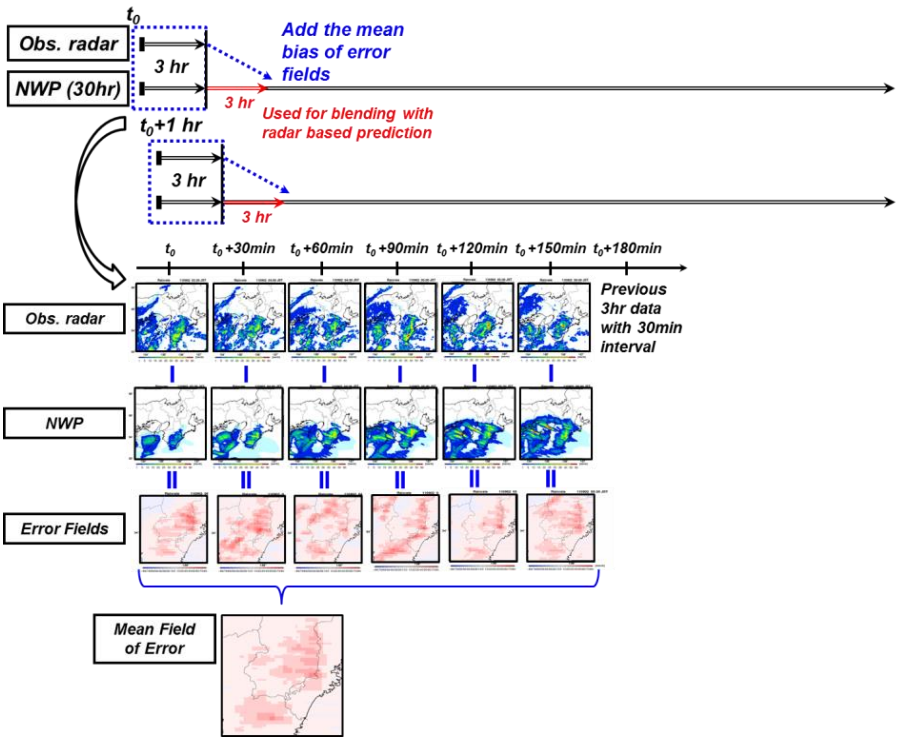

Figure 7.5 Procedure of NWP updating using error-field scheme.

NWP Updating with Transposition Scheme

The transposition scheme considering orographic rainfall introduced in Chapter 6 is also used for the NWP updating and blending with radar-based prediction from improved radar image extrapolation method. Figure 7.6 shows the proposed process for NWP updating using transposition of rainfall fields considering orographic rainfall. As stated in Chapter 6, at first, ensemble NWP rainfall is separated into orographic and non-orographic rain fields using the extraction of topography effect. Then the non-orographic rainfall fields are examined by the transposition scheme to produce additional ensemble information for QPF location error correction, and ensemble NWP rainfall fields are calculated by recombining the transposition results of non-orographic rain fields with the orographic rainfall. After 6 hours from the starting of the ensemble NWP rainfall forecast, the recombined ensemble rain fields

are spatially verified by MLIT C-band composite radar data with error indexes, which are critical success index (CSI) and root mean square error (RMSE) to find out the best ensembles and transposed locations. And for the NWP updating and blending with radar-based prediction, the best 20 transposed ensemble domains from the CSI and RMSE verification are selected, and give information to the next NWP updating step with 1 hr interval. These updated 3 hours forecast data in transposed NWP rainfall are then used to run the blending method, which merges the updated NWP rainfall with radar-based prediction from the improved radar image extrapolation method.

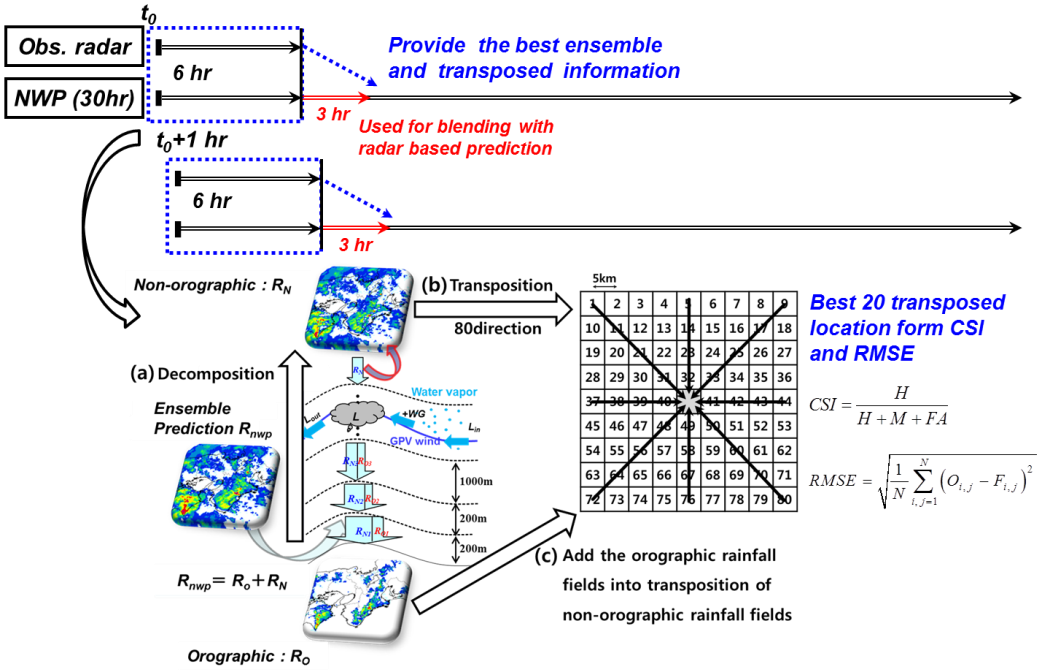

Figure 7.6 Procedure of NWP updating using transposition scheme

7.2.4 Blending NWP with Radar-based Prediction

To make optimized short-term rainfall prediction until 3 hrs ahead, the results of the radar-based prediction considering orographic rainfall and error-field scheme with each updated ensemble NWP rainfall based on the error-field scheme and the transposition scheme integrated using a blending method proposed in this chapter. The blending forecast outputs are produced and updated with 1 hr time step intervals according to merging weights, which are computed from the expected skills of the radar-based prediction and the updated NWP forecast.

In the blending of the radar based prediction with updated NWP rainfall using error-field scheme, given the starting time t_o of the ensemble NWP rainfall forecast for a given event, the blending method with updated NWP rainfall using error-field scheme is configured to start a blend forecast after 6 hrs (t_o+6h) until 3 hrs ahead (t_o+9h) on a 30 hr forecast window of ensemble NWP rainfall forecast because it takes 3 hrs for the calculation of mean bias between observed radar and original ensemble NWP rainfall in updating step, and also takes 3hrs for the calculation of weights for first blending forecast step.

On the other hand, in the blending of the radar-based prediction with updated NWP rainfall using transposition scheme, the blending method is configured to start a blend forecast after 9 hrs (t_o+9h) until 3 hrs ahead (t_o+12h) because it takes 6 hrs for the calculation of the best 20 transposed ensemble domains from the CSI and RMSE verification, and also takes 3hrs for the calculation of weights for first blending forecast step. Then, a 1 hr forecasting time step interval after 6 hrs and 9 hrs for blending forecasts using error-field scheme and transposition scheme, respectively, is adopted and updated at 1km resolution on the 100 km × 100 km domain of verification area shown in Figure 7.2.

For the calculation of weights for the blending forecast step, one needs to investigate several indexes and thresholds prior to setting the optimal blending procedure over the verification area. In order to compute the weights in a suitable way, we used the tested indexes, which are CSI and RMSE, to consider each characteristic for the lead times of 30, 60, 90, 120, 150, and 180 min and the thresholds of 0.1, 0.5, 1.0, 5.0, 10.0 and 20.0 mm/h.

$$CSI = \frac{H}{H + M + FA} \tag{7.9}$$

$$RMSE = \sqrt{\frac{1}{N}\sum_{i,j=1}^{N}\left(O_{i,j} - F_{i,j}\right)^2} \tag{7.10}$$

where N is the total grid cells (100 × 100) in verification area, $O_{i,j}$ and $F_{i,j}$ are the observed and forecasted rainfall of each grid cell at forecast time t, H is the number of correct forecasts over the threshold (i.e., when the rainfall that is forecasted is also observed), and M is the number of times rainfall is not forecasted but is observed. FA is the number of times rainfall is forecasted but not observed.

At t_o+6h time point in the blending with updated NWP rainfall using the error-field scheme, CSI and RMSE indexes of updated NWP rainfall and radar prediction are computed from the previous 3 hrs (t_o+3h) to 3 hrs ahead (t_o+6h) compared with previous observed radar data for the lead times of 30, 60, 90, 120, 150, and 180 min and the thresholds of 0.1, 0.5, 1.0, 5.0, 10.0, and 20.0 mm/h. High thresholds restrict rain events to heavy rains, while low thresholds not only represent light rains but also consider all rains from light to heavy rains. Therefore, estimated CSI and RMSE indexes from the lead times of 30, 60, 90, 120, 150 and 180 min and the 5 mm/h threshold, which can be take into account a suitable threshold for both light and

heavy rains, are used for each merging weight of updated NWP rainfall forecast and radar-based prediction. And estimated CSI and RMSE from t_o+3h to t_o+6h are introduced in the equations (7.11) and (7.12) with square type to estimate the weights for the blending forecast from t_o+6h until 3 hrs. In RMSE index, low value has preference, so it was subtracted from 1. Through these weights of updated NWP rainfall and radar-based prediction by computing CSI and RMSE indexes from t_o+3h to t_o+6h, two coefficients are computed as follow equation (7.13) with average value of two weights. Coefficients of NWP and radar depend on the prediction lead time because the accuracy of each method depends on the prediction lead time. The sum of two coefficients of NWP and radar is 1, and computed coefficient of each lead time from t_o+3h to t_o+6h gives information to hybrid blending forecasts from t_o+6h to t_o+9h in case of the blending with the error-field scheme. Finally, the hybrid blending forecast is computed from equation (7.14), and blending forecasts are updated with a 1 hr time step interval after 6 hrs in case of error-field scheme.

On the other hand, in the blending with updated NWP rainfall forecast using the transposition scheme, at t_o+9h time point, CSI and RMSE indexes of updated NWP forecast and radar-based prediction are computed from previous 3 hrs (t_o+6h) to 3 hrs ahead (t_o+9h), and estimated CSI and RMSE indexes from the lead times of 30, 60, 90, 120, 150, and 180 min and the 5 mm/h threshold are used for each merging weight of updated NWP rainfall and radar-based prediction. However, in case of blending with error-field scheme, 11 ensemble members for blending with radar-based prediction are equal to that after the NWP updating, whereas in case of blending with transposition scheme, the selected best 20 ensemble members from the CSI and RMSE verification are changed in each 6 hrs transposition step. For this reason, the weights from equations (7.11) and (7.12) could not be used for own ensemble member; therefore, we used the coefficients of updated NWP rainfall and radar prediction with the average weights of the selected best 20 ensemble members in each NWP updating step based on equation (7.15). And computed coefficient of

each lead time from t_o+6h to t_o+9h gives information to hybrid blending forecasts from t_o+9h to 3 hrs ahead (t_o+12h). Finally, the hybrid blending forecast is computed from equation (7.16), and blending forecasts are updated with a 1 hr time step interval.

$$w_{nwp,i,1} = \frac{CSI_{nwp,i}^2}{CSI_{radar}^2 + CSI_{nwp,i}^2}$$
$$w_{nwp,i,2} = 1 - \frac{RMSE_{nwp,i}^2}{RMSE_{radar}^2 + RMSE_{nwp,i}^2} \tag{7.11}$$

$$w_{radar,i,1} = \frac{CSI_{radar,i}^2}{CSI_{radar}^2 + CSI_{nwp,i}^2}$$
$$w_{radar,i,2} = 1 - \frac{RMSE_{radar,i}^2}{RMSE_{radar}^2 + RMSE_{nwp,i}^2} \tag{7.12}$$

$$C_{nwp,i} = \frac{w_{nwp,i,1} + w_{nwp,i,2}}{2}$$
$$C_{radar,i} = \frac{w_{radar,i,1} + w_{radar,i,2}}{2} \tag{7.13}$$

$$\begin{bmatrix} R_{blend,1} \\ R_{blend,2} \\ R_{blend,3} \\ \cdot \\ \cdot \\ R_{blend,10} \\ R_{blend,11} \end{bmatrix} = \begin{bmatrix} C_{radar,1} \\ C_{radar,2} \\ C_{radar,3} \\ \cdot \\ \cdot \\ C_{radar,10} \\ C_{radar,11} \end{bmatrix} \times R_{radar} + \begin{bmatrix} C_{nwp,1} \\ C_{nwp,2} \\ C_{nwp,3} \\ \cdot \\ \cdot \\ C_{nwp,10} \\ C_{nwp,11} \end{bmatrix} \times \begin{bmatrix} R_{nwp,1} \\ R_{nwp,2} \\ R_{nwp,3} \\ \cdot \\ \cdot \\ R_{nwp,10} \\ R_{nwp,11} \end{bmatrix} \tag{7.14}$$

$$C_{nwp} = \frac{1}{N}\sum_{i=1}^{N}\frac{w_{nwp,i,1} + w_{nwp,i,2}}{2}$$
$$C_{radar} = \frac{1}{N}\sum_{i=1}^{N}\frac{w_{radar,i,1} + w_{radar,i,2}}{2} \quad (7.15)$$

$$\begin{bmatrix} R_{blend,1} \\ R_{blend,2} \\ R_{blend,3} \\ \cdot \\ \cdot \\ R_{blend,19} \\ R_{blend,20} \end{bmatrix} = C_{radar} \times R_{radar} + C_{nwp} \times \begin{bmatrix} R_{nwp,1} \\ R_{nwp,2} \\ R_{nwp,3} \\ \cdot \\ \cdot \\ R_{nwp,19} \\ R_{nwp,20} \end{bmatrix} \quad (7.16)$$

where $w_{nwp,i,1}$ and $w_{nwp,i,2}$ are weights from CSI and RMSE calculation of each member of ensemble NWP rainfall, $w_{radar,1}$ and $w_{radar,2}$ are weights from CSI and RMSE calculation of radar prediction outputs, C_{nwp} and C_{radar} are coefficients of ensemble NWP rainfall and radar prediction for blending of each lead time, i is ensemble members of NWP (11 ensemble members in case of blending with error-field scheme and 20 ensemble members in case of blending with transposition scheme), R_{nwp} and R_{radar} are outputs of each grid cell from ensemble NWP and radar prediction, and R_{blend} is the forecasted blending rainfall with NWP and radar of each grid cell.

7.3 Results and Discussion

7.3.1 Verification Results of Rainfall Prediction

Improved Radar Image Extrapolation Method

As the view into the performances of each radar prediction method, Figure 7.7 shows accumulated rainfall by MLIT C-band composite radar data and its corresponding radar prediction results with 3 hrs lead time and scatter plots during typhoon Talas event. The prediction result by advection of translation model could not represent the accumulated rainfall distribution over 1,000 mm in mountainous regions, whereas the prediction result considering orographic rainfall expressed the orographic rainfall distribution generated from orographic effect, and the prediction result combining orographic rainfall and error-field scheme could reproduce the accumulated rainfall distribution compared with observed radar rainfall.

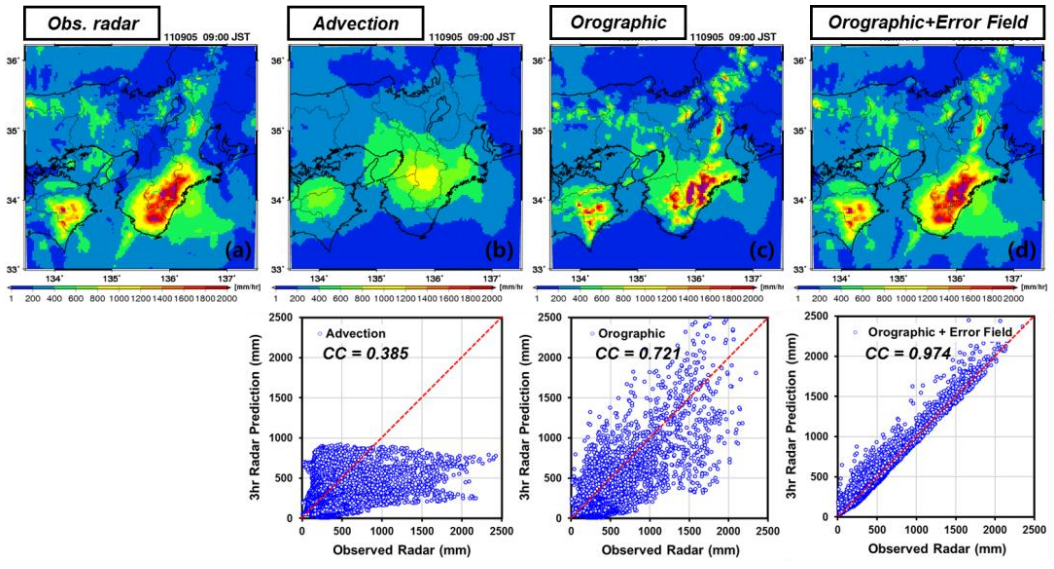

Figure 7.7 Accumulated rainfall results with 3 hrs lead time and scatter plots by each method during typhoon Talas

And a simple verification measure using correlation coefficient was adopted for the purpose of the performance assessment of each prediction method. The correlation coefficient has been computed as follows:

$$corr = \frac{\mathrm{cov}(F,O)}{\sigma_F \sigma_O} = \frac{N\sum_{i=1}^{N} F_i O_i - \sum_{i=1}^{N} F_i \sum_{i=1}^{N} O_i}{\sqrt{\left[N\sum_{i=1}^{N} F_i^2 - \left(\sum_{i=1}^{N} F_i\right)^2\right]\left[N\sum_{i=1}^{N} O_i^2 - \left(\sum_{i=1}^{N} O_i\right)^2\right]}} \quad (7.17)$$

where F is the prediction rainfall, O_i is the observed radar rainfall, cov is the covariance of F and O, σ_F and σ_O are the standard deviations of F and O, respectively, and N is the number of grid cells within the domain.

Table 7.1 shows the computed correlation coefficients for each prediction method. The correlation coefficient does not measure the forecast accuracy and does not take into account the bias in the forecasts. However, it is able to describe the association between the forecasts dataset and the reference dataset (e.g., corr = 1 indicates a perfect positive linear relationship between forecasts and reference observations). Therefore, even though the correlation coefficient cannot be considered an exhaustive measure of forecasts quality, it was considered suitable to provide a comparative analysis of the observed radar rainfall and each prediction method.

Table 7.1 Computed correlation coefficients for each prediction method.

Translation model	Orographic rainfall	Orographic + error field
0.385	0.721	0.974

From these results, Figure 7.7 suggests that improved radar image extrapolation method considering both orographic rainfall and the error-field scheme predicted accurately the accumulated rainfall amount and spatial location compared with the observed radar rainfall, and the scatter plots of each prediction method show that improved radar prediction method combining orographic rainfall and error-field scheme had better results than other prediction methods.

And CSI and RMSE were used again to investigate the performance of each prediction method as well as the use of the calculation of weights to blend the ensemble NWP forecast and radar-based prediction. The performance of each prediction method was estimated by selecting increasing rainfall intensity thresholds of 0.1, 0.5, 1.0, 5.0, 10.0, and 20.0 mm/h and increasing lead time of 30, 60, 90, 120, 150, and 180 min during the target forecast period (2011/09/02 03:00 ~ 09/04 09:00 JST, 54 hrs).

Figure 7.8 shows one of prediction results of average values of CSI and RMSE during the target forecast period with increasing lead time and 5 mm/h rainfall threshold. The average CSI decreases with lead time between 30 min and 3 hrs for all prediction methods, but the CSI of improved prediction method considering both orographic rainfall and error field was maintained over 0.7 value with lead time, and it provided the best result over other methods in spatial forecast location. In the average RMSE with lead time, proposed radar prediction method also improved the accuracy from 90 min to 180 min lead time. On the other hand, the simple advection by translation model provided the best RMSE index from 30 min to 60 min lead time. This result implies that simple radar image extrapolation produces a suitable prediction result in case of very short-range prediction of an extreme typhoon event.

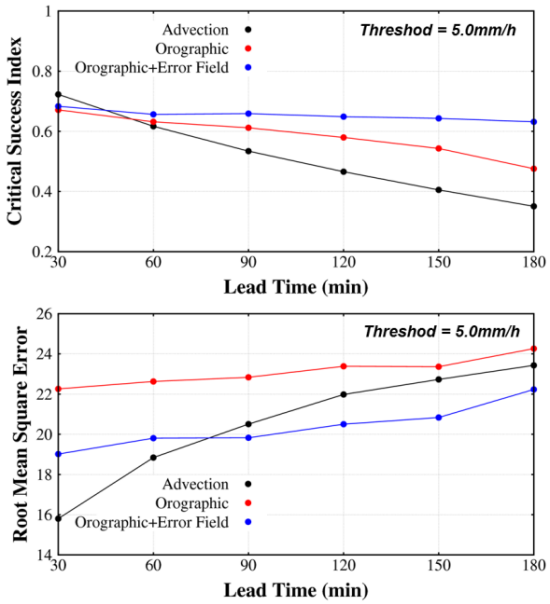

Figure 7.8 Average values of CSI and RMSE of each radar prediction result

NWP Updating with Error-Field Scheme

Figure 7.8 shows average values of CSI and RMSE of updated NWP rainfall by error-field scheme with lead time and 5 mm/h rainfall threshold compared with the radar prediction considering orographic rainfall and error-field scheme. In CSI results, all ensembles were maintained to be closed to 0.8 values. In RMSE results, average RMSE has from 17 to 18 value with lead time except for 1 member (member 8 in Figure 2.5) over the 21 value. Through the comparison between updated NWP rainfall and radar prediction result, the average CSI and RMSE by updated NWP rainfall produced higher performances than radar prediction result. It can be explained by Figure 7.10. In a previous study, CSI and RMSE results of raw control run during 2 sets of ensemble prediction outputs (1st forecast: 2011/09/02 03:00 ~ 09/03 09:00 JST, 30 hrs; 2nd forecast: 2011/09/03 03:00 ~ 09/04 09:00 JST, 30 hrs) had low values because forecasted rain field movement was faster as the lead time was longer, so the rainfall forecast pattern has been deviated from verification area.

In this situation, mean bias by error fields of observed radar and NWP give to raw NWP forecasting. As a result, updated NWP has been improved through the accurate spatial information from mean field of error structure (Figure 7.10).

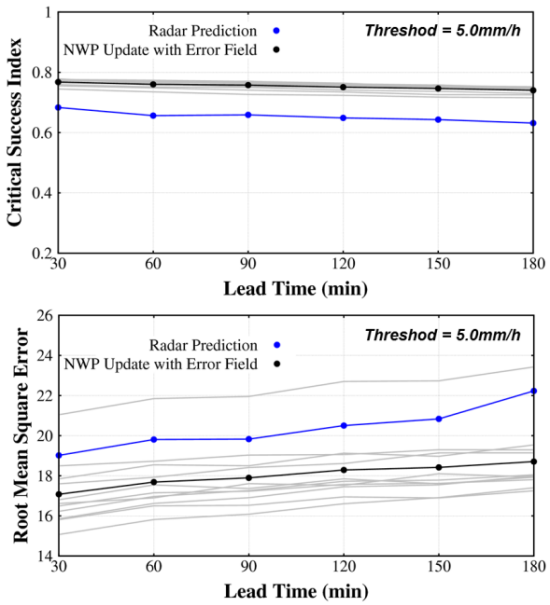

Figure 7.9 Average values of CSI and RMSE of updated ensemble NWP rainfall using error-field scheme

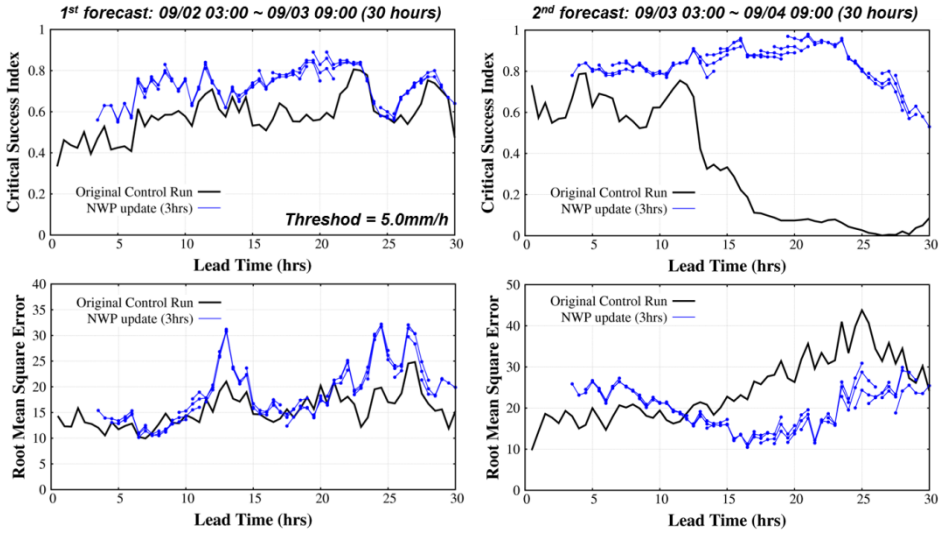

Figure 7.10 Average values of CSI and RMSE for control run of original ensemble NWP and updated NWP rainfall for 3 hrs lead time with 1 hr interval

NWP Updating with Transposition Scheme

Figure 7.11 shows average values of CSI and RMSE of updated NWP rainfall by transposition scheme with lead time and 5 mm/h rainfall threshold compared with the radar prediction considering orographic rainfall and error-field scheme. In CSI results, all ensembles were maintained to be closed to 0.6 values. In RMSE results, average RMSE has from 20 to 22 value. Through the comparison between updated NWP rainfall and radar prediction result, contrary to updated NWP rainfall with error-field scheme, the average CSI and RMSE of radar prediction produced higher performances than updated NWP rainfall result. This is because the transposition scheme is not a method for the bias correction, just the QPF location error correction, so transposition scheme could improve the forecast performance by more than original ensemble NWP rainfall, which is indicated in the original control run result of Figure 7.10. However, radar prediction considering the orographic rainfall and bias correction from error-field scheme provided better results than the updated NWP rainfall in CSI and RMSE verification.

Figure 7.12 shows comparison of updated ensemble NWP rainfall using error-field scheme and transposition scheme in terms of average values of CSI and RMSE with lead time and 5 mm/h rainfall threshold. From this result, the updated NWP rainfall considering bias correction from the error-field scheme provided better results than that considering location correction from the transposition scheme.

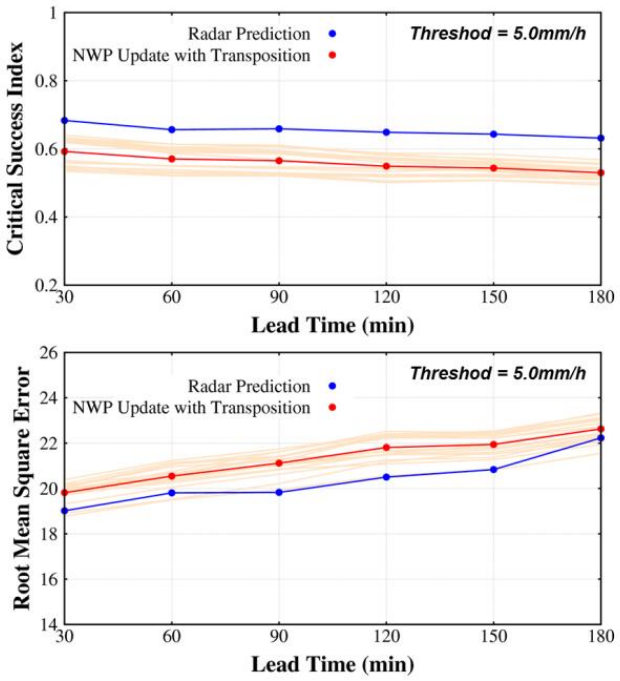

Figure 7.11 Average values of CSI and RMSE of updated ensemble NWP rainfall using transposition scheme

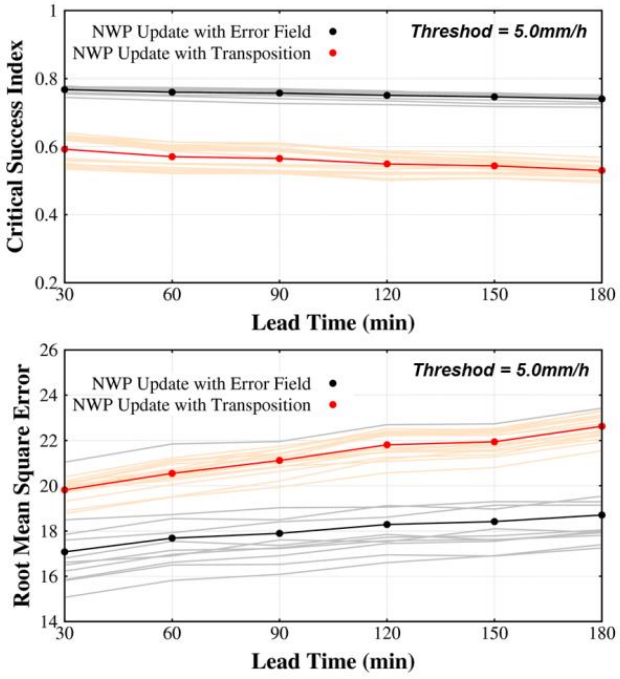

Figure 7.12 Comparison of updated ensemble NWP rainfall using error-field scheme and transposition scheme

Blending with Error-Field Scheme

As stated above, the radar-based prediction considering orographic rainfall and error-field scheme with updated ensemble NWP rainfall was blended up to 3 hrs with 1 hr time step according to weights, which are computed from the CSI and RMSE. The estimated weights from CSI and RMSE indexes of updated NWP forecast and radar prediction are computed from the previous 3 hrs (t_o+3h) to 3 hrs ahead (t_o+6h) for the calculation of blending coefficient, and computed coefficient of each lead time from t_o+3h to t_o+6h gives information to hybrid blending forecasts from t_o+6h to t_o+9h in case of the blending with the error-field scheme.

In the use of estimated coefficient in the blending step, we considered 3 different methods. The first method is the use of the coefficient of same lead time before 3 hr (e.g., the blending coefficient for 1 hr lead time (t_o+7h) at t_o+6h time point and use of the estimated coefficient of 1 hr lead time (t_o+4h) at t_o+3h time point). The second method is the use of the average coefficient of prior same lead time for time series statistical analysis (e.g., the blending coefficient for 1 hr lead time (t_o+16h) at t_o+15h time point and use of the average coefficient of 1 hr lead time (t_o+7h, +10h and +13h) at t_o+6h, +9h and +12h time point). The third method is the use of the average coefficient from prior 3 hrs until 3 hrs ahead (e.g., the blending coefficient for all lead time from t_o+6h to t_o+9h and use of the average coefficient of all lead time from t_o+3h to t_o+6h).

Figure 7.13 shows average CSI and RMSE results among 3 different blending methods with regard to the estimation of coefficient with lead time and 5 mm/h threshold. Case A means the method using the coefficient of same lead time before 3 hr, Case B means the method of the average coefficient of prior same lead time for time series statistical analysis , and Case C means the method of the average coefficient from prior 3 hrs until 3 hrs ahead as stated above. Through Figure 7.13,

we confirmed that average CSI and RMSE results of three methods are almost the same performance. These results can be explained by the estimated coefficient used in blending of the updated NWP rainfall using error-field scheme and radar-based prediction with lead time represented in Figure 7.14. The estimated coefficient is also almost constant with lead time by the bias correction from error-field scheme, so average CSI and RMSE results of three methods are almost the same performance in Figure 7.13. In this chapter, the coefficient of same lead time before 3 hr (Case A) is used for blending of updated NWP rainfall and radar-based prediction.

Figure 7.15 shows average values of CSI and RMSE among radar-based prediction considering orographic rainfall and error-field scheme, updated NWP rainfall with error-field scheme, and blending of radar prediction and updated NWP rainfall with lead time and 5 mm/h threshold. Through Figure 7.15, the blending of updated NWP rainfall using error-field scheme and radar prediction improved the rainfall prediction accuracy with lead time than the results of radar prediction and updated NWP rainfall.

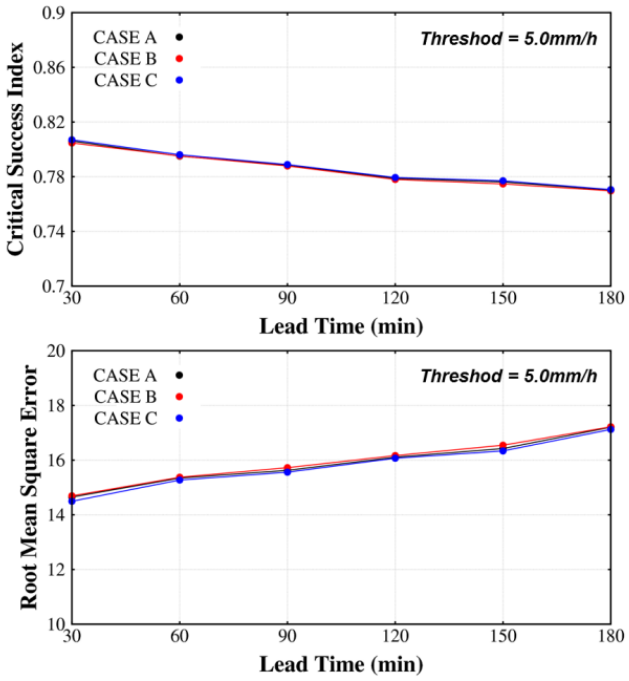

Figure 7.13 Comparison of average CSI and RMSE results among three different blending methods with regard to the estimation of coefficient

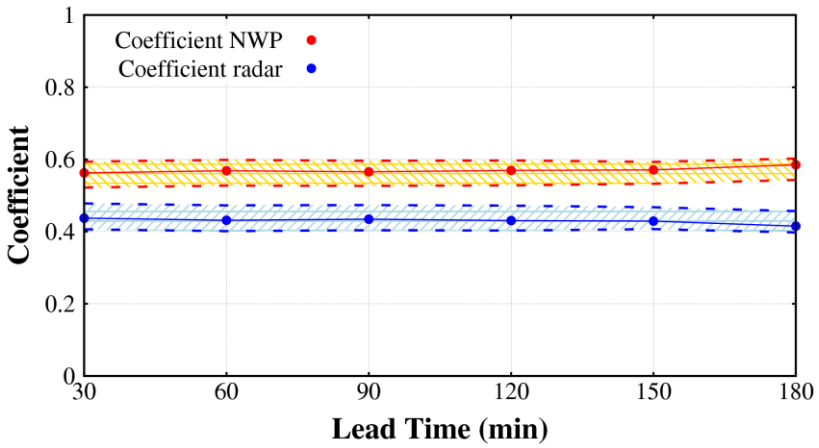

Figure 7.14 Estimated coefficient used in blending of the updated NWP rainfall using error-field scheme and radar-based prediction

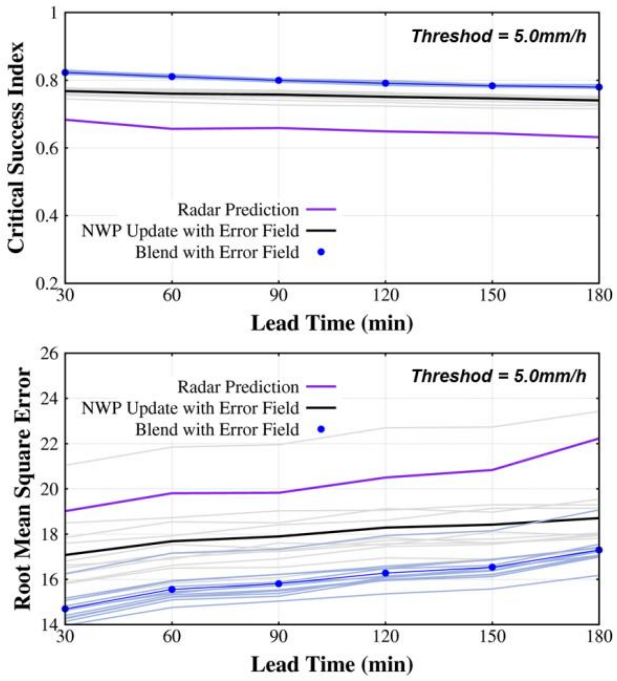

Figure 7.15 Average values of CSI and RMSE among radar prediction, updated NWP rainfall with error-field scheme, and blending forecast

Blending with Transposition Scheme

Figure 7.16 shows average values of CSI and RMSE among radar-based prediction considering orographic rainfall and error-field scheme, updated NWP rainfall with transposition scheme, and blending results with lead time and 5 mm/h threshold. Figure 7.17 represents comparison result of blending using error-field scheme and transposition scheme. From Figure 7.16, the blending of updated NWP rainfall using transposition scheme and radar prediction could provide better prediction accuracy with lead time than the results of radar prediction and updated NWP rainfall alone. However, the blending result considering bias correction from error-field scheme had a higher performance than the result considering QPF location correction from transposition scheme represented in Figure 7.17. And Table 7.2 and 7.3 represent comparisons of average CSI and RMSE values with lead time and all rainfall intensity thresholds. From these results, the improvement achieved by merging the radar prediction with the updated NWP rainfall using error-field scheme becomes more appreciable as the forecasts advance in lead time and the rainfall intensities become higher.

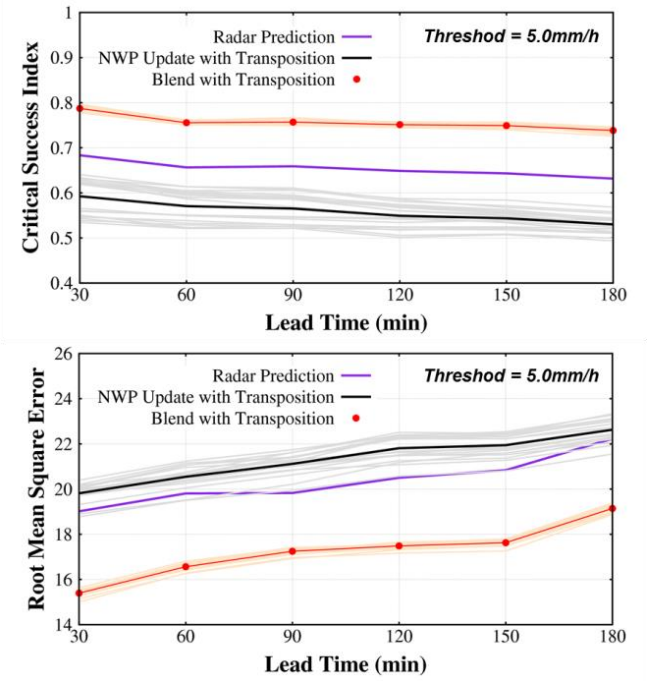

Figure 7.16 Average values of CSI and RMSE among radar prediction, updated NWP rainfall with transposition scheme, and blending forecast

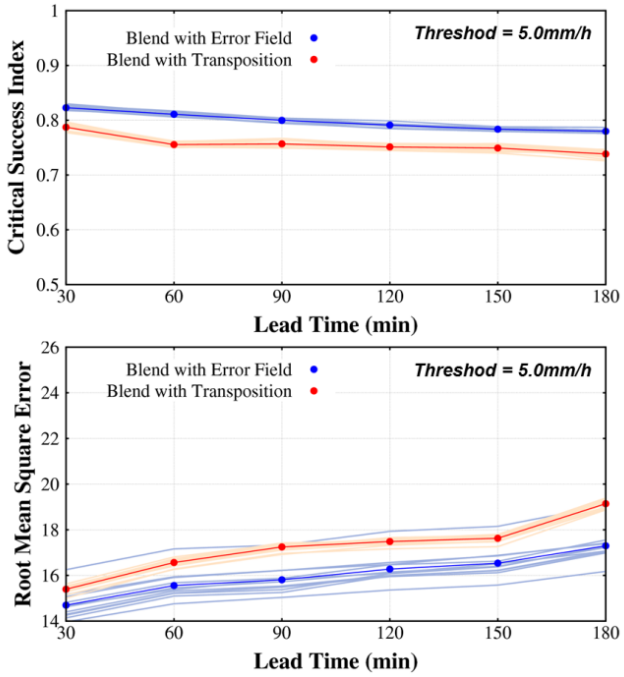

Figure 7.17 Comparison of average values of CSI and RMSE of blending results using error-field scheme and transposition scheme

Table 7.2 Average CSI value among radar prediction, NWP updating, and blending with lead time and thresholds

Lead Time	Type	Thresholds (mm)					
		0.1	0.5	1.0	5.0	10.0	20.0
60 min	Radar Prediction	0.81	0.79	0.78	0.66	0.55	0.38
	NWP update (Transposition)	0.89	0.82	0.77	0.57	0.43	0.23
	NWP update (Error)	0.94	0.92	0.90	0.76	0.65	0.45
	Blend (Transposition)	0.96	0.93	0.91	0.76	0.64	0.42
	Blend (Error)	**0.97**	**0.95**	**0.93**	**0.81**	**0.71**	**0.51**
120 min	Radar Prediction	0.80	0.78	0.77	0.65	0.54	0.38
	NWP update (Transposition)	0.88	0.81	0.75	0.55	0.41	0.22
	NWP update (Error)	0.94	0.91	0.89	0.75	0.64	0.44
	Blend (Transposition)	0.95	0.92	0.90	0.75	0.63	0.41
	Blend (Error)	**0.96**	**0.94**	**0.93**	**0.79**	**0.69**	**0.49**
180 min	Radar Prediction	0.80	0.78	0.77	0.63	0.52	0.36
	NWP update (Transposition)	0.87	0.80	0.74	0.53	0.40	0.21
	NWP update (Error)	0.94	0.91	0.89	0.74	0.63	0.42
	Blend (Transposition)	0.95	0.92	0.89	0.74	0.60	0.38
	Blend (Error)	**0.96**	**0.94**	**0.92**	**0.78**	**0.68**	**0.47**

Table 7.3 Average RMSE value among radar prediction, NWP updating, and blending with lead time and thresholds

Lead Time	Type	Thresholds (mm)					
		0.1	0.5	1.0	5.0	10.0	20.0
60 min	Radar Prediction	17.92	18.02	18.10	19.81	23.07	31.65
	NWP update (Transposition)	18.58	18.66	18.74	20.55	24.10	32.94
	NWP update (Error)	16.17	16.21	16.27	17.8	20.56	28.58
	Blend (Transposition)	15.29	15.32	15.37	16.56	19.47	27.91
	Blend (Error)	**14.41**	**14.43**	**14.46**	**15.56**	**18.08**	**25.90**
120 min	Radar Prediction	18.63	18.72	18.79	20.50	23.84	32.30
	NWP update (Transposition)	19.76	19.85	19.94	21.81	25.43	34.19
	NWP update (Error)	16.79	16.83	16.88	18.29	21.18	29.26
	Blend (Transposition)	16.23	16.26	16.31	17.48	20.38	28.97
	Blend (Error)	**15.15**	**15.17**	**15.20**	**16.28**	**18.84**	**26.77**
180 min	Radar Prediction	20.28	20.37	20.44	22.23	25.77	35.26
	NWP update (Transposition)	20.51	20.62	20.72	22.63	26.32	35.03
	NWP update (Error)	17.25	17.29	17.33	18.71	21.56	29.73
	Blend (Transposition)	17.79	17.84	17.90	19.14	22.22	31.03
	Blend (Error)	**16.14**	**16.16**	**16.19**	**17.30**	**19.94**	**28.01**

7.3.2 Application in Hybrid Flood Forecasting

The proposed approach for ensemble NWP updating and the blending with radar prediction has been applied to the flood forecasting in the viewpoint of hybrid forecasting on two sub-catchments, which are Futatsuno (356.1km^2) and Nanairo (182.1km^2) dam catchments for the largest flood event by typhoon Talas of 2011. Figure 7.18 represents the strategy for hybrid flood forecasting using blending and updated NWP results. At first, the blending result with updated NWP rainfall and radar prediction is configured to start a blend forecast after 6 hrs (t_o+6h: error field scheme) and 9 hrs (t_o+9h: transposition scheme) until 3 hrs ahead (t_o+6h and t_o+9h: error field scheme, t_o+9h and t_o+12h: transposition scheme). Then updated NWP rainfall is used for post-flood forecasting after 3 hr from 6 hrs (t_o+6h: error-field scheme) and 9 hrs (t_o+9h: transposition scheme) up to a 30-hr forecast window. And this process is continued with a 1 hr time step interval.

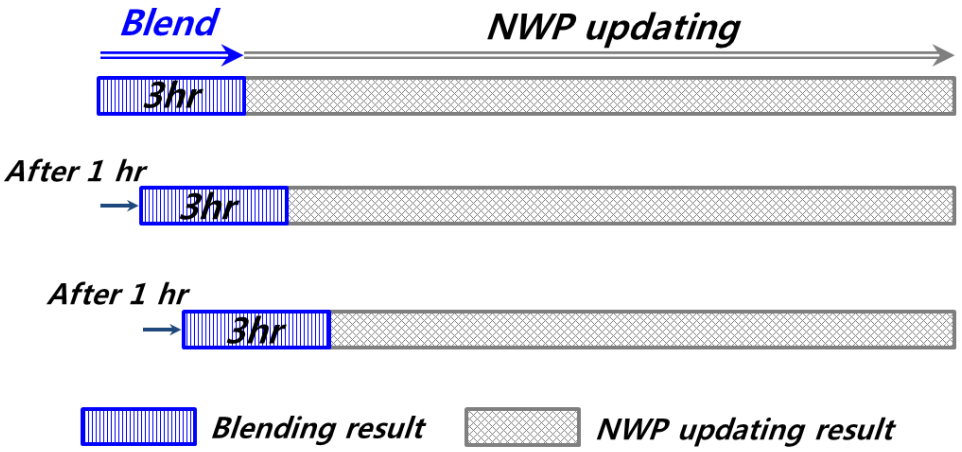

Figure 7.18 Strategy for hybrid flood forecasting with blending and updated NWP rainfall

Figures 7.19 ~ 7.22 show the ensemble flood forecasting using the original 11 ensemble members and the hybrid flood forecasting with blending and updated NWP rainfall after 6, 9, 12, 15, 18, 21, and 24 hrs considering bias correction by error-field scheme in the rising limb and peak discharge period over the Futatsuno and Nanairo dam catchment. Each figure illustrates a complete set of the forecasted discharge for the ensemble range (grey range), the ensemble mean (blue curve), and the simulation result using observed radar rainfall (black curve) and observed discharge data of catchment outlet point (red point).

Through the Figure 7.19, 3 hrs forecasting from the blending result is well matched to observed discharge in overall time period. And the ensemble mean and spread from the combination of blending and updated NWP rainfall by error-field scheme could represent the peak value and cover the observed discharge until the starting point of the hybrid flood forecasting at 18 hrs. However, the hybrid flood forecasting is over-predicted from the starting point of 18 hrs and 21 hrs. It can be explained by the bias between observed and predicted data expressed in Figure 3.3 of Chapter 3. In Figure 3.3, the observed rainfall intensity from 15 to 21 hrs lead time in 2nd forecast period increases, whereas the predicted ensemble NWP mean rainfall decreases and is under-predicted from 15 to 21 hrs lead time, so mean bias between observed and predicted data is largely estimated. The post-flood forecasting using updated NWP rainfall in hybrid flood forecasting at + 18 hrs and + 21 hrs starting point in Figure 7.19 uses the large mean bias estimated by 3-hr comparisons between observed and predicted data from 15 to 18 hrs and from 18 to 21 hrs lead time, respectively, so the hybrid flood forecasting is over-predicted from the starting point of 18 hrs and 21 hrs. In the 2nd forecast period (peak discharge period, Figure 7.20), the ensemble mean and spread of the original ensemble forecasting could not represent the peak discharge, whereas hybrid flood forecasting with combination of blending and updated NWP rainfall by error-field scheme provided the accuracy improvement of ensemble mean value and covered the observed discharge in peak

discharge period in overall updating step.

Through the result of hybrid flood forecasting in the rising limb period over the Nanairo dam catchment expressed by Figure 7.21, the ensemble mean and spread is similar to a curve shape of the observed discharge, but it is over-predicted generally. In this chapter, simulated discharge from the observed radar rainfall used the as the initial condition for hybrid flood forecasting in each updating step, and simulated discharge from the observed radar rainfall (Black curve) is over-predicted compared with the observed discharge. This led to over-prediction of hybrid flood forecasting. In the 2nd forecast period (peak discharge period, Figure 7.22), the ensemble mean value and spread of the original ensemble forecasting are under-predicted compared with the peak discharge, whereas hybrid flood forecasting outperforms original flood forecasting, and the ensemble spread could cover and represent the peak discharge impeccably in the overall updating step.

The results of the hybrid flood forecasting from the combination of blending and updated NWP rainfall considering bias correction by error-field scheme are reflected in the verification results using bias index according to elapsed time with blending time step in Figure 7.23. From the bias correction by error-field scheme, the accuracy of hybrid flood forecasting is improved compared with the ensemble flood forecasting using the original 11 ensemble members. And the bias of ensemble mean and spread are close to 1 value in each updating step.

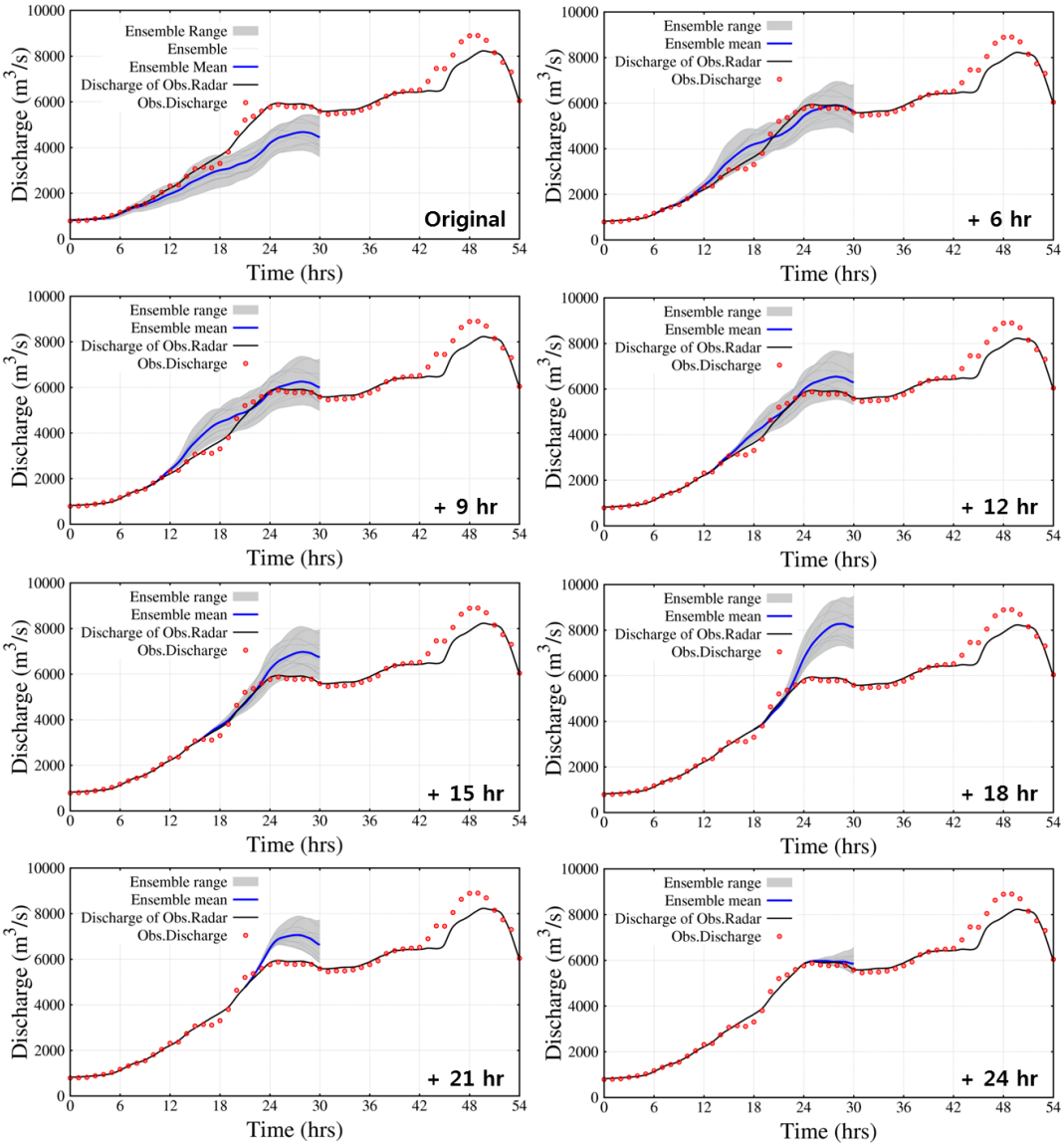

Figure 7.19 Hybrid flood forecasting considering bias correction by error-field scheme in the rising limb period over the Futatsuno dam catchment

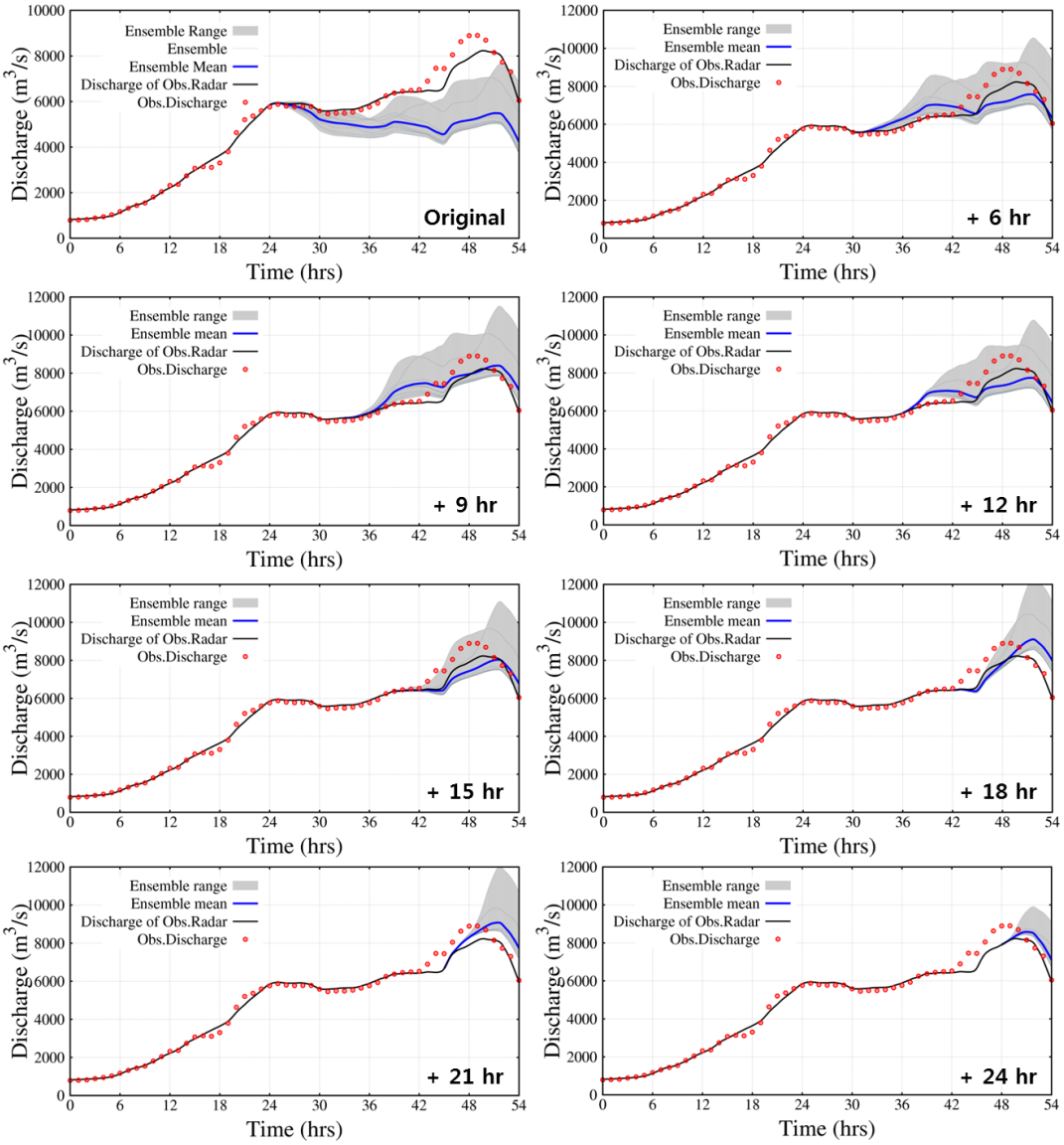

Figure 7.20 Hybrid flood forecasting considering bias correction by error-field scheme in the peak discharge period over the Futatsuno dam catchment

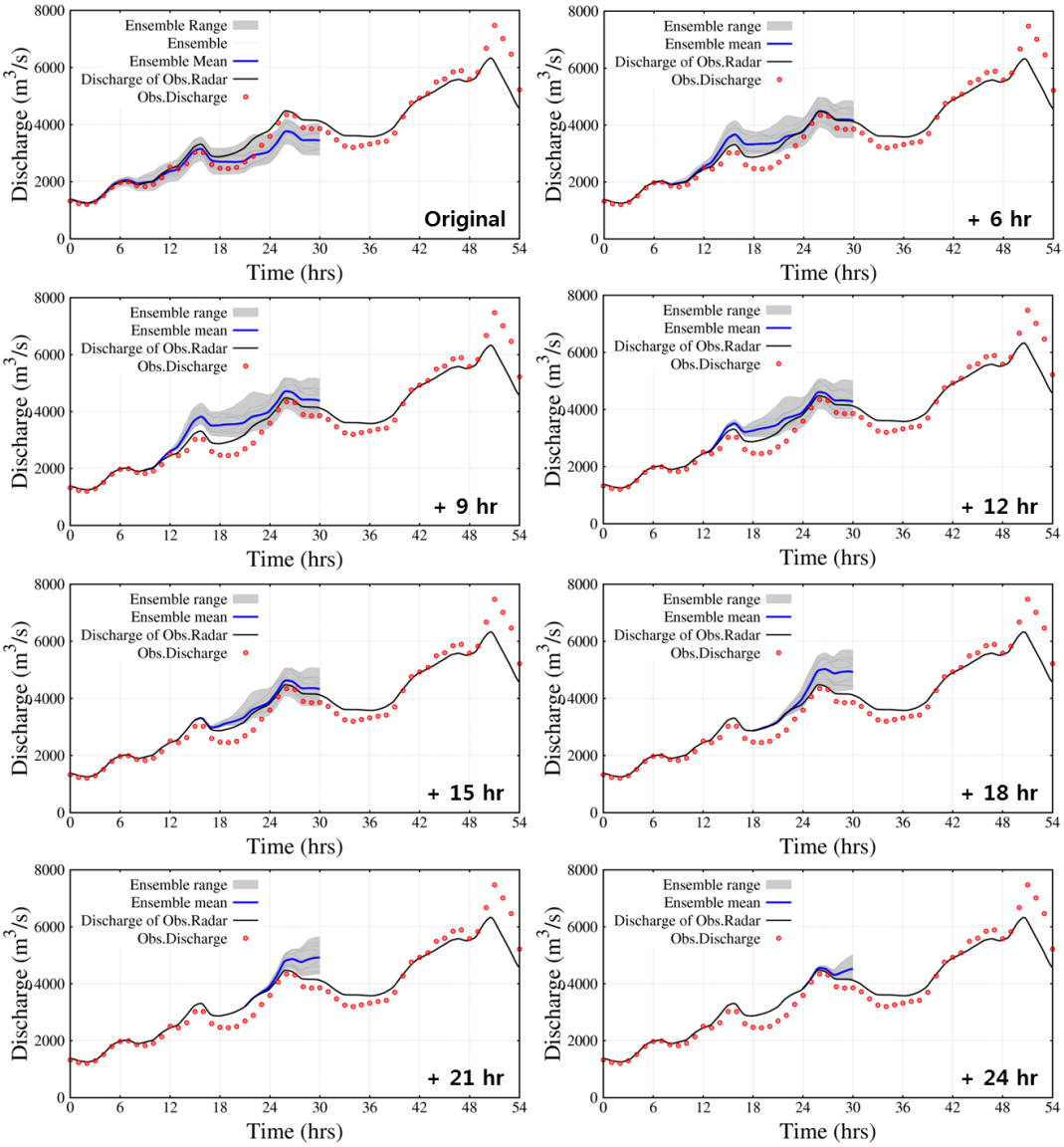

Figure 7.21 Hybrid flood forecasting considering bias correction by error-field scheme in the rising limb period over the Nanairo dam catchment

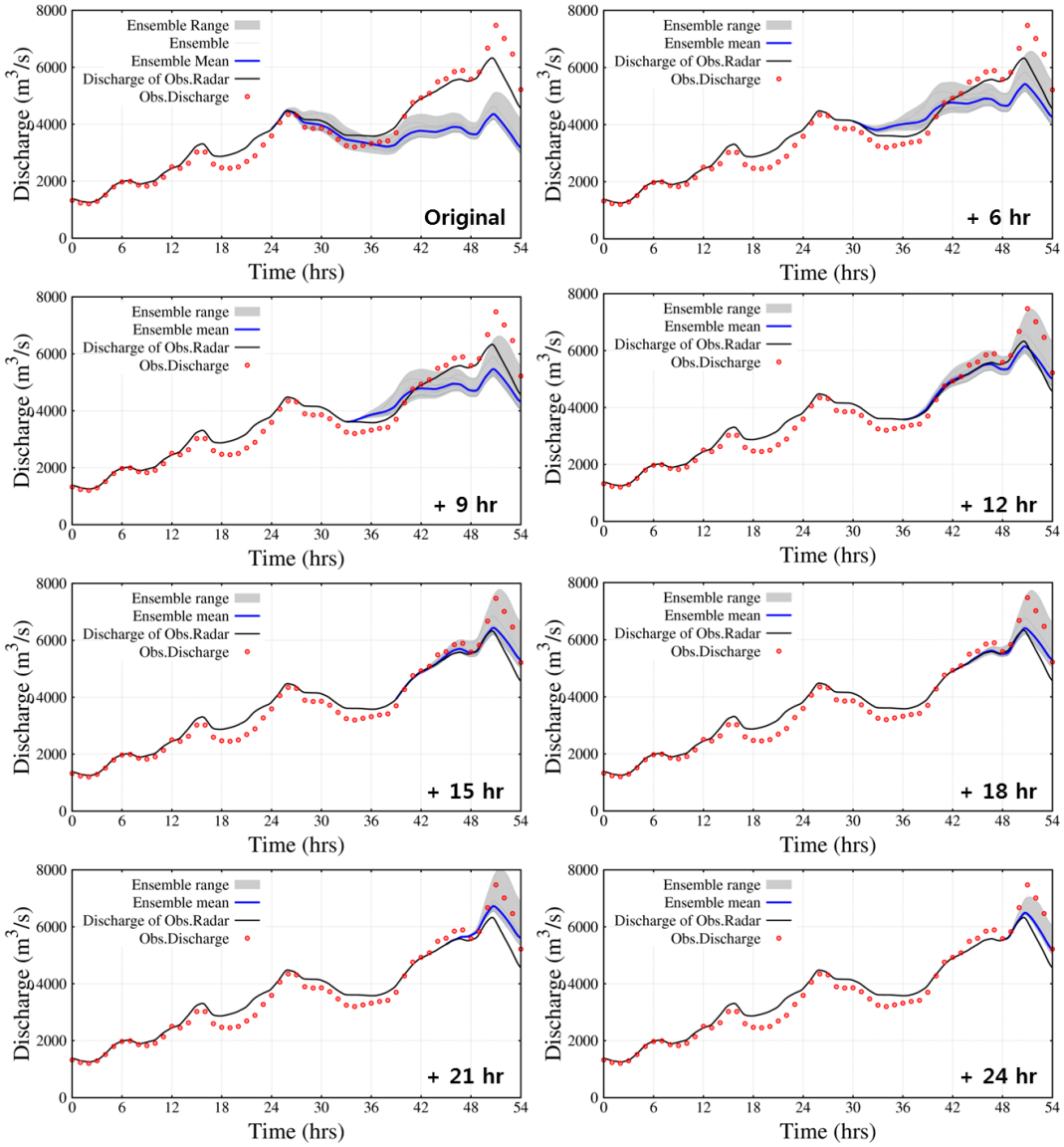

Figure 7.22 Hybrid flood forecasting considering bias correction by error-field scheme in the peak discharge period over the Nanairo dam catchment

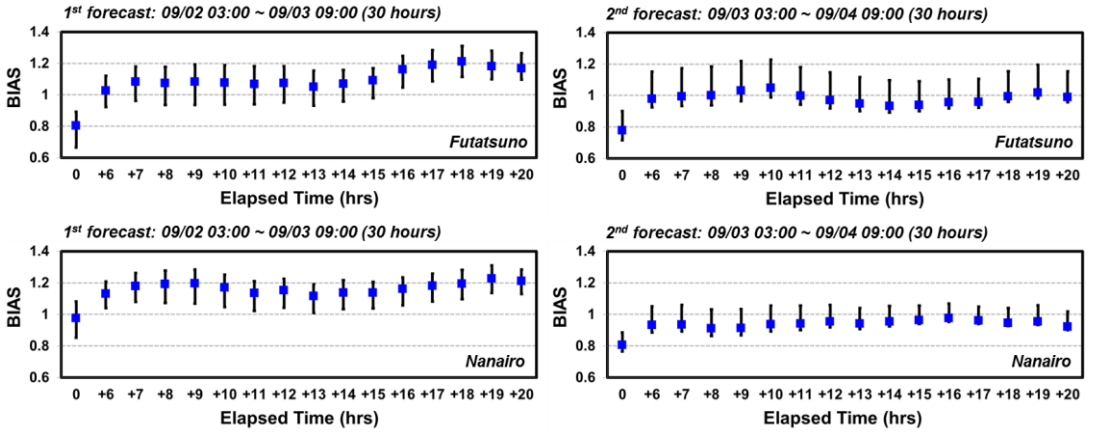

Figure 7.23 Verification results of hybrid flood forecasting considering bias correction by error-field scheme

Figures 7.24 ~ 7.27 show the ensemble flood forecasting using the original 11 ensemble members and the hybrid flood forecasting with blending and updated NWP rainfall after 9, 12, 15, 18, and 21 hrs considering QPF location correction by error-field scheme in the rising limb and peak discharge period over the Futatsuno and Nanairo dam catchment. Through the result of hybrid flood forecasting expressed by Figures 7.24 ~ 7.27, 3-hr forecasting from the blending result is close to observed discharge in overall time period, and the blending and updated NWP rainfall based on QPF location correction by transposition scheme could reduce the width of ensemble spread in the flood forecasting. However, ensemble mean value and spread from the combination of blending and updated NWP rainfall by transposition scheme could not represent the peak value or cover the observed discharge. These results considering QPF location correction by transposition scheme are also reflected in the verification results using bias index according to elapsed time with blending time step in Figure 7.28.

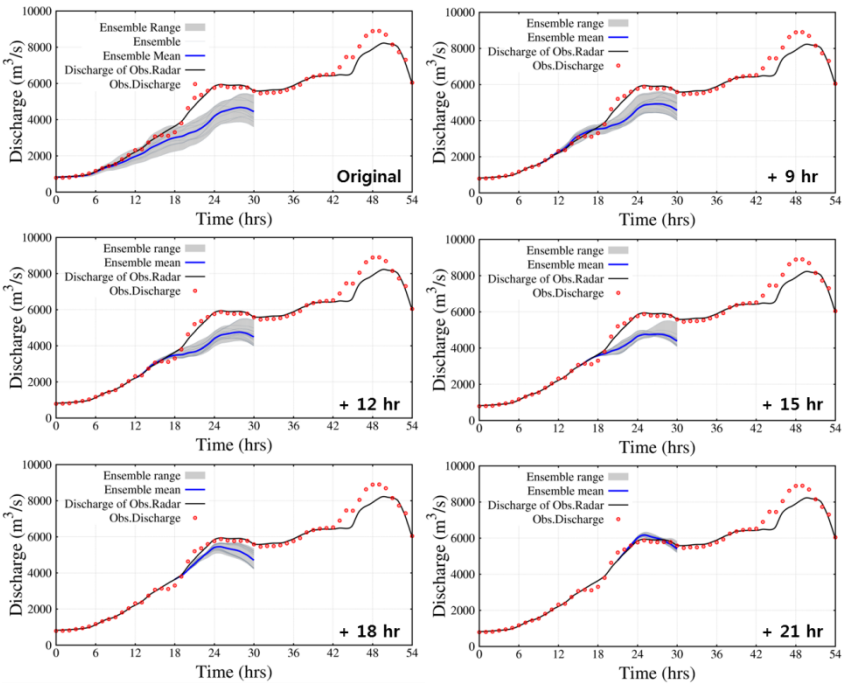

Figure 7.24 Hybrid flood forecasting considering location correction by transposition scheme in the rising limb period over the Futatsuno dam catchment

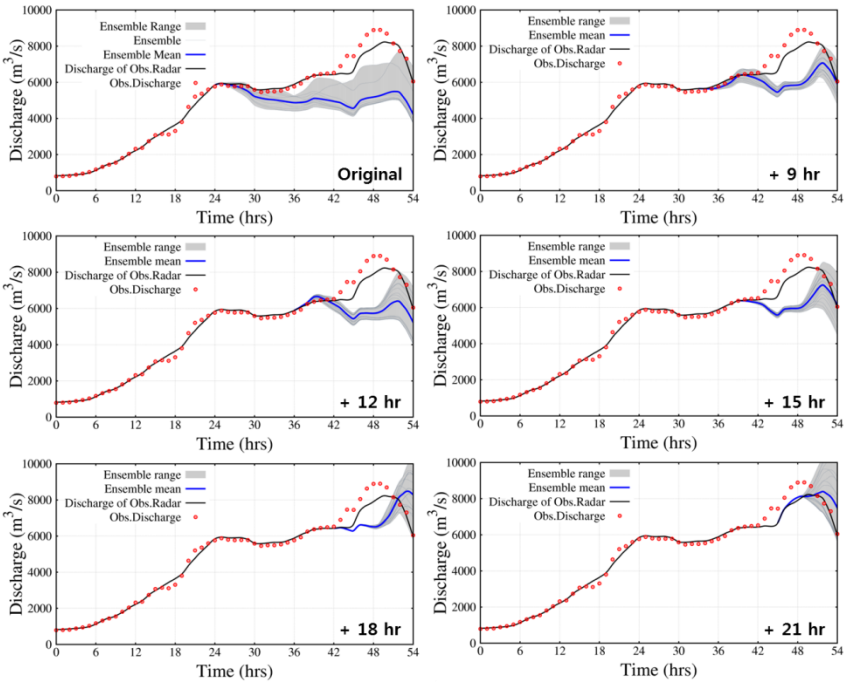

Figure 7.25 Hybrid flood forecasting considering location correction by transposition scheme in the peak discharge period over the Futatsuno dam catchment

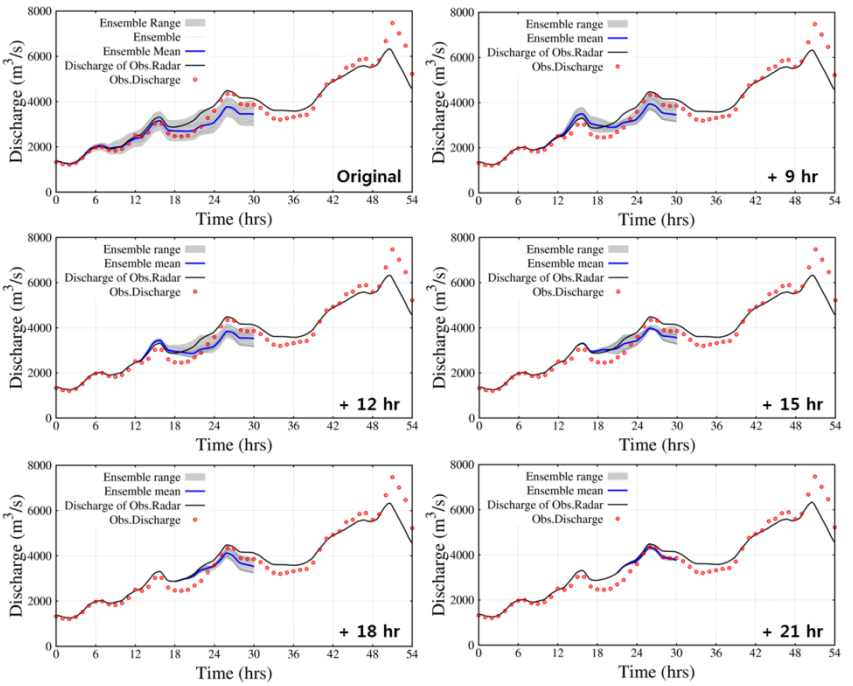

Figure 7.26 Hybrid flood forecasting considering location correction by transposition scheme in the rising limb period over the Nanairo dam catchment

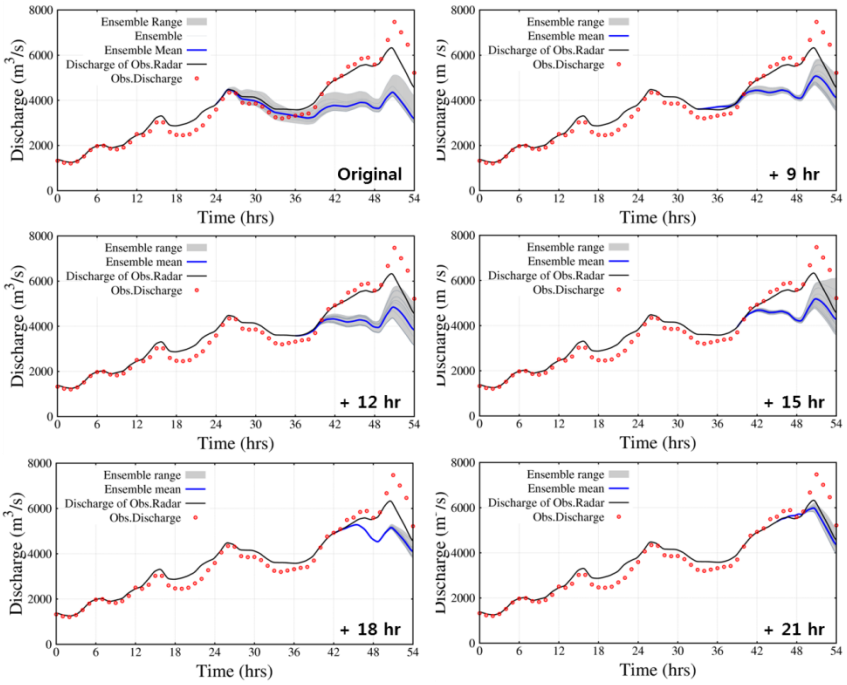

Figure 7.27 Hybrid flood forecasting considering location correction by transposition scheme in the peak discharge period over the Nanairo dam catchment

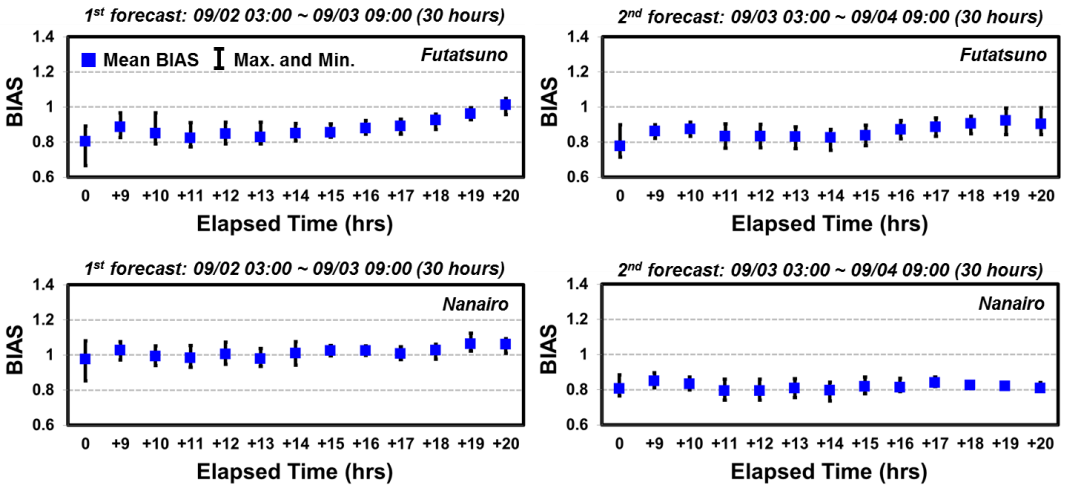

Figure 7.28 Verification results of hybrid flood forecasting considering QPF location correction by transposition scheme

7.4 Summary

This chapter attempted to improve the accuracy of rainfall and flood forecasting by blending the advantages of ensemble information of NWP rainfall forecast and radar-based prediction in viewpoint of the hybrid forecast. For this objective, improved radar-based image extrapolation was implemented with consideration of orographic rainfall identification and the error fields, and ensemble NWP rainfall with 30-hr forecast time were also updated using error-field scheme and transposition scheme. Finally, updated NWP rainfall and improved radar prediction were blended with time-varying weights through CSI and RMSE, and then the proposed blending method was verified through 2011's largest rainfall event and is applied to the hybrid flood forecasting on two sub-catchments, which are Futatsuno (356.1km^2) and Nanairo (182.1km^2) dam catchments. The results of this chapter lead to the following conclusions:

Improved radar image extrapolation method with consideration of orographic rainfall identification and the error fields showed better performance than other radar prediction methods in spatial forecast location in verification results of accumulated rainfall distribution, correlation coefficient, CSI and RMSE indexes.

Ensemble NWP rainfall were improved with quantitative bias correction using mean field bias of error fields, and updated NWP rainfall produced higher performances than radar prediction results considering the orographic rainfall and the error-field scheme. Updated NWP rainfall considering QPF location correction by the transposition scheme also outperformed the ensemble flood forecasting using the original 11 ensemble members, but radar prediction considering orographic rainfall and the error-field scheme provided better results than the updated NWP rainfall in CSI and RMSE verification.

The improvement achieved by merging the radar prediction with the updated NWP rainfall becomes more appreciable as the rainfall forecasts advance in lead time and the rainfall intensities become higher in case of both the error-field scheme and the transposition scheme. And hybrid flood forecasting with combination of blending and updated NWP rainfall by error-field scheme and by transposition scheme could improve the under-predicted part of original ensemble NWP rainfall in rising limb and peak discharge period over the two catchments. The newly proposed method based on bias correction shows sufficient reproducibility in peak discharge value compared with the result based on QPF location correction in updated flood forecasting, whereas the blending based on transposition scheme could reduce the width of ensemble spread, which is expressed as the uncertainty, in the flood forecasting. From these results, the bias correction by error-field scheme added to each ensemble member appears to significantly enhance the ensemble's utility and provide a more effective way than the QPF location correction by transposition scheme for accuracy improvement in rainfall and flood forecasting areas.

Chapter 8

Concluding Remarks

This study discussed high-resolution ensemble information mainly from numerical weather prediction (NWP) model based forecast and partly from radar based forecast for the application of real-time flood forecasting with a distributed hydrologic model. This study mainly consists of three parts:

1) Investigation of the applicability of ensemble forecasts of numerical weather prediction (NWP) model for flood forecasting area.

2) Assessment of the uncertainty propagation of rainfall forecast into hydrological response with catchment scale through distributed rainfall-runoff modeling based on the forecasted ensemble results of numerical weather prediction (NWP) model.

3) Development of the real-time flood forecasting for the accuracy improvement based on the QPF location correction and quantitative bias correction using the transposition scheme and error field scheme, respectively, in viewpoint of the hybrid forecast.

From these main objectives, acquired results are provided as follows:

In Chapter 3, Ensemble rainfall from numerical weather prediction (NWP) model with 30hr forecast time and 2 km horizontal resolution are verified temporally and spatially to assess whether they can produce suitable rainfall predictions or not during the Typhoon Talas event. Then flood forecasting is carried out over the two

catchments, which are Futatsuno (356.1 km^2) and Nanairo (182.1 km^2) dam catchments of Shingu river basin, located in Kii Peninsula of the Kinki area, Japan. The results show that although ensemble rainfall could catch the rainfall pattern and produced more suitable results compared with deterministic control run, the uncertainty of ensemble NWP rainfall was also significant at longer lead times. Flood forecasts driven by ensemble outputs showed that in general it has a large proportion of under and over predictions at short lead times and exhibited a negative bias at longer lead times. Despite the deficient performance for longer lead times, it was shown that the ensemble flood forecast provides additional information to the deterministic forecast.

In Chapter 4, the uncertainty propagation of rainfall forecast into hydrological response with catchment scale through distributed rainfall-runoff modeling based on the forecasted results of Chapter 3 was investigated. The results show the fact that uncertainty variability occurs sensitively and diversely at the same time in different catchments, and small catchments have sensitive variability of uncertainty. Therefore, it should be careful in case of flood forecasting in small catchment due to the large variability of uncertainty.

Chapter 5 proposes pre-processing methodologies based on appropriate members and a transposition scheme of ensemble forecast outputs from numerical weather prediction (NWP) model for the accuracy improvement of flood forecasting in the Futatsuno and the Nanairo dam catchments. First, the selection of appropriate members is investigated by comparison of spatial distributions between observed radar rainfall and forecasted ensemble rainfall. And selected ensemble information is applied into the next forecast period to assess the accuracy improvement of flood forecasting. Second, as an approach for the accuracy improvement of the flood forecasting, transposition method, which is spatial shift of ensemble rainfall distributions considering the correction of misplaced predicted rainfall distributions,

is introduced. Finally, above two methods are integrated in order to use advantages of characteristics of each method at the same time and apply into the next forecast period to confirm the accuracy improvement of the flood forecast skill. The results show that, in the flood forecast using selected ensemble members, this method can improve the accuracy of the mean value with conserving the best value between the original and selected ensemble members over two catchments. And the ensemble flood forecasting using transposition of NWP rainfall fields produced better results than the original and selected ensemble members, in terms of the best values of flood forecast skill in all periods over the two catchments. Finally, the integration of the selected and transposition methods recovered the accuracy of the mean values for two periods over the Nanairo catchment, compared with the use of the transposition method alone, although the mean values from using the selected ensemble method have outstanding accuracy.

Chapter 6 aimed to enhance the transposition method proposed in Chapter 5 and to propose newly real-time updating method for flood forecasting using transposition of ensemble rainfall distributions considering orographic rainfall. At first, ensemble forecast rainfalls from NWP model are separated into orographic and non-orographic rainfall fields using atmospheric variables of GPV data and the extraction of topography effect. Then the non-orographic rainfall fields are shifted by the transposition scheme to produce additional ensemble information. And newly ensemble rainfall fields are calculated by recombining the transposition results of non-orographic rainfall fields with separated orographic rainfall. Then the additional ensemble information is applied into hydrologic model for post-flood forecasting with 6 hours interval. The results show that the newly proposed method for real-time updating for flood forecasting could enhance the under-predicted part of original ensemble flood forecast and improve the accuracy of post-flood forecasting with 6 hours updating interval. However, the transposition scheme focuses on QPF location error correction considering the orographic rainfall but not predicted bias correction,

which is quantitative correction using the difference between observed and predicted rainfall. For this reason, it is possible to be vulnerable when forecasted rainfall intensity is under-predicted and suitable spatial distribution fails compared with observed reference data. Therefore, bias correction and/or hybrid products with radar based prediction are required to be more reliable hydrologic prediction.

Chapter 7 attempted to improve the accuracy of rainfall and flood forecasting with blending the advantages of ensemble information of NWP rainfall forecast and radar based prediction in viewpoint of the hybrid forecast. For this objective, improved radar based image extrapolation was implemented with consideration of orographic rainfall identification and the error fields, and ensemble NWP rainfall with 30 hours forecast time were also updated using error field scheme and transposition scheme. Finally, updated NWP rainfall and improved radar prediction are blended with time-varying weights through CSI and RMSE, then the proposed blending method is verified through 2011 largest rainfall event and is applied into the hybrid flood forecasting on two sub-catchments. The results show that the improvement achieved by merging the radar prediction with the updated NWP rainfall becomes more appreciable as the rainfall forecasts advance in lead time and the rainfall intensities become higher in case of both the error field scheme and the transposition scheme. And hybrid flood forecasting with combination of blending and updated NWP rainfall by error field scheme and by transposition scheme could improve the under-predicted part of original ensemble NWP rainfall in rising limb and peak discharge period over the two catchments.

The newly proposed method based on bias correction shows sufficient reproducibility in peak discharge value compared with the result based on QPF location correction in updated flood forecasting, whereas the blending based on transposition scheme could reduce the width of ensemble spread, which is expressed as the uncertainty, in the flood forecasting. From these results, the bias correction by

error field scheme added to each ensemble member appears to significantly enhance the ensemble's utility and provided a more effective way than the QPF location correction by transposition scheme for accuracy improvement in rainfall and flood forecasting areas.

Bibliography

Atencia, A., Rigo, T., Sairouni, A., More1, J., Bech, J., Vilaclara, E., Cunillera, J., Llasat, M.C. and Garrote, L. (2010) Improving QPF by blending techniques at the Meteorological Service of Catalonia. Natural Hazards and Earth System Sciences, Vol. 10, pp. 1443-1455.

Bartholmes, J. and Todini, E. (2005) Coupling meteorological and hydrological models for flood forecasting. Hydrology and Earth System Sciences, Vol. 9, pp. 333-346.

Bartholmes, J., Thielen, J., Ramos, M. and Gentilini, S. (2009) The European Flood Alert System EFAS – Part 2: Statistical skill assessment of probabilistic and deterministic operational forecasts. Hydrology and Earth System Sciences, Vol. 13, pp. 141-153.

Bogner, K. and Kalas, M. (2008) Error correction methods and evaluation of an ensemble based hydrological forecasting system for the Upper Danube catchment. Atmospheric Science Letters, Vol. 9, pp. 95-102.

Bowler, N., Pierce, C. and Seed, A. (2006) STEPS: A probabilistic precipitation forecasting scheme which merges an extrapolation nowcast with downscaled NWP, *Q. J. Roy. Meteorol. Soc.*, Vol. 132, pp. 2127-2155.

Buizza, R., Miller, M. and Palmer, T.N. (1999) Stochastic representation of model uncertainties in the ECMWF ensemble prediction system. *Quarterly Journal of the Royal Meteorological Society*, Vol. 125, pp. 2887-2908.

Buizza, R., Houtekamer, P.L., Toth, Z., Pellerin, G., Wei, M. and Zhu., Y. (2005) A comparison of the ECMWF, MSC, and NCEP Global Ensemble Prediction Systems. Monthly weather review, Vol. 133, No. 5, pp. 1076-1097.

Cloke, H.L. and Pappenberger, F. (2009) Ensemble flood forecasting: a review. *Journal of Hydrology*, Vol. 375, pp. 613-626.

Cuo, L., Pagano, T.C. and Wang, Q.J. (2011) A review of quantitative precipitation forecasts and their use in short- to medium-range streamflow forecasting. *Journal of Hydrometeorology*, Vol. 12, pp. 713-728.

Demeritt, D., Cloke, H., Pappenberger, F., Thielen, J., Bartholmes., J. and Ramos. M.H. (2007) Ensemble predictions and perceptions of risk, uncertainty, and error in flood forecasting. *Environmental Hazards*, Vol. 7, No. 2, pp. 115-127.

De Roo, A., Bartholmes, J., Bates, P.D., Beven, K., Bongioannini-Cerlini, B., Gouweleeuw, B., Heise, E., Hils, M., Hollingsworth, M., Holst, B., Horritt, M., Hunter, N., Kwadijk, J., Pappenburger, F., Reggiani, P., Rivin, G., Sattler, K., Sprokkereef, E., Thielen, J., Todini, E., Van Dijk, M. (2003) Development of a European flood forecasting system. *International Journal of River Basin Management*, Vol. 1, No. 1, pp. 49-59.

Duan, Q., Sorooshian, S. and Gupta, V.K. (1994) Optimal use of the SCE-UA global optimization method for calibrating watershed models. *Journal of Hydrology*, Vol. 158, pp. 265-284.

Ebert, E. (2001) Ability of a Poor Man's Ensemble to Predict the Probability and Distribution of Precipitation. *Monthly Weather Review*, Vol. 129, pp. 2461-2480.

Ebert, E. and McBride, J. (2000) Verification of precipitation in weather systems: Determination of systematic errors. *Journal of Hydrology*, Vol. 239, pp. 179-202.

Gneiting, T. and Raftery, A.E. (2005) Weather forecasting with ensemble methods. *Science*, Vol. 310, pp. 248-249.

Golding, B.W. (1998) Nimrod: A system for generating automated very short range forecasts. *Meteorological Applications*, Vol. 5, pp. 1-16.

Golding, B.W. (2009) Review - Long lead time flood warnings: reality or fantasy? *Meteorological Applications*, Vol. 16, pp. 3-12.

Gouweleeuw, B., Thielen, J., Franchello, G., de Roo, A. and Buizza, R. (2005) Flood forecasting using medium-range probabilistic weather prediction. Hydrology and Earth System Sciences, Vol. 9, No. 4, pp. 365-380.

Hamm, A. J. and Elmore, K. L. (2004) A validation of the NCEP SREF, Session 7 Verification Studies: Part II on 20th Conference on Weather Analysis and Forecasting/16th Conference on Numerical Weather Prediction.

Hlavcova, K., Szolgay, J., Kubes, R., Kohnova, S. and Zvolensky, M. (2006) Routing of numerical weather predictions through a rainfall–runoff model. In: Marsalek, J., Stancalie, G. and Balint, G. (Eds.), *Transboundary Floods: Reducing Risks through Flood Management, Springer, NATO Science Series, Dordecht, Netherlands*, pp. 57-68.

Honda, Y. and Sawada, K. (2008) A new 4D-Var for mesoscale analysis at the Japan meteorological agency. CAS/JSC WGNE, *Res. Act. Atmos. Ocea. Model*, Vol. 38, pp. 01.7-01.8.

Hopson, T. and Webster, P. (2008) Three-Tier flood and precipitation forecasting scheme for south-east asia. Available at (http://cfab2.eas.gatech.edu/).

Hsiao L.F. et al. (2013) Ensemble forecasting of typhoon rainfall and floods over a mountainous watershed in Taiwan. Journal of Hydrology, Vol. 506, pp. 55-68.

Komma, J., Reszler, C., Blöschl, G. and Haiden, T. (2007) Ensemble prediction of floods - catchment non-linearity and forecast probabilities. *Natural Hazards Earth*

System Sciences, Vol. 7, pp. 431-444.

Kwadijk, J. (2003) EFFS – European Flood Forecasting System. Final report of Contract EVG1-CT-1999-00011 (http://effs.wldelft.nl).

Kim, S., Tachikawa, Y., Sayama, T. and Takara, K. (2009) Ensemble flood forecasting with stochastic radar image extrapolation and a distributed hydrologic model. *Hydrological Processes*, Vol. 23, pp. 597–611.

Leahy, C.P., Srikanthan, S., Amirthanathan, G. and Sooriyakumaran, S. (2007) Objective Assessment and Communication of Uncertainty in Flood Warnings, *Extended abstracts of presentations at the 5th Victorian Flood Management Conference*.

Lee, G., Tachikawa, Y. and Takara, K. (2008) Assessment of prediction uncertainty under scale-dependant condition of rainfall runoff modeling, *Annuals of Disaster Prevention Research Institute, Kyoto University*, No. 51B, pp. 29-50.

Legg, T.P. and Mylne, K.R. (2004) Early warnings of severe weather from ensemble forecast information. *Weather and Forecasting*, Vol. 19, pp. 891-906.

Lin, C., Vasic, S., Kilambi, A., Turner, B. and Zawadzki, I. (2005) Precipitation forecast skill of numerical weather prediction models and radar nowcasts. *Geophysical Research Letter*, Vol. 32, L14801.

Lorenz, E.N. (1969) Atmospheric Predictability as Revealed by Naturally Occurring Analogues. *Journal of the Atmospheric Sciences*, Vol. 26, pp. 636-646.

Matsubara, T., Kasahara, S., Shimada, Y., Nakakita, E., Tsuchida, K., and Takada, N. (2013) Study on applicability of information of typhoons and GSM for dam operation, *Ann. J. Hydraul. Eng, JSCE*, Vol. 69, No. 4, pp. I_367-I_372 (in Japanese with English abstract).

Nakakita, E., Ikebuchi, S., Nakamura, T., Kanmuri, M., Okuda, M., Yamaji, A. and Takasao, T. (1996) Short-term rainfall prediction method using a volume scanning radar and GPV data from numerical weather prediction. *J. Geophys. Res.*, Vol. 101 (D21), pp. 26181-26197.

Nakakita, E. and Terazono, M. (2008) Short-term rainfall prediction taking into consideration nonlinear effect of non-orographic rainfall on orographic rainfall. *Ann. J. Hydraul. Eng, JSCE*, Vol. 52, pp. 331-336 (in Japanese with English abstract).

Nakakita, E., Yoshikai, T. and Kim, S. (2012) Application of error-ensemble prediction method to a short-term rainfall prediction model considering orographic rainfall. *IAHS Publ. Proceedings of 2011International Weather Radar and Hydrology symposium, Exeter, UK*. Vol. 351, pp. 311-316.

Olsson, J. and Lindstrom, G. (2008) Evaluation and calibration of operational hydrological ensemble forecasts in Sweden. *Journal of Hydrology*, Vol. 350, pp. 14-24.

Palmer, T. (2002) The economic value of ensemble forecasts as a tool for risk assessment: from days to decades. *Quarterly Journal of the Royal Meteorological Society*, Vol. 128, pp. 147-174.

Palmer, T. and Buizza, R. (2007) Fifteenth anniversary of EPS, *ECMWF Newsletter* Vol. 114, pp. 14.

Pierce, C., Hardaker, P., Collier, C. and Haggett, C. (2001) GANDOLF: A system for generating automated nowcasts of convective precipitation, *Meteorological Applications*, Vol. 7, pp. 341-360.

Roulin, E. (2007) Skill and relative economic value of medium-range hydrological ensemble predictions. *Hydrology and Earth System Sciences*, Vol. 11, pp. 725-737.

Roulin, E. and Vannitsem, S. (2005) Skill of medium-range hydrological ensemble predictions. *Journal of Hydrometeorology*, Vol. 6, No. 5, pp. 729-744.

Saito, K., Fujita, T., Yamada, Y., Ishida, J., Kumagai, Y., Aranami, K., Ohmori, S., Nagasawa, R., Kumagai, S., Muroi, C., Kato, T., Eito, H. and Yamazaki, Y. (2006) The operational JMA nonhydrostatic meso-scale model. *Monthly Weather Review*, Vol. 134, pp. 1266-1298.

Saito, K. (2012) The JMA nonhydrostatic model and its application to operation and research. In: Yucel, I. (Eds.), *Atmospheric Model Applications, InTech*, pp. 85-110.

Schaake, J., Franz, K., Bradley, A. and Buizza, R. (2006) The hydrologic ensemble prediction experiment (HEPEX). *Hydrology and Earth System Sciences Discussions*, Vol. 3, pp. 3321-3332.

Schaake, J., Hamill, T.H., Buizza, R. and Clark, M. (2007) HEPEX: the hydrological ensemble prediction experiment. *Bulletin of the American Meteorological Society*, Vol. 88, No. 10, pp. 1541-1547.

Schaake, J., Perica, S., Mullusky, M., Demargne, J., Welles, E. and Wu. L. (2004) Pre-processing of atmospheric forcing for ensemble runoff prediction, *Proceedings of the 84th AMS Annual Meeting*.

Tachikawa, Y., Nagatani, G. and Takara, K. (2004) Development of stage-discharge relationship equation incorporating saturated–unsaturated flow mechanism. *Ann. J. Hydraul. Eng, JSCE*, Vol. 48, pp. 7-12 (in Japanese with English abstract).

Takasao, T. and Shiiba, M. (1988) Incorporation of the effect of concentration of flow into the kinematic wave equations and its applications to runoff system lumping. *Journal of Hydrology*, Vol. 102, pp. 301-322.

Tatehira, R. (1976) Orographic rainfall computation including cloud-precipitation interaction. *Tenki*, Vol. 23, pp. 95-100 (in Japanese).

Thielen, J., Schaake, J., Hartman, R. and Buizza, R. (2008) Aims, challenges and progress of the Hydrological Ensemble Prediction Experiment (HEPEX) following the third HEPEX workshop held in Stresa 27 to 29 June 2007. *Atmospheric Science Letters*, Vol. 9, pp. 29-35.

Toth, E., Brath, A. and Montanari, A. (2000) Comparison of short-term rainfall prediction models for real-time flood forecasting. Journal of Hydrology, Vol. 239, pp. 132-147.

Velazquez, J.A., Anctil, F., Ramos, M.H. and Perrin, C. (2011) Can a multi-model approach improve hydrological ensemble forecasting? A study on 29 French catchments using 16 hydrological model structures, *Advances in Geosciences*, Vol. 29, pp. 33-42.

World Meteorogical Organization (2011) Manual on flood forecasting and warning. (WMO-No. 1072), Geneva, Switzerland.

Xuan, Y., Cluckie, I. and Wang, Y. (2009) Uncertainty analysis of hydrological ensemble forecasts in a distributed model utilizing short-range rainfall prediction. *Hydrol. Earth Syst. Sci.*, Vol. 13, pp. 293-303.

Yu, W., Nakakita, E. and Yamaguchi, K. (2013) Assessment of probabilistic flood Forecasting using ensemble NWP rainfall with 30hr forecast time during typhoon events. *Advances in River Engineering*, *JSCE*, Vol. 19, pp. 235-240.

Yu, W., Nakakita, E., Kim, S. and Yamaguchi, K. (2014) Accuracy improvement of flood forecasting using pre-processing of ensemble numerical weather prediction rainfall fields. *Journal of Japan Society of Civil Engineers*, *Ser. B1 (Hydraulic Engineering)*, Vol. 70, pp. I_151-I_156.

Zappa, M., Rotach, M.W., Arpagaus, M., Dorninger, M., Hegg, C., Montani, A., Ranzi, R., Ament, F., Germann, U., Grossi, G., Jaum, S., Rossi, A., Vogt, S., Walser, A., Wehrhand, J. and Wunram, C. (2008) MAP D-PHASE; real-time demonstration of hydrological ensemble prediction systems. *Atmospheric Science Letters*, Vol. 9, pp. 80-87.